

Experimental Study on Loop Heat Pipe with Flat Evaporator

By

Huynh Phuoc Hien

A dissertation submitted in partial fulfillment of the
requirements for the degree of

Doctor of Engineering (Dr. Eng.)

in

Mechanical Engineering



Department of Science and Advanced Technology

Graduate School of Science and Engineering

Saga University, Japan

March 2019

ACKNOWLEDGEMENTS

I would like to express my deep gratitude to my supervisor, Professor Akio Miyara, who willingly accepted me as his doctoral student and kindly me to do this research. I am grateful to him for his patient guidance, valuable discussions and enthusiastic encouragements to this research work. My grateful thanks are also extended to Associate Professor Keishi Kariya who has enthusiastically helped and supported me since the first days of this research.

I would like to sincere thanks to Associate Professor Chieko Kondou of Nagasaki University for sharing with me her valuable experiences of this research.

I am also grateful to the Technical Support Division of Saga University, especially Mr. Masahito Kawahira and Mr. Muneharu Matsuoka for their important helps in fabrications the test section.

I also would like to extend my sincere thanks to the members of my dissertation committee, Professor Yuichi Mitsutake, and Professor Yoichi Kinoue for their time, comments and valuable ideas that helped me improve this study significantly.

I would like to thank to my home university, Ho Chi Minh City University of Technology (Vietnam) for allowing me the opportunity to continue my studies at the doctoral level. I would also like to express special thanks to the MEXT (Ministry of Education, Culture, Sports, Science and Technology), Japan to accept me as a Japanese Government sponsored student. Without their grant and support, this work would not have been possible.

From my heart, I am thankful to my parents who give me my life and have devoted their whole lives for nurturing and supporting me and my siblings. I also extend my thanks to all my brother, sisters and my brothers-in-law for their true love to me.

Finally, I would like to thank all my lab mates for their support. I would also like to express my gratitude to all my Japanese language teachers, Vietnamese friends and international students in Saga for making my Japan life more comfortable and enjoyable.

ABSTRACT

Loop heat pipe (LHP) is a passive two-phase heat transport device of which principle operation is based on the phase changing processes and the natural motivations such as capillary or gravitational force. Different with conventional heat pipe (HP), vapor and liquid phases in LHP flow in separated pipes and the fine pore wick occurring inside evaporator only. Hence, LHP accesses some favor characteristics such as flexibility, compact ability, high heat transfer capacity with low thermal resistance and high-reliability characteristics. LHP has been applied successfully and commonly in the thermal management systems belonging to orbital vehicles or machines like spacecraft, satellites, orbiters which operates in the zero-gravity environment. Nowadays, LHP is considered as one of potential solutions for the challenges that the cooling system of modern electronics devices facing such as high heat power and heat flux dissipation, stable and reliable performance and electricity consumption or environmental problem. There are numerous experimental and computational studies conducted to evaluate the performance as well as the phenomenon happening inside the LHP under the effects of different parameters. However, until now LHP has not approved the commercial situation as the normal HP does. One of the reasons can be caused by the complicated structure of evaporator, especially sintered porous wick that increases the LHP manufacturing cost. In this study, a new pattern of evaporator was proposed, and various experiments were conducted to find out the thermal performance of this evaporator as well as the whole LHP operating under different conditions including orientations, working fluids, cooling conditions. From the experimental results, the assumption above boiling and heat transfer process happening inside this evaporator was withdrawn. This assumption can be used as one of the factors to improve the design of LHP in the future.

The works done in this thesis can be summarized as follows

- Designing and fabricating the first pattern of LHP's evaporator. This pattern was accompanied with the sintered stainless-steel wick, and water was the working fluid inside the LHP. The LHP's performance was investigated under both gravity-assisted and horizontal orientation condition.

- In the experiment that LHP worked in condition advantage in gravity, the condenser was cooled by water at 27.5°C with mass flow rate at 27 kg/h, the LHP could operate stably in the range of 50 to 520 W (19.2 W/cm²) and maintain the temperature on the top surface of the heater not be higher than 105°C. The total thermal resistance of LHP reduced with heating power increment and had the minimum value of 0.149 K/W at the heating power of 520 W. For the target of cooling, this LHP could take the heat at the rate of 350 W (12.9 W/cm²) from the heater while the temperature on the top surface of heating block at 85°C. The start-up characteristics of the LHP under different heating power were also analyzed and discussed. The experimental results also included the changing of evaporation heat transfer coefficient on the heat flux. Through the results, an assumption about boiling phenomenon happening inside the evaporator was introduced. This experiment also examined the cooling performance of the LHP after turning off the heater.
- Within the horizontal condition, the performance of LHP was investigated when the inlet temperature of cooling water was adjusted at different values including 18.5°C, 28.5°C, 36.5°C. When cooled by water at 28.5°C, the LHP could operate in the range of heat load from 10 W to 94 W and maintain temperature at the top surface of heating block lower than 100°C; however, the LHP demonstrated the weak oscillating behavior under heat load at 10 W. Experimental results also show that the total thermal resistance of LHP, when cooled by water at 28.5°C and 36.5°C, are nearly equal together and smaller than the case that cooling water was set at 18.5°C. This result indicates that LHP can function efficiently with natural water without cooled in advance. Besides, the experiment of horizontal condition also found out the overcharged of working fluid is one of reasons caused the LHP behave different oscillation characteristics.
- However, the first pattern of the evaporator behaved some disadvantage in design, especially the vapor chamber and compensation chamber could connect with each other, so made the circulation weaker. Therefore, we designed and fabricated the second pattern of LHP's evaporator having some strong points such as prevent the connection between the vapor collector and compensation chamber, easy in changing the wick as well as the base of the evaporator. Within the second pattern, performance of LHP under gravity assisted condition was investigated when operating with different working fluids including water and ethanol. In the experiment, the evaporator's LHP was also equipped with stainless-steel wick. The results show that the performance of water LHP was almost

similar to one working with the first pattern of evaporator despite of the smaller elevation difference between evaporator and condenser (350mm \rightarrow 235mm). Comparison between water LHP and ethanol LHP, the LHP with water as working fluid had the better performance. In the case of water LHP, when heating power was changed from 33 to 535 W, the temperature at the top surface of the heating block raised from 38°C to 110°C. With the ethanol LHP, this temperature reached the value of 133°C at the heating power of 395 W. If temperature limitation of processors functioning inside the DC is recognized at 85°C, the cooling capability of LHP will be 220 W (8.1 W/cm²) and 350 W (12.9 W/cm²) corresponding to the working fluid was ethanol and water respectively. In addition, the discussion in the difference in boiling heating transfer characteristics as well as condenser performances in the cases that water and ethanol were used as working fluid was also presented in this experiment.

OUTLINES OF THESIS

The thesis includes 7 chapters, the chapter outline is listed as follows

- Chapter 1 begins with the introduction of data center (DC) and the challenges cooling systems in the DC facing. The end of this chapter presents the background of LHP and the relative studies on LHP with flat evaporator to cool the electronics devices.
- Chapter 2 describes the parameters of LHP including the specification of the two patterns of the evaporator, the sintered wick, the condenser, the vapor and liquid line as well as the heating block used in the experiment.
- Chapter 3 demonstrates the setup and results obtained from the experiment of investigation the performance of LHP with the first pattern of evaporator under gravity assisted condition.
- Chapter 4 is the experiment of LHP with the second pattern of the evaporator under gravity assisted condition with stainless-steel wick and water and ethanol as working fluids respectively.
- Chapter 5 shows the setup and results obtained from the experiment of investigation the performance of LHP with the first pattern of evaporator under horizontal condition.
- Chapter 6 presents the oscillating behavior of the LHP operating horizontally under overcharged condition.
- The conclusion and future study will be focused in the chapter 7.

TABLE OF CONTENTS

	ACKNOWLEDGMENTS	i
	ABSTRACTS	ii
	OUTLINES OF THESIS	v
	TABLE OF CONTENTS	vi
	LIST OF FIGURES	ix
	LIST OF TABLES	xiii
	NOMENCLATURE	xiv
1	INTRODUCTION	1
	1.1 DATA CENTER	2
	1.1.1 Definition of data center	2
	1.1.2 Basic requirements for safety operation of data center	3
	1.1.3 Energy and environment context	3
	1.2 LOOP HEAT PIPE	11
	1.2.1 Introduction of loop heat pipe	11
	1.2.2 Loop heat pipe theory	13
	1.2.3 Loop heat pipe for electronics cooling	15
	1.3 MOTIVATION OF THIS STUDY	23
2	LOOP HEAT PIPE DESCRIPTION	28
	2.1 EVAPORATOR'S DESIGN	28
	2.1.1 The first pattern of the evaporator	28
	2.1.2 The second pattern of the evaporator	31
	2.1.3 Sintered wick characteristics	33
	2.2 DESCRIPTION OF CONDENSERS	34

2.3	VACUUM AND CHARGING SYSTEM	35
2.4	THERMOCOUPLES USED IN THE EXPERIMENT	36
2.5	OTHER EQUIPMENT AND MEASUREMENT DEVICES	37
3	EXPERIMENTAL INVESTIGATION ON LHP PERFORMANCE UNDER GRAVITY-ASSISTED CONDITION – THE FIRST PATTERN OF EVAPORATOR	38
3.1	INTRODUCTION	39
3.2	EXPERIMENTAL SETUP	42
3.3	DATA REDUCTION	44
3.4	RESULTS AND DISCUSSIONS	46
3.4.1	Startup characteristics of the loop heat pipe	46
3.4.2	Cooling capacity and thermal performance of LHP	48
3.4.3	The evaporator heat transfer coefficient and assumption about boiling heat transfer phenomenon inside the evaporator	53
3.4.4	Cooling performance of loop heat pipe after turning off the heaters	56
3.5	CONCLUSION	57
4	EXPERIMENTAL INVESTIGATION ON LHP PERFORMANCE UNDER GRAVITY-ASSISTED CONDITION WITH DIFFERENT WORKING FLUIDS – THE SECOND PATTERN OF EVAPORATOR	60
4.1	INTRODUCTION	61
4.2	EXPERIMENTAL SETUP	62
4.3	DATA REDUCTION	64
4.4	RESULTS AND DISCUSSIONS	66
4.4.1	Cooling capacity and performances of water loop heat pipe and ethanol loop heat pipe	66
4.4.2	Thermal resistances comparison	70
4.4.3	Evaporator heat transfer coefficient and the boiling characteristics of evaporator operating with water and ethanol	74
4.5	CONCLUSION	77
5	LHP PERFORMANCE UNDER HORIZONTAL CONDITION – THE FIRST	79

	PATTERN OF EVAPORATOR	
5.1	INTRODUCTION	80
5.2	EXPERIMENTAL SETUP AND DATA REDUCTION	81
5.3	RESULTS AND DISCUSSIONS	83
	5.3.1 Performance of loop heat pipe when cooled by water at 28.5°C	83
	5.3.2 Loop heat pipe performance under different cooling conditions	86
5.4	CONCLUSION	88
6	OSCILLATING BEHAVIOR OF LOOP HEAT PIPE WHEN OPERATING UNDER OVERCHARGED CONDITION	90
6.1	INTRODUCTION	91
6.2	EXPERIMENTAL SETUP AND DATA REDUCTION	92
6.3	RESULTS AND DISCUSSIONS	95
	6.3.1 Performance of loop heat pipe when charged with 28.5 ml water	95
	6.3.2 Thermal performance of loop heat pipe after the first-time reducing amount of charged water	96
	6.3.3 Thermal performance of loop heat pipe after the second-time reducing amount of charged water	100
6.4	CONCLUSION	102
7	CONCLUSION	104
	APPENDIX	107
A	MANUFACTURED DRAWINGS	107
B	WICK'S SPECIFICATIONS	114
C	THERMOCOUPLES CALIBRATION RESULTS	118
D	THERMAL BALANCING & GRADIENT TEMPERATURE MEASUREMENT	122
E	EXPERIMENTAL UNCERTAINTY ANALYSIS	126

LIST OF FIGURES

1.1	Typical layout of data center	2
1.2	Power flow in a traditional data center	3
1.3	Electricity consumption by different sectors in data center	4
1.4	Electricity consumption worldwide in data center	5
1.5	Carbon footprint in data center in 2002 and predicted in 2020	5
1.6	Using the rotating wheel heat exchanger to reduce the cooling load on the chiller system	6
1.7	The Aquasar cooling system applied to QS22 Blade server module	7
1.8	Different stages of data center	8
1.9	The projections of maximum heat flux and power dissipation for microprocessor chip	9
1.10	Schematic diagram of (a) traditional heat pipe (b) LHP	11
1.11	a) Analytical LHP scheme b) Diagram of the LHP working cycle	13
1.12	a) Disk-shaped evaporator; b) Rectangular evaporator; c) Evaporator with longitudinal replenishment	15
1.13	External view of ammonia LHPs with disk-shaped evaporator	17
2.1	(a) LHP's evaporator with longitudinal replenishment (b) LHP's evaporator with opposite replenishment	29
2.2	Structure drawing of the first pattern evaporator	29
2.3	Geometry of the inner surface of the evaporator	30
2.4	Method of fixing the evaporator on the heating block	31
2.5	Outline of the second pattern of evaporator	31
2.6	Assembly of the second pattern of evaporator	32
2.7	The fin and vapor grooves machined on the evaporator base	33
2.8	Stainless-steel powder [3], and the stainless-steel sintered wick used in the	34

experiment	
2.9	Description of condensers used in the experiments 34
2.10	Charging and vacuum system for LHP experiment 35
3.1	Schematic diagram of experiment setup 42
3.2	a) Geometry of the inner surface the evaporator b) Temperature gradient measurement 42
3.3	The real setup of the experiment 43
3.4	Startup of the LHP at heating power of 50 W 46
3.5	Startup of the LHP at heating power of 125 W 46
3.6	Startup of the LHP at heating power of 270 W 47
3.7	Changing of temperatures T_{s1} , T_{s2} on the heating power 49
3.8	Temperature of working fluid at different positions of LHP collected during the operating period 50
3.9	Temperature distribution inside the loop heat pipe at various heating power from 50 to 520 W 51
3.10	Changing of different thermal resistances on heating power 52
3.11	Effect of heat flux on the evaporator HTC 54
3.12	Relation between heat flux and excess temperature 54
3.13	Assumption of boiling phenomenon under different magnitude of heat flux 55
3.14	Cooling performance of the LHP after turning off the heaters 57
4.1	Schematic diagram of experiment 62
4.2	Temperature gradient measurement 62
4.3	Evaporator structure 63
4.4	Real setup of experiment before insulating the evaporator 63
4.5	Temperature T_{s1} at different heating power in the experiments of water LHP and ethanol LHP 66
4.6	Temperature distribution of working fluid inside the ethanol LHP 68
4.7	Temperature distribution of working fluid inside the water LHP 68
4.8	Temperature distribution inside the water LHP (200 W to 350 W, interval: 69

	25 W)	
4.9	Temperature distribution inside the ethanol LHP (from 200 W to 250 W, interval: 25 W)	69
4.10	Total thermal resistance of water and ethanol LHP varied with heating power	70
4.11	Changing of evaporator thermal resistance on heating power in the experiments of water and ethanol LHP	71
4.12	Changing of condenser thermal resistance on heating power in the experiments of water and ethanol LHP	72
4.13	Temperature distribution on the outer wall of condenser	73
4.14	Thermal contact resistance	74
4.15	Evaporator HTC in the in the experiments of water and ethanol LHP	75
4.16	Evaporator HTC in the in the experiment introduced in chapter 3 (water is working fluid)	75
4.17	Assumption about boiling heat transfer mechanism under condition that heat flux is higher than 100 kW/m ²	76
5.1	Schematic of experiment and the real setup	81
5.2	Temperature gradient measurement	81
5.3	Startup progresses of LHP at different heating power	83
5.4	Temperature T_{s1} and temperatures of working fluid in the LHP varied with heating power	84
5.5	Total thermal resistance R_t and evaporator thermal resistance R_e	85
5.6	Evaporator heat transfer coefficient h_e	86
5.7	Total thermal resistance R_t and temperature T_{s1} at different inlet temperature of cooling water	87
5.8	Schematic of LHP with different components of pressure loss when working fluid circulates inside	87
6.1	Schematic diagram of experimental setup	92
6.2	Vacuum and charging system	93
6.3	Temperature in the base of evaporator T_4 and temperatures at different positions of LHP (CR was 61%)	95
6.4	Assumption of phase distribution when LHP operating at CR was 61%	96

6.5	Temperature in the base of evaporator T_4 and temperatures at different positions of LHP after the first time of reducing amount of charged water (heating power at 45 W – CR was around 58.7%)	96
6.6	Phase distribution when LHP operating at the heating power at 45 W and CR was around 58.7%.	97
6.7	Temperature in the base of evaporator T_4 and temperatures at different positions of LHP after the first time of reducing amount of charged water (heating power at 25 W – CR was around 58.7%)	98
6.8	Phase distribution when LHP operating at the heating power at 25 W and CR was around 58.7%.	99
6.9	Temperature in the base of evaporator T_4 and temperatures at different positions of LHP after the first time of reducing amount of charged water (heating power at 50 W – CR was around 58.7%)	100
6.10	Phase distribution when LHP operating at the heating power at 50 W and CR was around 58.7%.	100
6.11	Temperature in the base of evaporator T_4 and temperatures at different positions of LHP after the second time of reducing amount of charged water (heat input power at 45W – CR was around 53%)	101
6.12	Total thermal resistance of LHP under the first and the second time of reducing working fluid	102

LIST OF TABLES

1.1	Classification of LHPs	12
1.2	Some previous studies on LHP	19
2.1	Specification of some processors	29
2.2	Specification of stainless-steel sintered wick	33
2.3	Condenser's specification	35
2.4	Thermocouple functions	36
2.5	Temperature difference estimating	36
2.6	Specification of other equipment and measurement devices	37
3.1	Main parameters of LHP	42
3.2	Uncertainty values	43
4.1	Main parameters of LHP	62
4.2	Uncertainty values	62
6.1	Main specifications of the LHP	93
6.2	Volumes of different sections of the LHP	93

NOMENCLATURE

Abbreviation

CC	: compensation chamber
DC	: data center
HP	: heat pipe
HTC	: heat transfer coefficient
LHP	: loop heat pipe
L-V	: liquid - vapor

Symbol

		SI unit
A	: heating area	m^2
c_p	: specific heat	$J/(kg \cdot K)$
CR	: charging ratio	%
C_{sf}	: experimental constant in Rohsenow equation	-
g	: gravitational acceleration	m/s^2
h_e or h_{e-T}	: evaporator heat transfer coefficient obtained from vapor temperature	$W/(m^2 \cdot K)$
h_{e-P}	: evaporator heat transfer coefficient obtained from vapor pressure	$W/(m^2 \cdot K)$
h_{fg}	: latent heat of working fluid	J/kg
ID/OD	: pipe inner and outer diameter	m
k	: thermal conductivity	$W/(m \cdot K)$
K	: permeability of porous material	m^2
l	: pipe length	m
m_{wa}	: cooling water mass flow rate	kg/s
n	: experimental constant in Rohsenow equation	-
Pr	: Prandtl number	-
q	: heat flux	W/m^2
Q	: heating power	W
Q_c	: heat released from condenser to cooling water	W
R	: thermal resistance	K/W

T	: temperature	°C
V	: volume	m ³
	: voltage	V

Greek letters

δ	: wick thickness	m
δ	: uncertainty	%
δ_1	: distance between thermocouples T ₁ , T ₂ , T ₃	m
ΔT	: temperature difference	°C
ΔP	: pressure drop	Pa
ΔV	: voltage difference	V
δ_2	: distance from the evaporator bottom surface to thermocouple T ₄	m
ε	: porosity	%
μ	: absolute viscosity	Pa.s
ν	: kinematic viscosity	m ² /s
ρ	: density	kg/m ³
σ	: surface tension	N/m
ω	: velocity	m/s

Subscripts

1, 2, 3, 4, 5	Order of thermocouples inserted to heating block, base of evaporator and outer wall of condenser
a	: ambient
bf	: base of fins
c	: condenser
cc	: compensation chamber
ci	: condenser inlet
co	: condenser outlet
cci	: compensation chamber inlet
ct	: contact interface
e	: evaporator
l	: liquid
s1	: top surface of heating block
s2	: bottom surface of evaporator

sat : saturation sate
t : total
v : vapor
w : wall
w : wick
wa-i : cooling water at inlet of condenser
wa-o : cooling water at outlet of condenser

Chapter 1

INTRODUCTION

The development of techniques such as online searching, social networking, cloud computing, etc. have approached the great progress to become inseparable demand of human. This tendency promotes to the dramatically development of data center (DC), but also leads some challenges to this industry. One of the challenges relates with cooling system due to the gain of heat power and heat flux generated from the electronic devices. Moreover, environmental concerns have been paying attention at this moment. This chapter present the DC, heat pipe loop heat pipe background as well as the literature review on relative studies of applying loop heat pipe (LHP) in cooling systems of DC.

1.1 DATA CENTER

1.1.1 Definition of data center

According to [1], data center (DC) is a large-capacity facility (up to 500 000 m²) in which are gathered Information Technology (IT) equipment, such as servers or processors, and support systems designed to provide a safe and reliable environment for IT equipment. For more clearly, from [2], DC is defined as computing structures housing a large number of Information and Communications Technology (ICT) devices installed for processing, storing and transmitting information. They are also equipped with data storages, network routers, switches, redundant power supplies, redundant data communications connections, and environmental controls such as air conditioners and fire suppression systems and often multi-stage high-level security access systems [1]. Fig 1.1 demonstrates the simple layout of the DC plant.

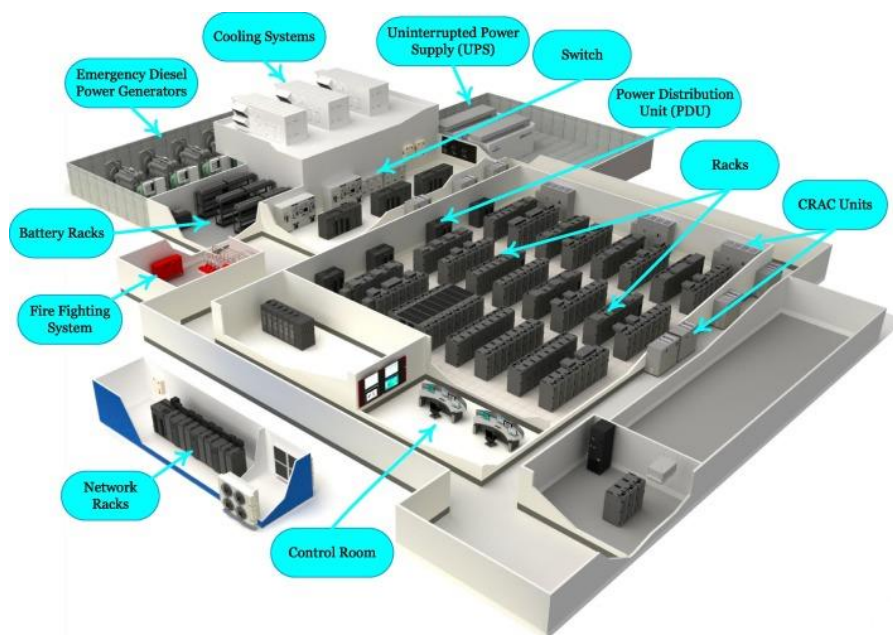


Figure 1.1: Typical layout of the DC [2]

Basing on their functions, the equipment in the DC can be classified into four categories [3] that are

- Power equipment includes power distribution units (PDUs), generators, uninterruptible power supply systems (UPSs), switchgears, and batteries.
- Cooling equipment consists of chillers, computer room air-conditioning (CRAC) units, cooling towers and plumbing system

- Servers, network, storage nodes and supplemental devices such as keyboards, monitors, workstations and laptop belong to IT equipment group.
- The fourth category is miscellaneous components load that are lighting and firing systems.

Although energy consumption of IT equipment could be considered effective, it is important to improve the energy efficiency of the three sections with ensuring the reliable and safe performance of the DC. Some metrics for evaluating the energy efficiency of DC are presented in section 1.1.3.

1.1.2 Basic requirements for safety operation of DC

Besides contributing to human daily activity such as online searching, social networking, telecommunication, banking, online shopping, cloud computing, etc. DC also support for the military and security operation in defense organizations. Therefore, DC should satisfy the stringent requirement during operating lifespan.

- Information security (InfoSec): the DC has to offer the secure environment which minimizes the chances of security breach.
- Business continuity: because the DC's client such as companies rely on their information systems to run their operations. If a system becomes unavailable, company operations may be damaged or stopped completely, it requests the DC to make sure it overcomes serious incidents or disasters and resumes its normal operation within a reasonably short period. This is accomplished through redundancy of mechanical cooling and power systems (including emergency backup power generators) serving the data center along with fiber optic cables.

1.1.3 Energy and environment context

a) Energy consumption

Figure 1.2 demonstrates schematic of power flow in a typical DC and the electricity distribution to each section is shown in Fig 1.3. While the electricity consumed by the demand – side systems such as processors, server power supplies, or storage and communication equipment take for around 52% total consumption, the energy used for operating the traditional cooling system account for 38 % of total. The rest of energy belongs to the lighting and building switchgear.

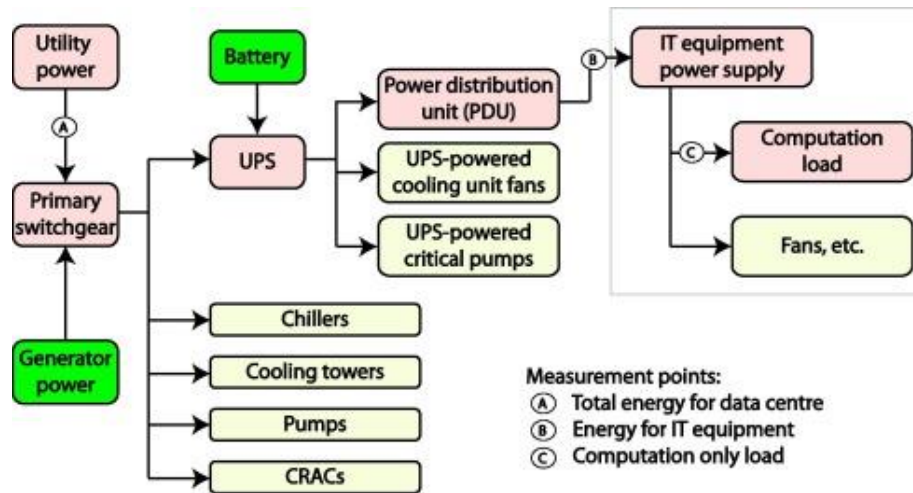


Figure 1.2: Power flow in a traditional DC [2]

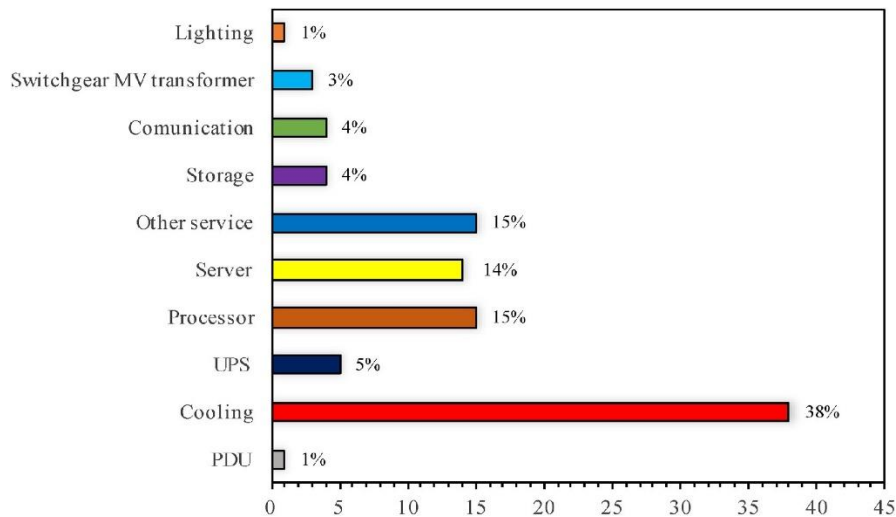


Figure 1.3: Electricity consumption by different sectors in DC [4]

The worldwide electricity usage in data centers has increased double from 2000 to 2005. In 2005, the electricity used by DC reach 152 billion kWh per year, as shown in Fig 1.3. This growth of the electricity consumption represents approximately 10% per year. In 2005, electricity consumed by data centers was about 1% of world electricity use, this ratio represents between 1.1 and 1.5% of the world electricity use by 2010. The lower bound figures demonstrate the situation that DC electricity consumption increased 20 to 33% compared to 2005. The Japanese Ministry of Economy predicted that the electricity consumption can be five times greater in 2025. The strong electricity usage, particularly in cooling, has made energy efficiency become the top of the agenda for both datacom businesses and policy makers.

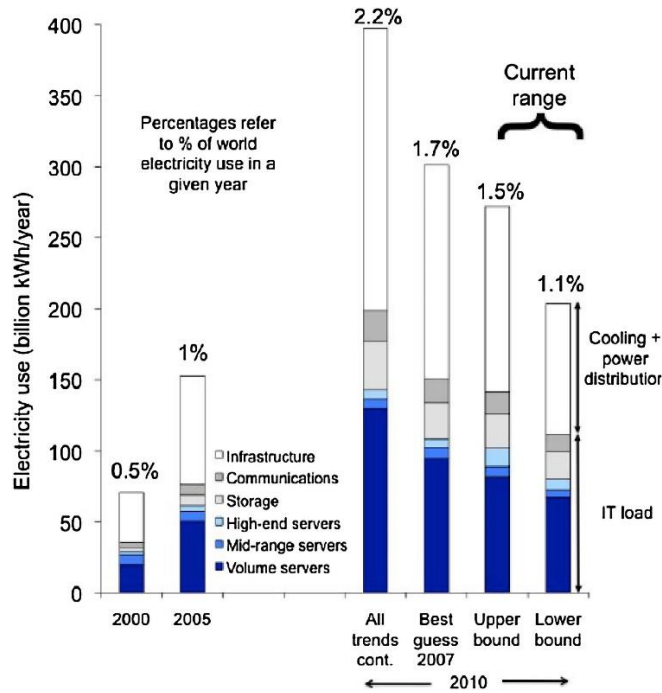


Figure 1.4: Electricity consumption worldwide in data center [5]

b) Carbon footprint

Due to the electricity consumption has increased date after date, the emission of CO₂ from DC activities has been increasing. In 2002 the global DC footprint was 76 MtCO₂e and it is expected to reach the value of 259 MtCO₂ in 2020 or grow up at the rate of 7% per year [1].

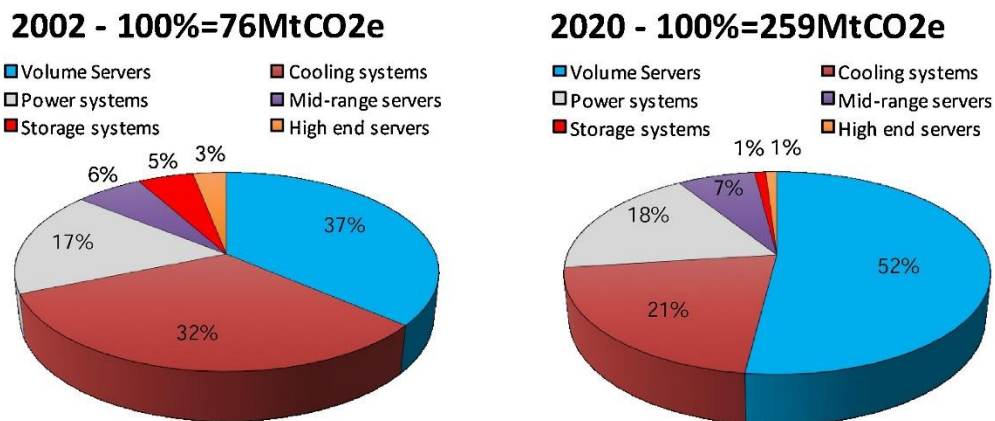


Figure 1.5: Carbon footprint in DC in 2002 and predicted in 2020 [6]

The prediction of carbon footprint in 2020 indicates that improvement the efficiency of the cooling systems is the inevitable trend of the future DC that can reduce the electricity consumption as well as the carbon emission from the activities of DC.

c) Metrics for energy efficiency of DC

The Power Usage Effectiveness (PUE) is suggested by the Green Grid initiative as a fraction of total power of the DC P_{DC} to that used by the IT equipment P_{IT} . It is defined to assess the energy efficiency of DC over the year.

$$PUE = \frac{P_{DC}}{P_{IT}} \quad (1.1.a)$$

$$PUE = \frac{P_{cooling} + P_{power} + P_{lighting} + P_{IT}}{P_{IT}} \quad (1.1.b)$$

The data center operates more effectively if value of PUE closes to 1, or power consumption by other section not IT closes to zero. The proper design of DC should have the value of PUE not higher than 1.6.

However, the parameter PUE itself does not consider the opportunity of energy recovery inside the DC. Therefore, the Green Grid defined another metrics named Energy Reuse Effectiveness (ERE) as

$$ERE = \frac{P_{cooling} + P_{power} + P_{lighting} + P_{IT} - P_{reues}}{P_{IT}} \quad (1.2)$$

From the Eq 1.2, reusing energy dissipated from the electronic devices for other purposes such as warming buildings, heating water, etc. is another method to increase the efficiency performance of the DC. Yin Zhang et al [7] introduced the technology that uses the wheel heat exchanger as shown in Fig 1.6. In this method, temperature of the fresh air is reduced by the exhaust air from the air-conditioned room by the rotating wheel heat exchanger before entering the evaporator. This method can decrease the cooling load on the chiller system.

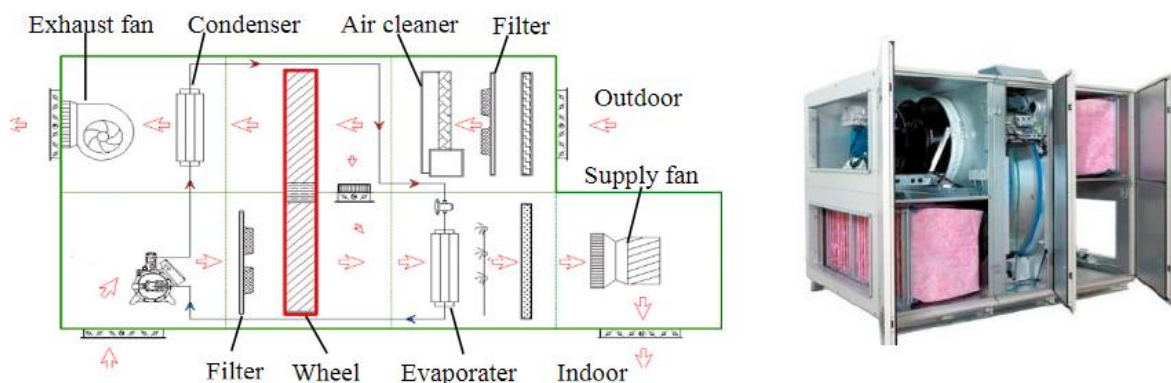


Figure 1.6: Using the rotating wheel heat exchanger to reduce the cooling load on the chiller system [7]

Another recovery energy method in DC is using hot water to cool the supercomputer. It was reported that IBM has delivered successfully to Swiss Federal Institute of Technology Zurich (ETH Zurich) the first-of-a-kind hot water-cooled supercomputer Aquasar whose electronics is cooled by the hot water to reuse the heat generated from the electronics for warming the building [8]. They show that the energy consumption 40% less than in the case of traditional air-cooling method while the temperature of processor can be kept well below 85°C. From this idea, M.A Cherysheva et al [9] suggested a copper-water LHPs for energy-efficient cooling systems of supercomputers. In their study, the performance of LHP when operating with cooling water controlled at various value from 20°C to 80°C. Their results show that their LHP's performance varies slightly with the changes in the condenser cooling temperature in the range below 40°C. It indicates the feasibility utilization LHP to recovery the energy generated from electronic device.

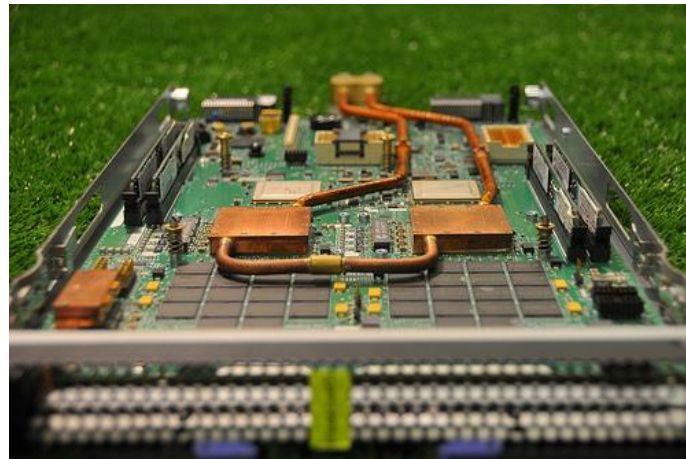


Figure 1.7: The Aquasar cooling system applied to QS22 Blade server module [10]

d) Temperature and heat load ranges

With the extreme development of DC, dissipated energy flux on the floor of the room that traditional DC operates inside was between 430 and 861 W/m²; however, it has been increased at least by 10 times (6458 – 10764 W/m²) while the cooling load from the normal room with the same size is only around 40 – 86 W/m². Therefore, design and manufacture of thermal management systems is one of the most challenging aspects of DC design: they must be capable of handling the increasing thermal loads while maintaining the temperature of electronic components at a safe operational level [11]. It is necessary to have accurate and reliable information about the maximum thermal loads and temperature limits in each component of a DC to design systems properly.

Rambo and Joshi [12] considered high power racks with heat dissipation of 57 kW in a model for DC airflow and heat transfer. Marcinichen et al. [13] indicated that in designing cooling system for today's data centers, the assumed heat capacity for the racks is between 10 and 15 kW. However, if rack is filled with supercomputer servers, it can generate in excess of 60 kW of heat.



Figure 1.8: Different stages of DC [14]

Figure 1.8 displays the combination different stages to create the DC. The DC consists many enclosures or servers from where heat is generated due to the major heat dissipated devices such as processors, memory modules, voltage regulators, chipsets, and power supplies operating inside. Between of them, the processor is the most challenge to the thermal management due to their high heat flux. Electricity used by the processors that almost converts into heat takes around 50% of total power consumption of the servers while taking up minimum servers area [15]. This challenge is caused by the miniaturization of electronics. In 1960s, there were 50 to 1000 components installed on the chip, but in 2006, the chip with the density 100 million transistors per square centimeter was already manufactured. As presented in Fig. 1.9, it is predicted that in 2020, heat power generated from chip can reach 360 W while the maximum heat flux can increase to the value of 190 W/cm²[16]. However, microprocessors are not the only power dissipation components in a typical server: an individual hard disk can dissipate powers as high as 12 W per each element, and up to 20–30 % of the total power supply can be consumed by mass storage devices [11].

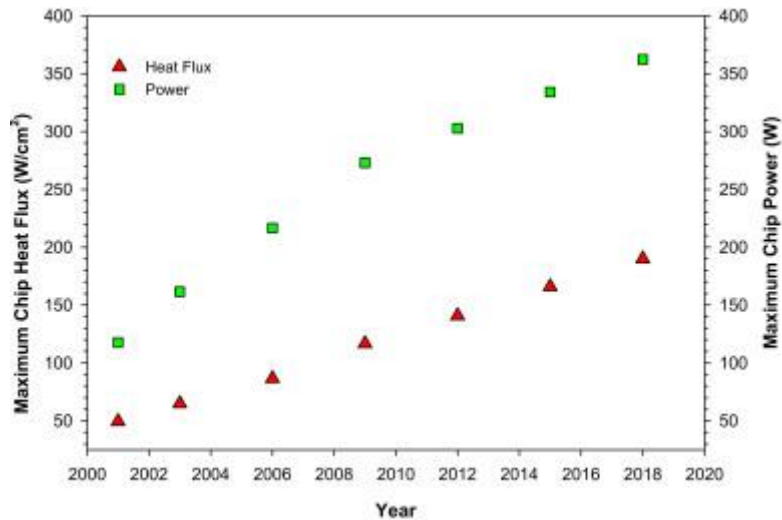


Figure 1.9: The projections of maximum heat flux and power dissipation for microprocessor chip

The limitation of the electronics thermal management research considers 85 °C as the maximum allowable junction temperature for the safe and effective operation of microprocessors [11]. However, there are few different suggested values of the limitation operating temperature of the processor or microprocessor. For example, Schmidt and Notohardjono [17] recommended 100°C is the maximum operating temperature of processor. On the other hand, this parameter was suggested at the value of 78°C by Ohadi et al [18]. The value 85°C is also the suggested as the limitation temperature of DIMM (Dual in-line memory module). However, it is often recommended that the hard drive disk driver should operate at the temperature not higher than 40°C – 45°C for long period lifespan. However, both of heat power and heat flux dissipated from such devices is not a serious problem that can be solved by normal air-cooling method.

From the above sections, the modern cooling method has not only the reliable, sufficient cooling capacity but also being friendlier with the environment or saving electricity consumption characteristics. LHP, a novel catalogue of the heat pipe (HP), can be considered as one of the potential solutions. LHP is also a passive two-phase heat transfer device operating in the same way as the HP. Heat supplied to evaporator makes a liquid turn into vapor, then flow to the condenser where vapor releases heat to the heat sink and become liquid again. However, in the LHP vapor and liquid phases flow in separated tubes and where is no capillary structure or wick placed on, but porous wick is only installed in evaporator, so the LHP can avoid entrainment limit and operate with the lower pressure loss to circulate the working fluid comparing to the conventional HP. Consequently, the LHP has the higher heat transfer capacity, smaller thermal resistance and more flexible characteristics than normal HP [19]. Besides,

working fluid is circulated inside the LHP by the capillary or gravity effect, no mechanical component functioning is required like the other active two-phase cooling methods. It means that both of electricity consumption and operating cost can be reduced while the lifespan and reliable performance can be higher. Moreover, in the fields of DC thermal management, it is feasible to arrange the position of evaporator lower than condenser to utilize the gravity in circulating the fluid, or the cooling capacity can be gained dramatically than when LHP operates horizontally or anti-gravity condition.

1.2 LOOP HEAT PIPE

1.2.1 Introduction of loop heat pipe

The beginning of the LHP can be considered from 1972 when the first such device with heat transfer capacity of about 1 kW and length of 1.2 m was created and examined successfully by the two scientists from Ural Polytechnical Institute that are Gerasimov and Maydanik [20].

The existence of the LHP was regarded as an alternative to the conventional heat pipe (HP) in the field of aerospace technology where require the heat transfer device much less sensitive to the change of orientation in the gravity field. With the traditional heat pipe, due to the capillary structure lies along the whole HP's body as shown in Fig. 1.10, when the HP operates horizontally or against the gravity force with the long heat transfer distance, the flow rate of working fluid circulating in the LHP or the heat transfer capacity will be decided by the relation between the hydraulic resistance and the capillary head pressure. The first term hydraulic resistance is directly proportional to the effective pore radius of the wick and the heat transfer distance or the length of the heat pipe while the capillary head is inversely proportional to the wick's pore radius. It means that reducing the wick pore radius could increase the capillary head, but at the same time it also causes the hydraulic resistance stronger. Therefore, it seems to be impossible to create the traditional heat pipe that can satisfy both of long heat transfer distance and high heat transfer capacity when functioning in horizontal or antigravity, micro gravity condition.

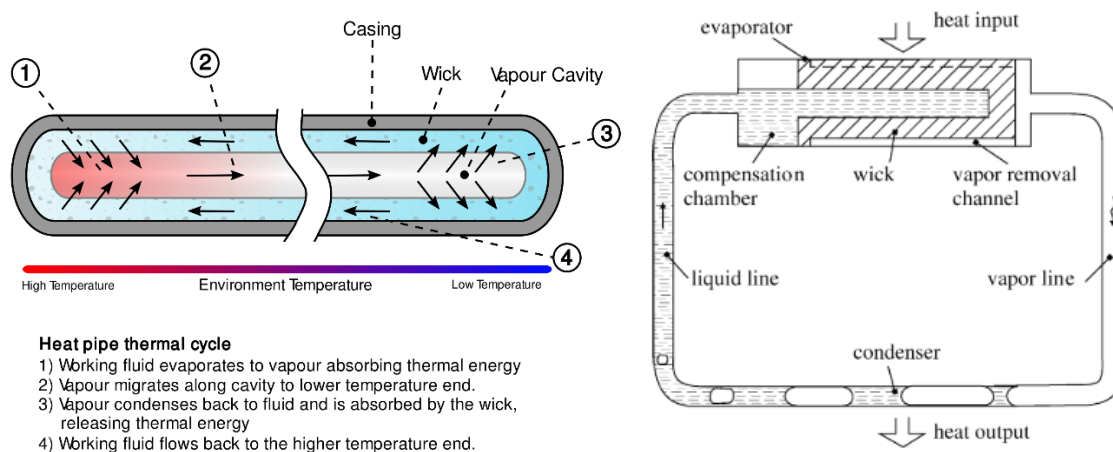


Figure 1.10: Schematic diagram of (a) traditional heat pipe (b) LHP

Because the LHP can be classified as a special branch of HP, it owns the advantages all of advantages of traditional HP such as compact ability, lightweight, reliable characteristics, no

power consumption for fluid circulating. Besides, the LHPs also has their own advantages, and some sides that can overcome the drawback of the conventional HP.

- Using the fine-pore wicks is feasible. In the LHP, it is possible to use the fine-pored wick that is sintered from nickel, titanium and copper powders and has effective pore of 0.7 to 15 μm for creating the sufficient capillary force, especially in the case of low-temperature working fluid with low surface tension.
- Minimum the distance of liquid moving in the capillary structure. As mentioned about, there is no wick installed in the liquid line of the LHP, liquid only penetrates through the wick from the compensation chamber to enter the evaporation zone.
- Due to the vapor and liquid lines of the LHP are separated together, as a result, the entrainment limitation in which liquid is prevented to return the evaporator due to the high pressure of the vapor flow can be eliminate. In addition, almost smooth tubes are used as vapor and liquid pipe-lines, the pressure loss in the adiabatic can be smaller.
- The evaporation normally happens on the wick surface or the mini channel grooves on the evaporator wall, therefore the evaporator heat transfer coefficient can be enhanced.
- The size as well as geometry of condenser can be selected independently with the structure of evaporator. It makes the LHP to be adapted easier to the conditions of heat exchange with an external heat sink.

The various LHP can be classified basing upon some criterion such as LHP dimensions, evaporator shape, condenser design, temperature range, etc. Table 1.1 demonstrate the different types of LHP grouped by different criterion [19]

Table 1.1: Classification of LHPs [19]

Classification of LHPs			
LHP design	LHP dimensions	Evaporator shape	Evaporator design
<ul style="list-style-type: none"> • Conventional (diode) • Reversible • Flexible • Ramified 	<ul style="list-style-type: none"> • Miniature • All the rest 	<ul style="list-style-type: none"> • Cylindrical • Flat disk-shaped • Flat rectangular 	<ul style="list-style-type: none"> • One butt-end compensation chamber • Two butt-end compensation chambers • Coaxial
Condenser design	Number of evaporators and condensers	Temperature range	Operating-temperature control
<ul style="list-style-type: none"> • Pipe-in-pipe • Flat coil • Collector 	<ul style="list-style-type: none"> • One • Two and more 	<ul style="list-style-type: none"> • Cryogenic • Low-temperature • High-temperature 	<ul style="list-style-type: none"> • Without active control • With active control

1.2.2 LHP theory

Figure 1.11 demonstrate the analytical LHP scheme and diagram of working cycle respectively.

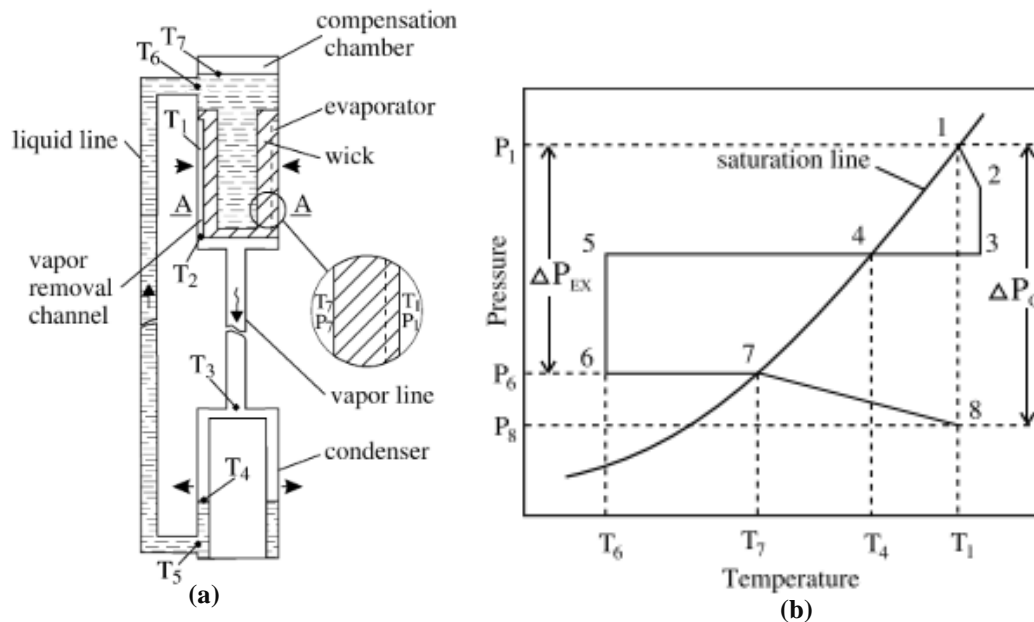


Figure 1.11: a) Analytical LHP scheme b) Diagram of the LHP working cycle [19]

The operation principle of the LHP also has some similar points with the conventional HP that are basing upon the phase changing process and utilizing the capillary force as the working motivation.

It is assumed that, before heating the liquid exists at the level A-A. When heat is applied to the evaporator, the liquid evaporates from the wick both in the evaporator zone (1) and the compensation chamber. The vapor generated in the evaporator zone flows and contacts with the heating wall, so the vapor pressure reduces while temperature raises up little (2) and higher than vapor in the compensation chamber. In this case the wick takes the role of thermal barrier. In addition, the superheated vapor in the evaporator zone cannot penetrate the compensation chamber through the saturated wick owing to the capillary force that keep the liquid inside. Here the wick plays as the hydraulic locks. The vapor continues to flow to the inlet of condenser (3). Both of temperature and pressure decrease when vapor flow from (2) to (3). The progress from (3) to (5) includes the de-superheat, condensation and subcooled progress. It is assumed that there is no pressure loss from (3) to (5). The pressure difference ΔP_{56} could include the pressure loss due to the hydrostatic resistance and the pressure loss caused by friction. Then, liquid at the stage (6) flow into the compensation chamber. At the same time, here comes part of the heat flow supplied to the evaporator, at the expense of which the working fluid is heated

to the temperature T_7 . The progress (7)–(8) corresponds to the liquid filtration through the wick into the evaporation zone. On this way the liquid may prove to be superheated, but its boiling-up does not take place owing to the short duration of its being in such a state. The point (8) determines the state of the working fluid in the vicinity of the evaporating menisci, and the pressure drop dP_{1-8} corresponds to the value of total pressure losses in all the sections of the working-fluid circulation.

From the above analysis, there are three condition for an LHP to function. The first one is the capillary condition. It is also the condition for conventional HP to operate.

$$\Delta P_c \geq \Delta P_v + \Delta P_l + \Delta P_g \quad (1.3)$$

ΔP_v pressure loss of working fluid during the motion of vapor state

ΔP_l pressure loss of working fluid during the motion of liquid state

ΔP_g pressure loss caused by the hydrostatic of the liquid column

ΔP_c capillary pressure created by the wick

The second condition is only for the LHP. This condition ensures the liquid to be displayed from the evaporator to the compensation chamber at the startup

$$\left. \frac{\partial P}{\partial T} \right|_{T_v} \Delta T_{1-7} = \Delta P_{EX} \quad (1.4)$$

Where:

$\left. \frac{\partial P}{\partial T} \right|_{T_v}$ is the derivative determined by the slope of the saturation line with T_v is the average temperature between T_1 and T_7

ΔP_{EX} is the sum of pressure losses in all the sections of circulation of the working fluid except the wick

The third condition is for preventing the liquid boiling in the liquid line due to the pressure loss and heating by the ambient.

$$\left. \frac{\partial P}{\partial T} \right|_{T_v} \Delta T_{4-5} = \Delta P_{5-6} \quad (1.5)$$

Where:

$\left. \frac{\partial P}{\partial T} \right|_{T_v}$ is the derivative determined by the slope of the saturation line with T_v is the average temperature between T_4 and T_5

ΔP_{5-6} is the sum of pressure loss from the state (5) to state (6)

From the second condition, the working fluid should have the high value of dP/dT to minimum the temperature difference ΔT_{1-7} and ΔT_{4-6} as small as possible.

1.2.3 Loop heat pipe for electronics cooling

Because of owning the outstanding advantages, LHP quickly became the common cooling method applied in space technology. The first flight experiment in condition of microgravitational condition was carried out in the 1989 aboard the Russian spacecraft. The first actual application of LHPs took place in 1994 aboard. After that, the application of LHP in the thermal management system became more popular not only in Russian spacecraft such as Chinese meteorological FY-IC, American satellites Hughes-702, Nasa Aura satellites (2004) or American spacecraft ICESar (2003), GOES N-Q (2006)

However, nowadays the dramatically development of the electronics, especially the device functioning in the DC like processors, offers the serious challenges to the traditional cooling. These challenges relate to the cooling capacity and the heat power or heat flux generated from the devices as well as efficient energy consumption of the DC. With the advantages mentioned above, the LHP has been considered as one of potential solution for the modern electronics cooling in future. However, the processor has the flat surface, it is better to use the LHP with the flat evaporator to improve the contact and avoid using the “saddle” or the cylinder-plane between the LHP and devices [21]. Therefore, the study of LHP with flat evaporator has become the noticeable topic that has been paying attention from many research groups all over the world.

Basing on the geometry of the evaporator, the LHP with flat evaporator could be divided into three groups such as flat disk-shaped evaporator, flat rectangular-shaped evaporator, evaporators with longitudinal replenishment.

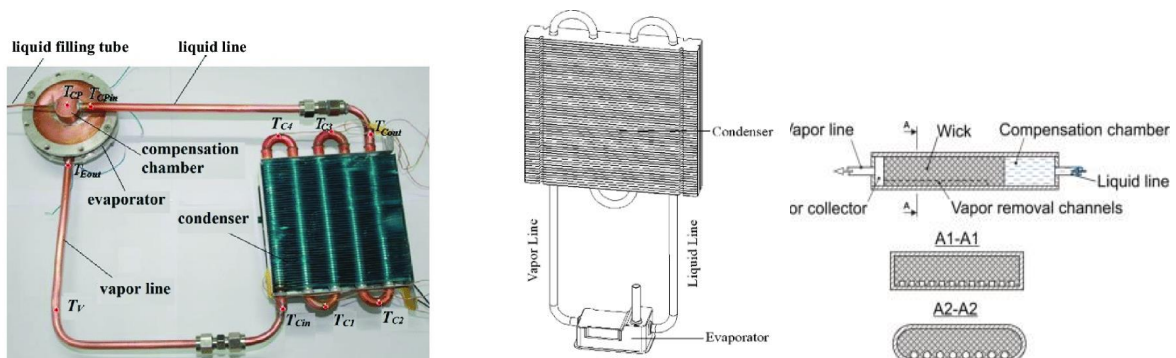


Figure 1.12: a) Disk-shaped evaporator; b) Rectangular evaporator; c) Evaporator with longitudinal replenishment

Firstly, Yu. F. Maidanik et al [22] conducted the test of LHP with flat disk-shaped evaporators and water working inside. However, the wall temperature belonged the range from 103°C to 147°C when heat load changed from 150 W to 400 W. The LHP operated at high temperature could be caused by the low value of dP/dT of water. In the ref [23], the LHP with stainless-steel disk-shaped evaporator and stainless-steel wick was investigated. Water was also selected as working fluid in this study. However, when operating at 75 W, the wall temperature reach 145°C while the vapor temperature was around 130°C. From 2009 to 2011, R. Singh et al [24]–[26] carried out the experiment on LHP with disk-shaped evaporator with different type of wick material such as Nickel, copper mono-porous and copper bi-porous. Water was also working fluid in these experiments. The results indicate that bi-porous copper wick had the highest heat transfer coefficient and lowest evaporator resistance. However, the vapor temperature reached 93°C when heat load was 80 W. From the above result, almost the LHP with flat-disk shaped evaporator could not operate at high heat load and maintain the temperature below 85°C.

Although these above LHP did not show the effective performance, it seems that water is the common working fluid that was selected by various study. The low working pressure of water that make it become suitable for this design of evaporator to avoid the deformation.

However, there were other groups selecting ammonia as working fluid. In the studies [27], [28], the LHP with 30-mm diameter, 1-mm thickness disk-shaped evaporator was tested. The results have shown that its thermal resistance may be at level of 0.15°C/W and the temperature of its wall no higher than 60°C. The ammonia LHP with disk-shaped evaporator in the Ref [29],[30] could operate at the heat load of 130 W with evaporator thermal resistance of 0.19 K/W when cooled by the heat sink at 0°C. The evaporator and vapor temperature were 58°C and 32°C respectively. Despite of better results could be obtained from the experiment of LHP with flat disk-shaped with working fluid ammonia, their practical application will evidently be restricted by space technology and other specific filed only because of toxic and ecological problem.

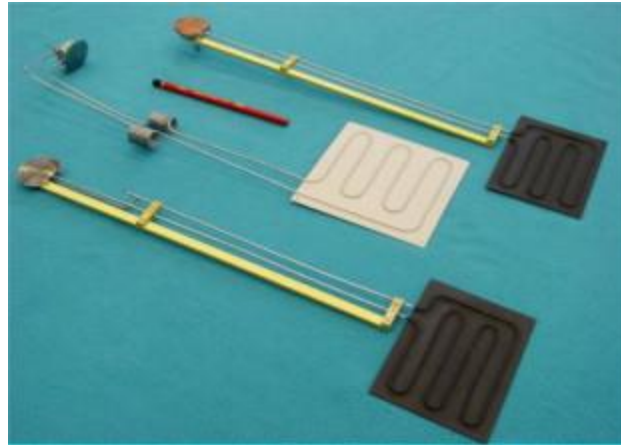


Figure 1.13: External view of ammonia LHPs with disk-shaped evaporator [27], [28]

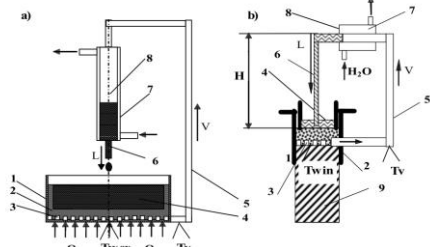
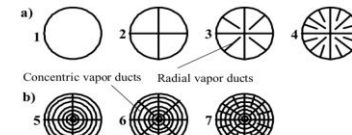
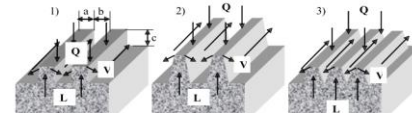
Beside water and ammonia, there are some working fluid that is less toxic than ammonia but has the lower freezing point than water such as ethanol and acetone. In Ref [31], the experiment of LHP with the disk-shaped evaporator 44 mm in diameter and 22 mm in thickness equipped with different wick material such as stainless-steel, nickel and titanium was conducted. Ethanol was working fluid of the LHP. The maximum heat load achieved at 120 W with thermal resistance of 0.62 K/W. In the Ref [32], another LHP with stainless steel disk-shaped evaporator 27 mm in diameter equipped with nickel wick could operate at 70 W while the vapor temperature reach 100°C. In the study conducted by H. Li et al [33], the LHP with disk-shaped evaporator equipped with bi-porous nickel wick and working fluid was methanol. With the condenser cooling temperature of 5°C, the evaporator and vapor temperature were at 70°C and 50°C respectively when heat load was adjusted at 100 W.

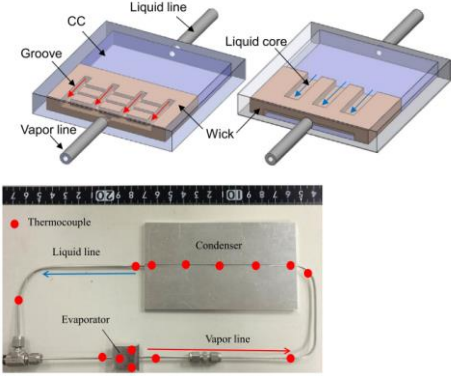
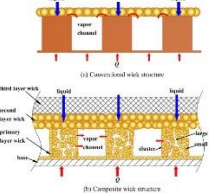
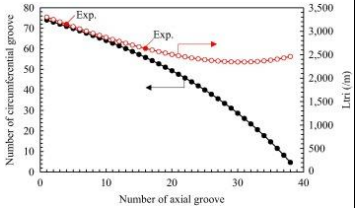
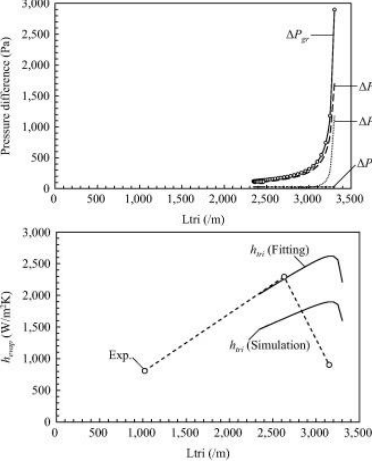
The rectangular – shaped evaporator with opposite replenishment demonstrated almost the same thermal performance with the disk-shaped evaporator group. With the experiment in Ref [34], the rectangular evaporator was tested with polypropylenes and working fluids were methanol, ethanol, acetone. This LHP could operate at heat load of 80 W and vapor temperature at 60°C when methanol was working fluid. In the study of Z. Lui et al [35], the LHP with rectangular evaporator was examined at different slopes while evaporator was below condenser. It was noticed that the acetone LHP could startup faster while the methanol could operate at higher heat power (120W). In the Ref [36], the LHP with evaporator dimension 30 mm x 30 mm x 15 mm was fabricated and tested under gravity assisted condition. The LHP could operate in the range of heat load from 10 to 600 W while evaporator temperature varied from 55 to 120°C.

One of the disadvantages of evaporator with opposite replenishment is the thickness depends on the size of compensation chamber. Therefore, some research group tried with the LHP with the longitudinal replenishment evaporator to reduce the thickness of evaporator. It was also stated that this design of evaporator could reduce the heat leak from the evaporation zone to the compensation chamber. In the study belonging to European project COSEE [37], the copper wick-water LHPs were developed and tested at different orientation from -90° to $+90^\circ$ and heat load from 20 to 100 W. The evaporator temperature did not over 90°C although temperatures of ambient and cooling medium were at 55°C . Yu. Maydanik et al [38] tried with this kind of evaporator using copper sintered wick and water as working fluid. Evaporator has the dimension $80 \times 42 \times 7$ mm. Their LHP could operate in the range of heat load from 5 to 900 W. The experiment was also conducted with different areas of the heater. With the 9 cm^2 heater, the evaporator temperature reach 100°C when heat load at 650 W. The experiment in Ref [39] has shown that the heat load of the LHP in previous study could be increased to 1200 W while evaporator temperature was at 110.4°C when the diameter of vapor line increased from ID 3.4mm to ID 5.4mm.

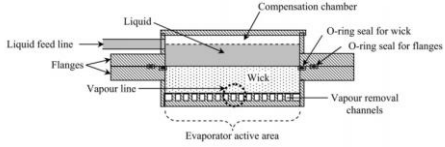
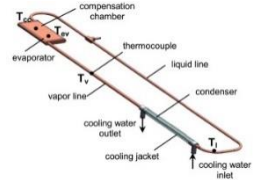
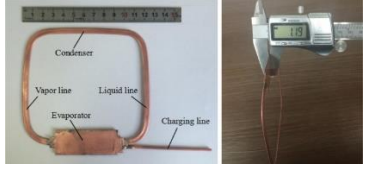
The following table summarizes the other studies that focus various designs of LHP's evaporator and different types of LHP such as miniature LHP, micro LHP, evaporator with longitudinal replenishment (ELR) LHP, LHP with parallel condensers.

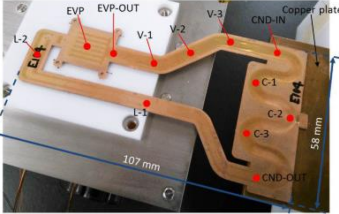

Table 1.2: Some previous studies on LHP

No	Reference	Loop heat pipe specifications	Objects and results
1	V.M. Kiseev - 2003 [40] <i>LHP, Steady-state behavior, HTC, capillary structure, flat evaporator</i>	LHP operating due to gravity Flat – disk shape evaporator Metal wick: (1) Titanium (55%, 3.8 μm; 33.9·10 ⁻¹⁴ m ² , 1.29 W/m·K) (2) Titanium (50%, 3.6 μm; 28.3·10 ⁻¹⁴ m ² , 1.77 W/m·K) (3) Nickel (65%, 0.65 μm; 2.2·10 ⁻¹⁴ m ² , 8.04 W/m·K) (4) Nickel chip of porous Ni (53%, 1.4 μm; 2.2·10 ⁻¹⁴ m ² , 9.16 W/m·K)	<p>Objects: Present some configurations of MLHP with flat plates of evaporators. The evaporator HTC was investigated by different configurations of the vapor ducts, working fluids (water and acetone) and capillary structures (Ni, Ti, thickness)</p>  <p>Fig. 1. Open LHP systems: 1 – LHP evaporator; 2 – capillary structure (wick); 3 – vapor ducts (grooves); 4 – compensation chamber (cavity); 5 – vapor line; 6 – liquid line; 7 – condenser; 8 – water cooler; 9 – copper heater; Tw ex, Tw in, Tv – thermocouples</p>  <p>Fig. 2. Configurations of vapor ducts (1 – 7): a) – only radial vapor ducts; b) – radial and concentric vapor ducts</p>  <p>Fig. 3. Geometry of concentric vapor ducts: 1 – rectangular vapor ducts; 2 – trapezoid vapor ducts; 3 – triangular vapor ducts</p> <p>Results: Optimal thickness is about 5 to 7mm with the Ni–No.3 & Ti–No.1, (Open LHP) With the Ni–No.3 and working fluid is acetone, $\xi = S_{vd}/S_{inp}$ should be around 0.4 to 0.5. The decreasing the sizes and distance between the concentric vapor ducts goes to intensification of heat transfer and the increase of HTC. The placement of concentric vapor grooves on an internal surface of the wall increase the heat HTC more than 10 – 30%.</p>
2	K. Fukushima - 2017[41] <i>Capillary force Heat transport LHP Porous PTFE</i>	Flat – rectangular evaporator New flat evaporator structure, micro LHP (Evaporator 20 x 10 x 3mm, 200mm in length transport line, Porous polytetrafluoroethylene wick 17 x 9 x 2 mm (PTFE) (50%, 2.2 μm, 6.48·10 ⁻¹⁴ , 0.25 W/m·K) Working fluid:	<p>Objects: Propose the wick with the liquid core Experimental and computational investigation was conducted Obtained the temperature distribution inside the evaporator and breakdown of heat load from the mathematical model.</p> <p>Results: From experiment, minimum R_{LHP} is 1.2 K/W and maximum $Q = 11$ W</p>

			
3	<p>Xianbing Ji - 2017 [42] <i>Multiscale, LHP, Composite porous wick, synergy</i></p>	<p>LHP with composite multiscale porous wick. Flat-disk shape evaporator Tilt angles: -90°, 0°, $+90^\circ$ CR = 38.5%, 51.3%; 64.1% Working fluid: water Evaporator: $\phi 80 \times 10$ (without CC thickness); $A_{\text{heating}} = 5\text{cm}^2$; 25cm^2 Vapor line: ID6/OD8 x 550mm; 650 mm; 750 mm Liquid line: ID6/OD8 x 300mm; 400 mm; 500 mm Condenser: 130 x 130 x 25; air cooling</p>	<p>Objects: Propose the composite multiscale porous wick to solve two problems” - To balance between vapor release and liquid flow resistances with capillary capacity. - High thermal conductivity for boiling HTC and small thermal conductivity to reduces heat leak to CC.</p>  <p>Wick includes 3 layers: - Primary layer was sintered from copper powder with different size (13, 37, 88, 149μm) - Second layer sintered from 149μm ($\delta = 2\text{mm}$) - Third layer was made of absorbent wool ($\delta = 2\text{mm}$)</p> <p>Changing the primary layer geometry. Results: This LHP can operate at the q of 40 W/cm^2 ($A_{\text{heating}} = 5 \text{ cm}^2$), T_c around 63°C.</p>
4	<p>M. Nishikawara - 2017 [43] <i>Capillary evaporator, capillary pumped loop, evaporator HTC, LHP, Optimized wick shape, 3-phase contact line</i></p>	<p>The wick material was PTFE wick bulk thermal conductivity is $0.25 \text{ W/m}\cdot\text{K}$. Case is stainless steel ($k = 16 \text{ W/m}\cdot\text{K}$) Minimum machined widths: 0.3mm (circumferential groove) & 0.4mm (axial groove)</p>  <p>Increasing axial groove will reduce number of circumferential grooves. For experimental examination, there are three wicks fabricated $L_{\text{tri}} = 3150/\text{m}$ (4 axial x 71 circumferential) $L_{\text{tri}} = 2630/\text{m}$ (16 axial x 56 circumferential) Classical wick with only 16 axial grooves and 1mm width of the groove</p>	<p>Objects: Optimize wick shape via calculation and experiment. The evaporator is maximized using only the length of a three-phase contact line (TPCL). $q = 2 \text{ W/cm}^2$ Effect of case and wick material as well as working fluid Results Effect of the TPCL on the groove pressure loss (by calculation) Comparison between evaporator HTC obtained using Eq.9 and that obtained through the experiments (ethanol)</p>  <p>Contribution of heat transport at TPCL was estimated at 0.87 when fitting to experiment results and 0.63 in the case of simulation Comparison of different working fluids and wick material, h_{tri} increased with wick's thermal conductivity. Value of h_{tri} was clearly higher for ammonia because of changes in interfacial HTC.</p>

5	<p>Jinliang Xu - 2014 [44] <i>Lhp, evaporator, heat transfer, modulated porous wick</i></p>	<p>LHP with flat-disk shape evaporator. Tilt angles: -90°, -60°, -30°, 0°, 90° (“-”: anti-gravity) Forced convective air cooling ($T_a = 22$ to 24°C) Working fluid: water Porous material includes 3 layers such as primary layer (in table), secondary copper table (2 mm - $149\mu\text{m}$) and third absorbent wool layer (2 mm - $r_{\text{pore}} = 20\mu\text{m}$) Evaporator: $\phi 80 \times 10$ (without CC thickness); $A_{\text{heating}} = 5\text{cm}^2$ Vapor line: ID6/OD8 x 550mm Liquid line: ID6/OD8 x 300mm Condenser: 130 x 130 x 25 CR = 38.5%, 51.3%; 64.1%, 64.1%, 76.9% Sintering process: oven temperature 900°C during 4h</p>	<p>Objects: to enhance pool boiling heat transfer by the modulated porous wick sintered on the heater wall. Three types of evaporator: MWE (microchannel/wick evaporator), MME (modulated monoporous wick evaporator), MBE (modulated biporous wick evaporator).</p> <p>The structure adjacent to the evaporator wall.</p> <table border="1"> <thead> <tr> <th>Run</th> <th>Schematic drawing of the structure adjacent to the evaporator wall</th> <th>Structure parameter (mm)</th> <th>Evaporator type and particle size (μm)</th> </tr> </thead> <tbody> <tr> <td>1</td> <td></td> <td>$h = 1.5, p = 1.5, w = 3.0$</td> <td>MWE, the porous wick is above microchannels</td> </tr> <tr> <td>2</td> <td></td> <td>$h = 1.5, p = 1.0, w = 3.0$</td> <td>MBE: 88 (78-92)</td> </tr> <tr> <td>3</td> <td></td> <td>$h = 1.5, p = 1.5, w = 2.0$</td> <td>MBE: 88 (78-92)</td> </tr> <tr> <td>4</td> <td></td> <td>$h = 1.5, p = 1.5, w = 3.0$</td> <td>MBE: 13 (10-14) MBE: 37 (25-42) MBE: 88 (78-92) MME: 149 (75-154)</td> </tr> <tr> <td>5</td> <td></td> <td>$h = 1.5, p = 1.5, w = 4.0$</td> <td>MBE: 88 (78-92)</td> </tr> <tr> <td>6</td> <td></td> <td>$h = 1.5, p = 2.0, w = 3.0$</td> <td>MBE: 78 (92)</td> </tr> <tr> <td>7</td> <td></td> <td>$h = 2.0, p = 2.0, w = 3.0$</td> <td>MBE: 88 (78-92)</td> </tr> </tbody> </table> <p>Results: MBE LHP shortens the startup and obtains the stable operation than MWE. MBE LHP can operate with heat flux at 40 W/cm^2 (heater heat flux) while T_c is around 63°C; ($R_t = 0.12\text{ K/W}$) Optimum CR = 51.3%; Operation anti-gravity condition is better than other with the properly design of MBE LHP Best geometric parameter of fin $h = 1.5\text{ mm}$; $p = 1.5\text{ mm}$; $w = 3\text{ mm}$ & best particle size: $88\mu\text{m}$</p>	Run	Schematic drawing of the structure adjacent to the evaporator wall	Structure parameter (mm)	Evaporator type and particle size (μm)	1		$h = 1.5, p = 1.5, w = 3.0$	MWE, the porous wick is above microchannels	2		$h = 1.5, p = 1.0, w = 3.0$	MBE: 88 (78-92)	3		$h = 1.5, p = 1.5, w = 2.0$	MBE: 88 (78-92)	4		$h = 1.5, p = 1.5, w = 3.0$	MBE: 13 (10-14) MBE: 37 (25-42) MBE: 88 (78-92) MME: 149 (75-154)	5		$h = 1.5, p = 1.5, w = 4.0$	MBE: 88 (78-92)	6		$h = 1.5, p = 2.0, w = 3.0$	MBE: 78 (92)	7		$h = 2.0, p = 2.0, w = 3.0$	MBE: 88 (78-92)
Run	Schematic drawing of the structure adjacent to the evaporator wall	Structure parameter (mm)	Evaporator type and particle size (μm)																																
1		$h = 1.5, p = 1.5, w = 3.0$	MWE, the porous wick is above microchannels																																
2		$h = 1.5, p = 1.0, w = 3.0$	MBE: 88 (78-92)																																
3		$h = 1.5, p = 1.5, w = 2.0$	MBE: 88 (78-92)																																
4		$h = 1.5, p = 1.5, w = 3.0$	MBE: 13 (10-14) MBE: 37 (25-42) MBE: 88 (78-92) MME: 149 (75-154)																																
5		$h = 1.5, p = 1.5, w = 4.0$	MBE: 88 (78-92)																																
6		$h = 1.5, p = 2.0, w = 3.0$	MBE: 78 (92)																																
7		$h = 2.0, p = 2.0, w = 3.0$	MBE: 88 (78-92)																																
6	<p>S.C. Wu - 2014 [45] <i>Wick structure, lhp, evaporator area, grooves</i></p>	<p>LHP with cylindrical stainless-steel evaporator ($\phi 16 \times 65$), water cooling Wick: nickel (ID/OD = $9/12.5$); largest $r_{\text{pore}} = 1.9 - 2.5\mu\text{m}$; $K = 1.3 - 3.25 \times 10^{-13}\text{ m}^2$, porosity: 63% - 67% Vapor line: ID5/OD6 x 470 Liquid line: ID4.5/OD6 x 585 Condenser: ID5/OD6.4 x 800 Working fluid: ammonia</p>	<p>Objects: fabricating and investigating the effects of increasing the number of grooves on a wick’s surface on the LHP’s performance.</p> <table border="1"> <tbody> <tr> <td>(a) A_9</td> <td>(b) A_8</td> <td>(c) A_{10}</td> </tr> <tr> <td></td> <td></td> <td></td> </tr> <tr> <td></td> <td></td> <td>$A_{310} = 25\%$</td> </tr> <tr> <td>(d) A_{12}</td> <td>(e) A_{14}</td> <td>(f) A_{16}</td> </tr> <tr> <td></td> <td></td> <td></td> </tr> <tr> <td>$A_{312} = 50\%$</td> <td>$A_{314} = 75\%$</td> <td>$A_{316} = 100\%$</td> </tr> </tbody> </table> <p>Results: 16-groove wick was easily damage; other wicks almost have the same properties such as porosity, K, pore radius. Sintering condition: 45 min at 600°C Increase the groove number increases the LHP’s performance; $Q = 500\text{ W}$, $R_t = 0.14\text{ K/W}$ There is a optimal number of groove on wick surface.</p>	(a) A_9	(b) A_8	(c) A_{10}						$A_{310} = 25\%$	(d) A_{12}	(e) A_{14}	(f) A_{16}				$A_{312} = 50\%$	$A_{314} = 75\%$	$A_{316} = 100\%$														
(a) A_9	(b) A_8	(c) A_{10}																																	
		$A_{310} = 25\%$																																	
(d) A_{12}	(e) A_{14}	(f) A_{16}																																	
$A_{312} = 50\%$	$A_{314} = 75\%$	$A_{316} = 100\%$																																	
7	<p>Jeehoon Choi - 2013 [46] <i>Miniature LHP, evaporator, sintering, contact conductance, thermal resistance</i></p>	<p>LHP with flat-disk shape evaporator. Nickel wick ($\phi 42 \times 3$), particles size: $3\mu\text{m}$, $P_{\text{capillary}} = 401\text{ kPa}$, $K = 0.99 \cdot 10^{-11}\text{ m}^2$, porosity = 64%, $k_{\text{eff}} = 9\text{ W/K}\cdot\text{m}$ CC: stainless-steel ($\phi 46 \times 7$) Vapor line: ID4.95/OD6.35 x 250 (copper) Liquid line: ID4.95/OD6.35 x 300 (stainless-steel) Forced convective air cooling Working fluid: water Horizontal orientation Heater surface area: $30 \times 30\text{ mm}^2$</p>	<p>Objects: explore a low-cost sintering method for fabricating the LHP’s evaporator. In this, the porous wick partially fills the vapor collection channel embedded in the evaporator’s base. There were two evaporators were fabricated</p> <table border="1"> <tbody> <tr> <td>(a)</td> <td>(b)</td> </tr> <tr> <td></td> <td></td> </tr> </tbody> </table> <p>The evaporator in Fig. b was fabricated with sintering procedure mentioned in section 2.2 of this paper.</p> <p>Results: Startup of LHP with the 2nd evaporator is shorter and more stable than one with “traditional”. The temperature</p>	(a)	(b)																														
(a)	(b)																																		

			<p>on the CC reduced significantly (34°C) with the evaporator with interpenetrated wick. Traditional LHP: 30 – 165 W; 80 – 141°C; 1.81 – 0.71 K/W LHP with interpenetrated wick/base plate: 30 – 180 W; 47 – 102°C; 0.76 – 0.43 K/W The lower temperature of the CC was explained because of the design of 2nd evaporator could help the wick and evaporator base contact perfectly → reduce the heat leakage to CC via the wall of evaporator</p>
8	Randeep Singh – 2008 [47] <i>Lhp, heat transfer, thermal performance, miniature lhp, flat evaporator, thermal control</i>	<p>Miniature LHP with flat disk shape copper evaporator (φ30 x 10mm) Working fluid: water Nickel wick δ = 3mm, (r_{pore} = 3-5μm; porosity: 75%) Air forced cooling condenser (T_a = 22 ± 2°C) Vapor line: φ2 x 150mm (copper) Liquid line: φ2 x 290mm (copper) Heater surface area: 25 x 25 mm Condenser: φ2 x 50mm</p>	<p>Objects: addressing thermal characteristics of miniature LHP with flat-disk shaped evaporator for the thermal control of the compact electronic equipment.</p>  <p>Results: startup at different heat load. Q = 5 – 70 W, R_{mLHP} = 5.66 – 0.17K/W, temperature of evaporator wall was slower than 100°C Oscillating behavior existed when Q was between 10 and 20W; this oscillation is explained because of the fluctuation of heat leaks from evaporator to CC and subcooled liquid temperature.</p>
9	M.A. Chernysheva – 2014 [9] <i>LHP, supercomputer, cooling system, operating temperature, thermal resistance</i>	<p>LHP with flat-oval evaporator (longitudinal replenishment evaporator) 80 x 42 x 7 mm, A_{active} = 32 x 42mm² 12 Vapor grooves φ1.8 x 33 Copper wick (porosity 43%, r_{pore} = 27μm) Vapor line: (1) ID4/OD5 x 305mm, (2) ID3/OD4 x 305mm Liquid line: ID3/OD4 x 810mm Condenser: ID4/OD5 x 160mm</p>	<p>Objects: cooling system with a LHP for thermal control of supercomputer Two LHP with different vapor pipe ID 4mm and 3mm inch was fabricated Test was conducted with Q from 20 to 600 W while temperature of cooling water was changed from 20 to 80°C.</p>  <p>Results: operating temperature of LHPs varies only slightly with changes in the condenser cooling temperature in the range below 40°C (variable conductance mode) It is more advantageous to use water-copper LHPs at condenser cooling temperature above 50°C.</p>
10	Guohui Zhou – 2016 [48] <i>Miniature LHP, ultrathin, thermal resistance, mobile electronic</i>	<p>Miniature LHP with flat evaporator (δ=1.2mm), vapor line, liquid line and condenser line (δ=1mm) Evaporator: 60 x 23 x 1.2 mm A_{active}: 15 x 9 Primary wick (inside evaporator): sintered from 10 layers 500mesh copper wire mesh) 50 x 21 x 0.8 (porosity: 65.2%,) Secondary wick (in liquid line) sintered from 4 layers 150 mesh copper wire mesh (δ=0.43mm) Liquid line: 105mm, vapor line: 105 mm. Condenser: 125mm. Natural cooling Orientation: horizontal, anti and assisted gravity. Working fluid: water</p>	<p>Objects: mLHP for mobile electronics</p>  <p>Results: LHP could startup at 2 W with temperature of evaporator of 43.9°C Q = 11 W, R_{LHP} = 0.11 K/W No noticeably different performance with different orientations. This mLHP provides a promising thermal management solution for cooling mobile electronics such as tablet or smart phone.</p>

11	Takeshi Shioga – 2015 [49] <i>Micro LHP, thermal resistance, heat leak, operation orientation</i>	Micro LHP fabricated by chemical-etching and diffusion bonding process Evaporator 20 x 17 x 0.6 mm Vapor line 5.6 x (1)0.4 & (2) 1 x 75 mm Liquid line 4 x 0.4 x 120 mm Condenser 5.6 x (1)0.4 & (2) 1 x 75 mm Working fluid: water	<p>Objects: Micro LHP for mobile electronics devices Effect of vapor & condenser thickness on μLHP performance</p>  <p>Results: μLHP could not work with vapor line & condenser line thickness at 0.4 mm. $Q = 5 \text{ W}$, $R_{LHP} = 0.8 \text{ K/W}$, $T_{\text{evaporator}} = 50.5^\circ\text{C}$. $Q = 15 \text{ W}$, $R_{LHP} = 0.32 \text{ K/W}$ Heat leak was estimated around 11%. Slight dependence of LHP on its operating orientation</p>
12	Ji Li – 2013 [50]	Evaporator: 30 x 30 x 15 mm. Gravity assisted operation Connecting line: ID 5mm Copper wick (porosity 50%, $r_{\text{pore}} = 65\mu\text{m}$, $K = 6 \times 10^{-11}\text{m}^2$) $A_{\text{Heater}} = 25 \times 25 \text{ mm}^2$ Condenser size: 120 x 80 x 50 mm ³	<p>Objects: experimental study of copper-water LHP with dual parallel condensers, especially for high power LED illumination applications.</p>  <p>Results: At $Q = 300 \text{ W}$, $R = 0.4^\circ\text{C/W}$; with $T_{\text{air}} = 15^\circ\text{C}$, $Q = 0 - 100\text{W}$, $T_{\text{junction}} < 75^\circ\text{C}$. At low heat loads, un-predicable non-uniform performance of the condenser causes the unstable behavior of the LHP.</p>

1.3 MOTIVATION OF THIS STUDY

In this study, a new pattern of evaporator that has the crossing grooves or the array of fins on the inner surface was suggested. This suggestion can avoid machining the grooves on the wick surface that can damage or change the surface characteristics of the wick. Besides, it also guarantees the sufficient space for evaporation as well as paths for vapor flow out easily, so prevent vapor forming inside the wick. Various experiments were conducted in this research to find out the thermal performance of this evaporator, condenser as well as the LHP operating under different conditions including orientations, working fluids, cooling conditions. From the experimental results, the assumption above boiling and heat transfer process happen inside this type of evaporator was withdrawn. This assumption can be used as one of the factors to improve the design of LHP in future

REFERENCES

- [1] C. Nadjahi, H. Louahlia, and S. Lemasson, “Sustainable Computing : Informatics and Systems,” *Sustain. Comput. Informatics Syst.*, vol. 19, no. May, pp. 14–28, 2018.
- [2] A. Habibi and S. K. Halgamuge, “A Review on efficient thermal management of air- and liquid-cooled data centers : From chip to the cooling system,” *Appl. Energy*, vol. 205, no. May, pp. 1165–1188, 2017.
- [3] J. Dai, M. M. Ohadi, D. Das, and M. G. Pecht, *Optimum Cooling of Data Centers*. 2014.
- [4] J. Cho, T. Lim, and B. S. Kim, “Viability of datacenter cooling systems for energy efficiency in temperate or subtropical regions: Case study,” *Energy Build.*, vol. 55, pp. 189–197, 2012.
- [5] J. G. Koomey and D. Ph, “Growth in data center electricity use 2005 to 2010,” Oakland, CA, 2011.
- [6] E. Farnworth and J. C. Castilla-rubio, “SMART 2020 : Enabling the low carbon economy in the information age,” 2008.
- [7] M. Yin Zhang, Zhiyan Wei, “Free cooling technologies for data centers : energy saving mechanism and applications,” *Energy Procedia*, vol. 143, pp. 410–415, 2017.
- [8] IBM, “Made in IBM Labs: IBM Hot Water-Cooled Supercomputer Goes Live at ETH Zurich,” 2010. [Online]. Available: <https://www-03.ibm.com/press/us/en/pressrelease/32049.wss>. [Accessed: 08-Jan-2019].
- [9] M. A. Chernysheva, S. I. Yushakova, and Y. F. Maydanik, “Copper-water loop heat pipes for energy-efficient cooling systems of supercomputers,” *Energy*, vol. 69, pp. 534–542, 2014.
- [10] Wikipedia, “Aquasar,” 2018. [Online]. Available: <https://en.wikipedia.org/wiki/Aquasar>.
- [11] K. Ebrahimi, G. F. Jones, and A. S. Fleischer, “A review of data center cooling technology , operating conditions and the corresponding low-grade waste heat recovery opportunities,” *Renew. Sustain. Energy Rev.*, vol. 31, pp. 622–638, 2014.
- [12] Y. J. J. Rambo, “Modeling of data center airflow and heat transfer: state of the art and future trends,” *Distrib. Parallel Databases*, 21 (2007), pp. 193-225, vol. 21, no. 2–3, pp. 193–225, 2007.
- [13] J. B. Marcinichen, J. A. Olivier, and J. R. Thome, “On-chip two-phase cooling of datacenters: Cooling system and energy recovery evaluation,” *Appl. Therm. Eng.*, vol. 41, pp. 36–51, 2012.
- [14] N. Saye, “How to guides,” 2014. [Online]. Available: <https://blogs.mentor.com/roi/blog/2014/03/11/how-to-guides/>. [Accessed: 08-Jan-2019].
- [15] A. C. Kheirabadi and D. Groulx, “Cooling of server electronics: A design review of existing technology,” *Appl. Therm. Eng.*, vol. 105, pp. 622–638, 2016.

- [16] K. Zhang, Y. Zhang, J. Liu, and X. Niu, "Recent advancements on thermal management and evaluation for data centers," *Appl. Therm. Eng.*, vol. 142, no. June, pp. 215–231, 2018.
- [17] B. D. N. R. R. Schmidt, "High-end server low temperature cooling," *IBM J. RES. DEV.*, vol. 46, no. 6, pp. 739–751, 2002.
- [18] J. Q. M. Ohadi, "Thermal management of harsh-environment electronics," in *Twentieth Annual IEEE Semiconductor Thermal Measurement and Management Symposium*, 2004.
- [19] Y. F. Maydanik, "Loop heat pipes," vol. 25, pp. 635–657, 2005.
- [20] R. M. David Reay, Peter Kew, *Heat Pipe Theory, Design, and Applications*, Sixth Edit. 2014.
- [21] Y. F. Maydanik, M. A. Chernysheva, and V. G. Pastukhov, "Review: Loop heat pipes with flat evaporators," *Appl. Therm. Eng.*, vol. 67, no. 1–2, pp. 294–307, 2014.
- [22] K. A. G. Yu. F. Maidanik, Yu.G. Fershtater, S.V. Vershinin, V.G. Pastukhov, "Some results of loop heat pipes development, tests and application in engineering," in *Proceedings of the 5th International Heat Pipe Symposium*, 1996, pp. 406–412.
- [23] G. P. Celata, M. Cumo, and M. Furrer, "Experimental tests of a stainless steel loop heat pipe with flat evaporator," *Exp. Therm. Fluid Sci.*, vol. 34, no. 7, pp. 866–878, 2010.
- [24] R. Singh, A. Akbarzadeh, C. Dixon, and M. Mochizuki, "Theoretical modelling of miniature loop heat pipe," *Heat Mass Transf.*, vol. 46, no. 2, pp. 209–224, 2009.
- [25] R. Singh, A. Akbarzadeh, and M. Mochizuki, "Sintered porous heat sink for cooling of high-powered microprocessors for server applications," *Int. J. Heat Mass Transf.*, vol. 52, no. 9–10, pp. 2289–2299, 2009.
- [26] R. Singh, A. Akbarzadeh, and M. Mochizuki, "Effect of Wick Characteristics on the Thermal Performance of the Miniature Loop Heat Pipe," *J. Heat Transfer*, vol. 131, no. 8, p. 082601, 2009.
- [27] Y. F. M. M.A. Chernysheva, S.V. Vershinin, "Development and tests results of loop heat pipes with a flat evaporator," in *Proceedings of the 12th International Heat Pipe Conference, Moscow, Russia*, pp. 134–138.
- [28] Y. F. Maydanik, "Miniature loop heat pipes," in *Proceedings of the 13th International Heat Pipe Conference, Shanghai, China*, pp. 24–37.
- [29] B. B. Chen, W. Liu, Z. C. Liu, H. Li, and J. G. Yang, "Experimental investigation of loop heat pipe with flat evaporator using biporous wick," *Appl. Therm. Eng.*, vol. 42, pp. 34–40, 2012.
- [30] B. B. Chen, Z. C. Liu, W. Liu, J. G. Yang, H. Li, and D. D. Wang, "Operational characteristics of two biporous wicks used in loop heat pipe with flat evaporator," *Int. J. Heat Mass Transf.*, vol. 55, no. 7–8, pp. 2204–2207, 2012.
- [31] S. Z. A.A.M. Delil, V. Baturkin, Yu. Friedrichson, Yu. Khmelev, "Experimental

- results of heat transfer phenomena in a miniature loop heat pipe with a flat evaporator,” in *Proceedings of the 12th International Heat Pipe Conference, Moscow, Russia*, 2002, p. pp 126-133.
- [32] K. S. K. V.M. Kiseev, A.S. Nepomnyashy, N.L. Gruzdova, “Miniature loop heat pipes for CPU cooling,” in *Proceedings of the 7th International Heat Pipe Symposium, Jeju, Korea*, 2003, pp. 175–180.
- [33] H. Li, Z. C. Liu, B. Bin Chen, W. Liu, C. Li, and J. Yang, “Development of biporous wicks for flat-plate loop heat pipe,” *Exp. Therm. Fluid Sci.*, vol. 37, pp. 91–97, 2012.
- [34] J. H. Boo and W. B. Chung, “Experimental study on the thermal performance of a small-scale loop heat pipe with polypropylene wick-8,” *J. Mech. Sci. Technol.*, vol. 19, no. 4, pp. 1052–1061, 2005.
- [35] Z. Liu, D. Gai, H. Li, W. Liu, J. Yang, and M. Liu, “Investigation of impact of different working fluids on the operational characteristics of miniature LHP with flat evaporator,” *Appl. Therm. Eng.*, vol. 31, no. 16, pp. 3387–3392, 2011.
- [36] J. Li, D. Wang, and G. P. Peterson, “Experimental studies on a high performance compact loop heat pipe with a square flat evaporator,” *Appl. Therm. Eng.*, vol. 30, no. 6–7, pp. 741–752, 2010.
- [37] S. Becker, S. Vershinin, V. Sartre, E. Laurien, J. Bonjour, and Y. F. Maydanik, “Steady state operation of a copper e water LHP with a fl at-oval evaporator,” *Appl. Therm. Eng.*, vol. 31, no. 5, pp. 686–695, 2011.
- [38] S. Maydanik, Yu., Vershinin, “Development and investigation of copper–water loop heat pipes with high operating characteristics,” *Heat Pipe Sci. Technol.*, vol. 1, no. 2, pp. 151–162.
- [39] Y. Maydanik, S. Vershinin, M. Chernysheva, and S. Yushakova, “Investigation of a compact copper e water loop heap pipe with a fl at evaporator,” *Appl. Therm. Eng.*, vol. 31, no. 16, pp. 3533–3541, 2011.
- [40] V. M. Kiseev, A. S. Nepomnyashy, and N. L. Gruzdova, “Investigation of vapor generation into capillary structures of miniature loop heat pipes,” *V Minsk Int. Semin. “Heat Pipes, Heat Pumps, Refrig.*, pp. 201–207, 2003.
- [41] K. Fukushima and H. Nagano, “International Journal of Heat and Mass Transfer New evaporator structure for micro loop heat pipes,” *Int. J. Heat Mass Transf.*, vol. 106, pp. 1327–1334, 2017.
- [42] X. Ji, Y. Wang, J. Xu, and Y. Huang, “Experimental study of heat transfer and start-up of loop heat pipe with multiscale porous wicks,” *Appl. Therm. Eng.*, vol. 117, pp. 782–798, 2017.
- [43] M. Nishikawara and H. Nagano, “International Journal of Heat and Mass Transfer Optimization of wick shape in a loop heat pipe for high heat transfer,” *Int. J. Heat Mass Transf.*, vol. 104, pp. 1083–1089, 2017.
- [44] J. Xu, X. Ji, W. Yang, and Z. Zhao, “Modulated porous wick evaporator for loop heat pipes: Experiment,” *Int. J. Heat Mass Transf.*, vol. 72, pp. 163–176, 2014.

- [45] S. C. Wu, D. Wang, J. H. Gao, Z. Y. Huang, and Y. M. Chen, “Effect of the number of grooves on a wick’s surface on the heat transfer performance of loop heat pipe,” *Appl. Therm. Eng.*, vol. 71, no. 1, pp. 371–377, 2014.
- [46] J. Choi, B. Sung, C. Kim, and D. Borca-tasciuc, “Interface engineering to enhance thermal contact conductance of evaporators in miniature loop heat pipe systems,” *Appl. Therm. Eng.*, vol. 60, no. 1–2, pp. 371–378, 2013.
- [47] R. Singh, A. Akbarzadeh, and M. Mochizuki, “Operational characteristics of a miniature loop heat pipe with flat evaporator,” *Int. J. Therm. Sci.*, vol. 47, pp. 1504–1515, 2008.
- [48] G. Zhou, J. Li, and L. Lv, “An ultra-thin miniature loop heat pipe cooler for mobile electronics,” vol. 109, pp. 514–523, 2016.
- [49] T. Shioga and Y. Mizuno, “Micro loop heat pipe for mobile electronics applications,” *Annu. IEEE Semicond. Therm. Meas. Manag. Symp.*, vol. 2015–April, pp. 50–55, 2015.
- [50] J. Li, F. Lin, D. Wang, and W. Tian, “A loop-heat-pipe heat sink with parallel condensers for high-power integrated LED chips,” *Appl. Therm. Eng.*, vol. 56, no. 1–2, pp. 18–26, 2013.
- [51] E. Onogawa and H. Nagano, “Effect of Amount of Fluid Charge in Thermal Performance of Loop Heat Pipe,” *Therm. Sci. ...*, vol. 18, no. 1, 2010.
- [52] S. V. Vershinin and Y. F. Maydanik, “Investigation of pulsations of the operating temperature in a miniature loop heat pipe,” *Int. J. Heat Mass Transf.*, vol. 50, pp. 5232–5240, 2007.

Chapter 2

LOOP HEAT PIPE DESCRIPTION

This chapter presents the descriptions of different components belonging to the LHP such as two different patterns of the evaporator, capillary structures, condenser, connection lines as well as the vacuum and charging system. Both of two evaporators was fabricated by the Technical Support Division of Saga University. Besides, the specification of measuring instruments as well as other equipment are demonstrated in this chapter.

2.1 EVAPORATOR'S DESIGN

2.1.1 The first pattern of the evaporator

Due to the purpose of the LHP is cooling the electronics such as processors functioning in the DCs, the heat receiving surface of the LHP's evaporator should be the flat surface to improve the contact quality between the evaporator and the electronics, uniform the heat flux and temperature distribution on the active surfaces as well as eliminate the occur of mounting block at the evaporator. The evaporator investigated in this thesis belongs to the group named evaporator with opposite replenishment (EOA) in which liquid flows from the top to the bottom surface of the wick structure, as demonstrated in Fig 2.1(b). In the case of evaporator with longitudinal replenishment (ELR), Fig. 2.1(a), the liquid is supplied from the compensation chamber locating behind the wick structure or the liquid flows perpendicular to the heat flow rate. The evaporator with opposite replenishment has the simple structure, large liquid absorption surface; however, the evaporator can become thicker because the compensation chamber is above the capillary structure. Moreover, the heat leak from the evaporator to the compensation chamber through the wick will be more serious due to large cross section of the wick.

Figure 2.2 is the structure drawing of the first evaporator. The evaporator base and evaporator body belong to one cooper block. The evaporator has two parts which one is vapor collector and other is the space for the wick and compensation chamber. Separation between two parts is the copper plate that fixed by brazing method. In addition, there is a hole with 1mm diameter

and 22.5 mm in length was machined at the base of evaporator to install the thermocouples. The area of the top surface of the heating block and the bottom surface of evaporator have the same area which is 27 cm² (45mm x 60mm). This value was selected basing upon the specifications of some processors as shown in the table 2.1.

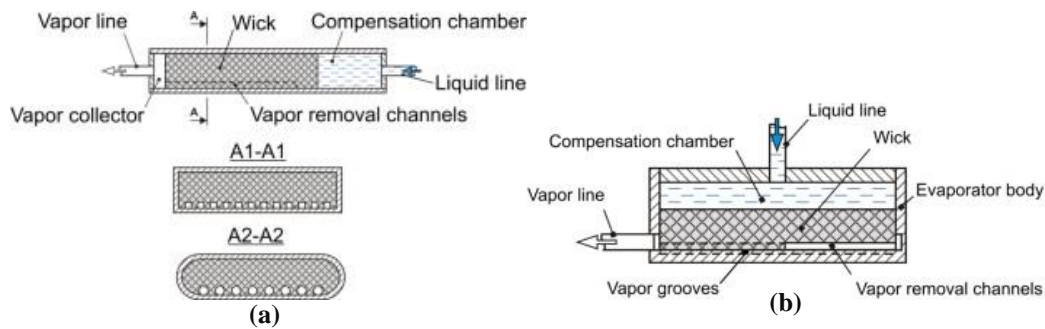


Figure 2.1: (a) LHP's evaporator with longitudinal replenishment (b) LHP's evaporator with opposite replenishment [1]

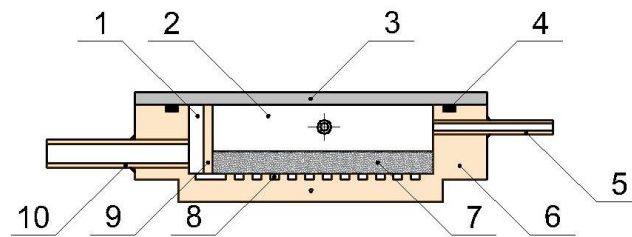


Figure 2.2: Structure drawing of the first pattern evaporator

1: vapor collector; 2: compensation chamber; 3: poly carbonate lid; 4: O-ring; 5: charging pipe; 6: copper evaporator body; 7: wick; 8: vapor grooves; 9: copper plate; 10: vapor pipe

Table 2.1: Specification of some processors

No	Modern	Thermal power design (W)	Case dimensions (mm x mm)	Heat flux (W/cm ²)
1	Core i7 5960X	140	52.5 x 45	5.9
2	Core i7 5930K	140	52.5 x 45	5.9
3	Core i7 4960X	130	52.5 x 45	5.48
4	Core i7 4930X	130	52.5 x 45	5.48
6	Core i7 3790X	150	52.5 x 45	6.3
7	Xeon E7 8891 v3	165	52 x 45	7.05
8	Xeon E7 8880 v3	150	52 x 45	6.41
9	Xeon E7 8890 v2	155	52 x 45	6.62
10	Itanium 9300	185/155/130	48.5 x 40.25	9.47/7.94/6.66
11	Itanium 9500	170/130	48.5 x 40.25	8.71/6.66

Figure 2.3 demonstrates the geometry of the inner surface of evaporator. Instead of machining the grooves on the wick surface, there is a crossing grooves system, or the array of fins fabricated on the inner wall of evaporator. This groove system provides paths for vapor to flow out evaporator easier and ensure space for boiling occurs. The groove also tolerates the liquid for the startup progress of the LHP. This design could help the cost of LHP fabrication lower due to avoiding mechanical processing on the capillary structure that can destroy or change the surface characteristics of the porous wick.

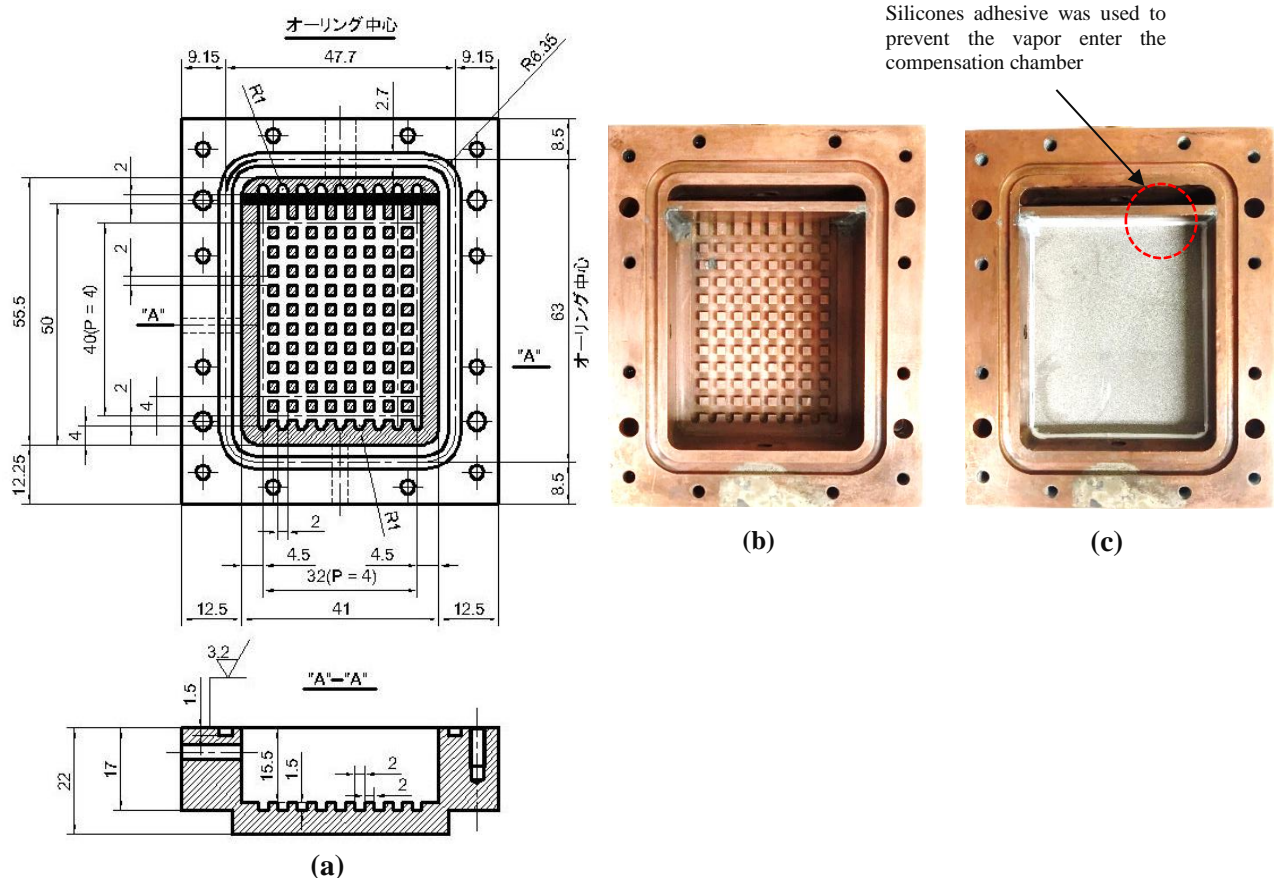


Figure 2.3: Geometry of the inner surface of the evaporator

a) Manufacturing drawing; b) The evaporator without wick; c) The evaporator with the stainless-steel wick

The LHP with this evaporator was investigated performance in the experiments introduced in the chapter 3, chapter 5 and chapter 6. The manufacture drawing of this evaporator is shown in appendix A-1

In all of experiment introduced in this thesis, the evaporator was fixed on the heating block by using the screws as shown in the Fig. 2.4. This design also improves the contact between the evaporator and the heating block.

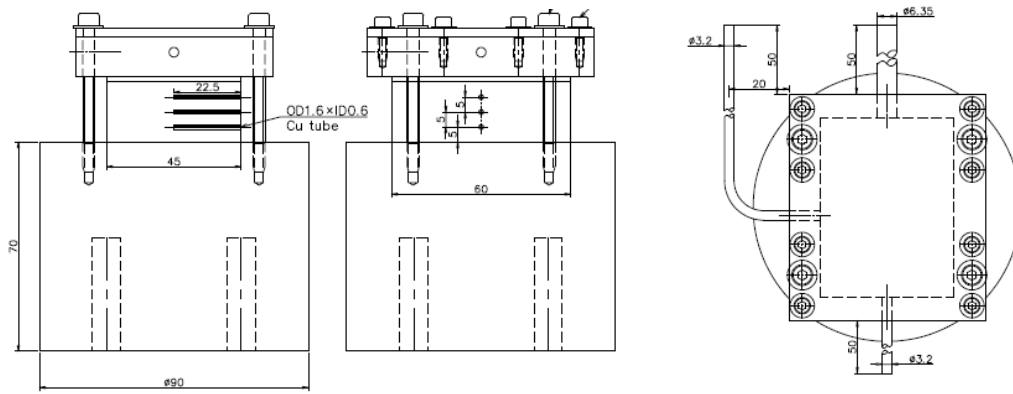


Figure 2.4: Method of fixing the evaporator on the heating block

2.1.2 The second pattern of the evaporator

Although the first pattern of evaporator could function successfully in the experiments with gravity-assisted condition and horizontal orientation. It still had some shortcomings that need to be eliminated such as

- Difficult in inserting or removing wick because of the tiny difference between the wick's dimension and the inner space of the evaporator.
- The contact between the wick and the fin cannot be ensured.
- Need to used silicone adhesive to prevent the vapor flow through the gaps between the wick and the evaporator wall as well as the connection between the vapor collector and compensation chamber. The using of silicone adhesive can limit the operation temperature of the LHP.
- Cannot try experiment with different vapor grooves or fin geometry.

Therefore, the new pattern of evaporator that can overcome the above shortcomings was designed and fabricated.

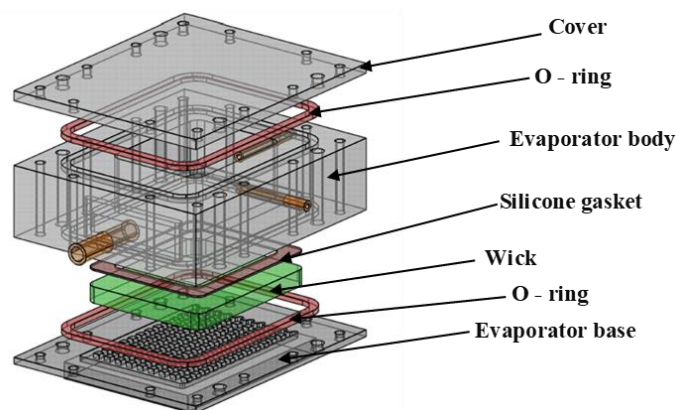


Figure 2.5: Outline of the second pattern of evaporator

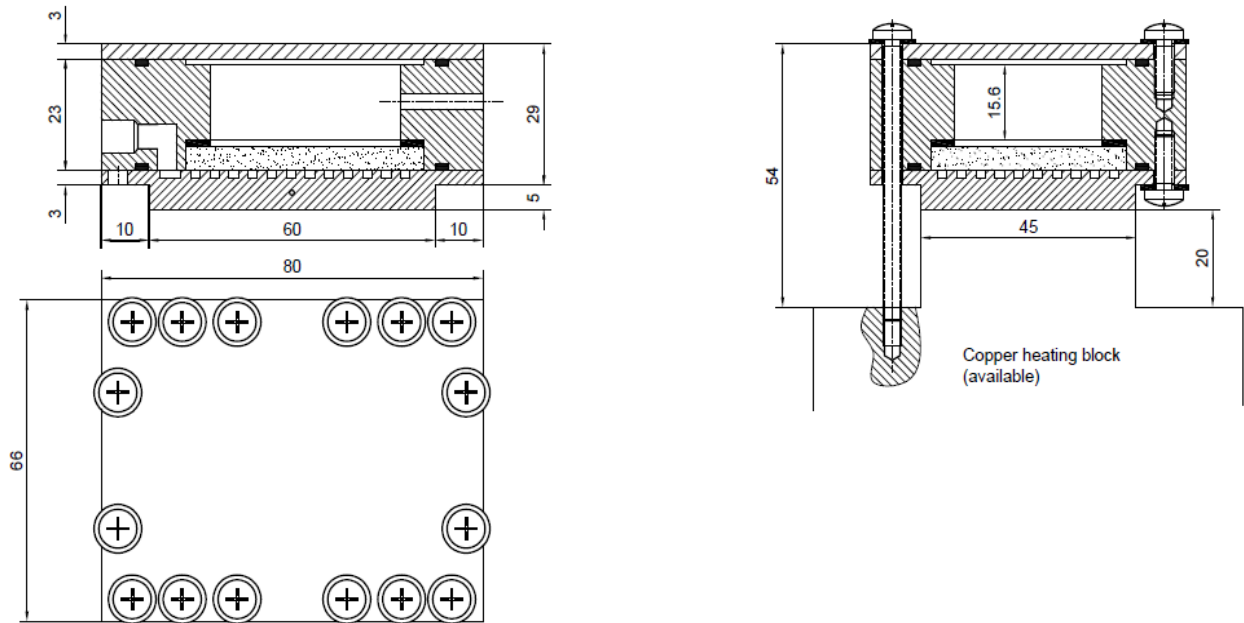


Figure 2.6: Assembly of the second pattern of evaporator

As displayed in Fig 2.5 and Fig 2.6, the second pattern of the evaporator includes three main parts that are the lid, body and evaporator base. The evaporator base is made from pure copper, the stainless steel is material of evaporator body and the lid is made from polycarbonate and stainless steel. The specifications of the fins or vapor grooves machined on surface of the evaporator base are like one of the first pattern (Fig 2.7). This pattern can prevent the vapor chamber connecting to the compensation chamber. With the compression capability of the silicone gasket, the contact between the wick and tip of the fins can be guaranteed while the vapor is also restrained to flow from vapor grooves to the compensation chamber through the gaps between surrounding area of the wick and inner wall of the evaporator. The new design also offers the advantage in changing the wick structure and the base of evaporator, so the experiments that find out the effect of wick characteristics and fin geometry in future can be conducted easier than the previous design.

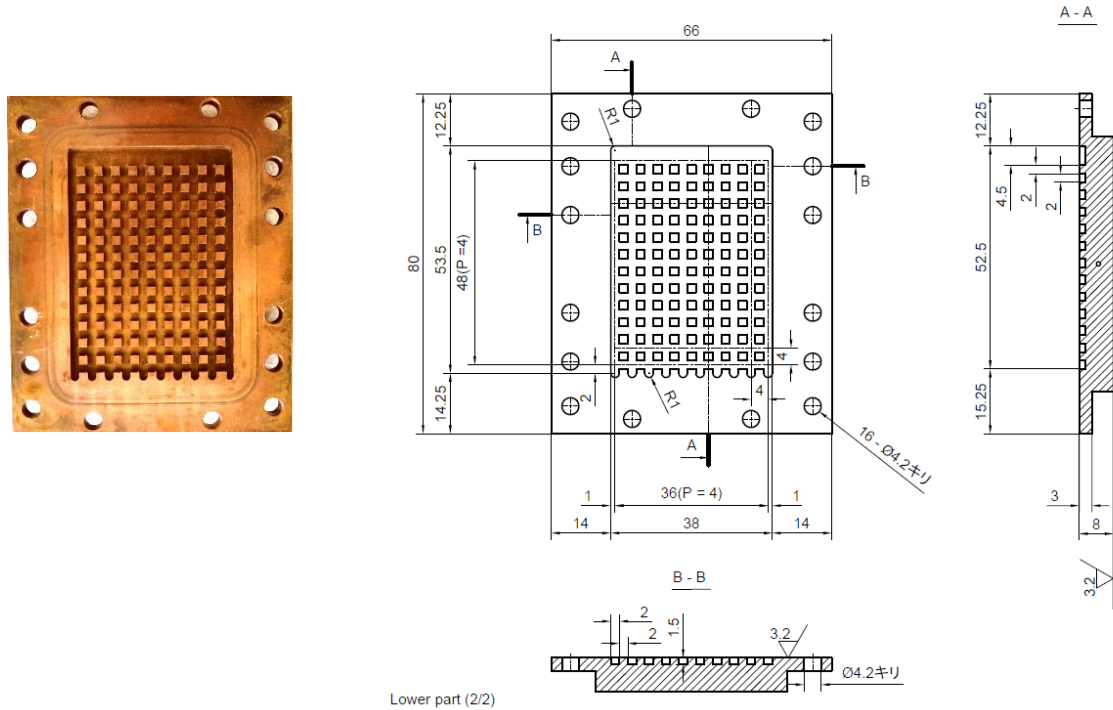


Figure 2.7: The fin and vapor grooves machined on the evaporator base

The manufacturing drawings are demonstrated in the appendix A-2. The experiment with this pattern is introduced in the chapter 4.

2.1.3 Sintered Wick Characteristics

The commercial stainless-steel sintered wick was selected as the capillary structure of the LHP. Stainless-steel was chosen because it has lower thermal conductivity ($k_{\text{bulb}} = 13.4 \text{ W/m}\cdot\text{K}$ at 300 K[2]) than copper so that the heat leak from the vapor groove to compensation chamber could be reduced.

Table 2.2: Specification of stainless-steel sintered wick [3]

Manufacture	SMC Corporation
Dimension (W x L x H), mm	41 x 50 x 5
Raw material	SUS316L equivalent
Sintering density, g/cm^3	4.2 to 5.2
Void ratio, %	36 to 48
Void ratio (Measuring), %	42.5
Permeability K , m^2	7.67×10^{-13}
Opening, μm	63
Sieve (mesh)	250

In the table 2.2, besides the void ratio obtained from the catalogue of manufacture, the experiment that measures the void ratio of the sintering wick was conducted. The measuring

methodology and results are introduced in the appendix B-1. In addition, the permeability of the wick was estimated based on the flow characteristic demonstrated in the appendix B-2.

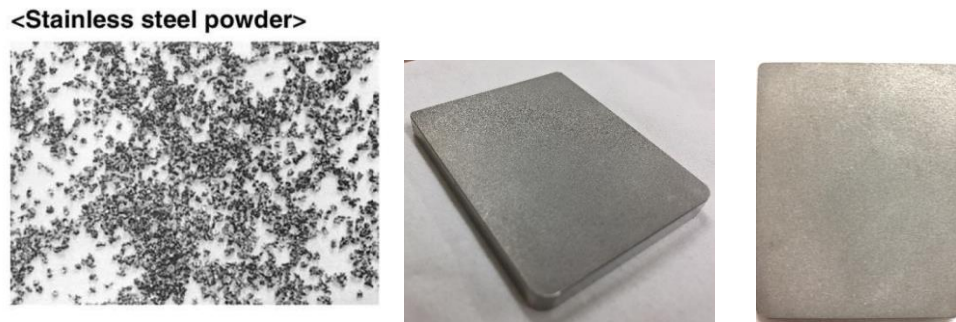


Figure 2.8: Stainless-steel powder [3], and the stainless-steel sintered wick used in the experiment

2.2 DESCRIPTION OF CONDENSERS

In this study, the double pipe counter flow heat exchanger was used as the condenser of the LHP. Cooling water flows in the annular area while the vapor condenses inside the copper tube. In the experiment with LHP operating at gravity – assisted condition (chapter 3 & chapter 4), the condenser is 600 mm in length while in the experiment of LHP with horizontal orientation, the 300 mm in length condenser is used (chapter 5 & chapter 6). The structure of condenser can be described in Fig 2.9 and table 2.3.

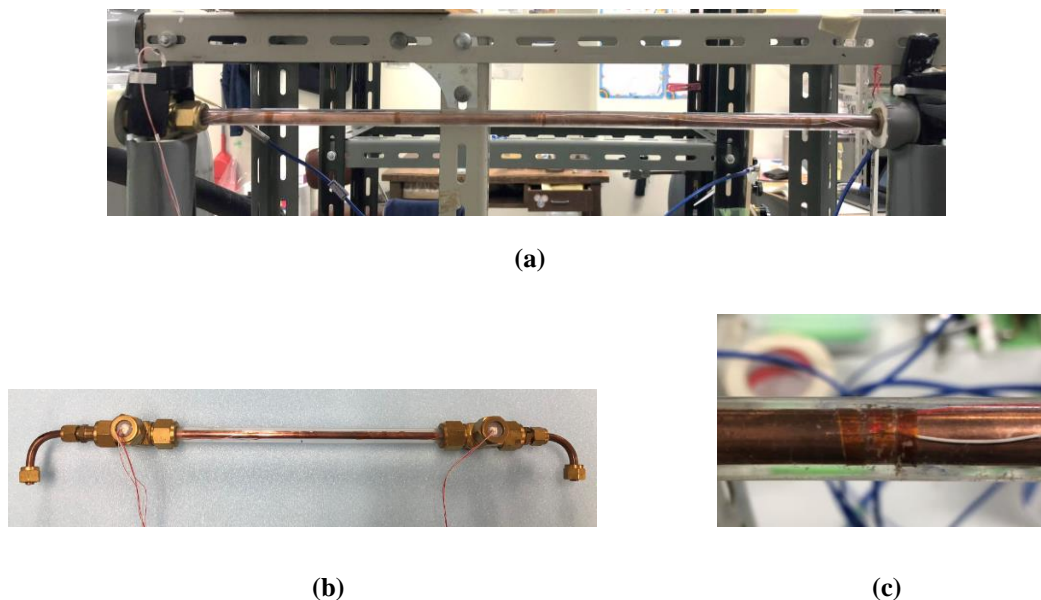


Figure 2.9: Description of condensers used in the experiments

- a) 600 mm condenser b) 300 mm condenser c) Fixing the T type thermocouples on the condenser outer surface

Table 2.3: Condenser's specification

	Inner tube	Outer tube
Material	Smooth Copper tube	Poly-carbonated resin
Length, mm	300 mm; 600 mm	300 mm; 600 mm
OD/ID, mm	6.35/4.35	13/9

Besides, the vapor pipe and liquid pipe of LHP is also copper smooth tube whose OD/ID are 6.35/4.35 mm and 3.2/1.5 mm respectively.

2.3 VACUUM AND CHARGING SYSTEM

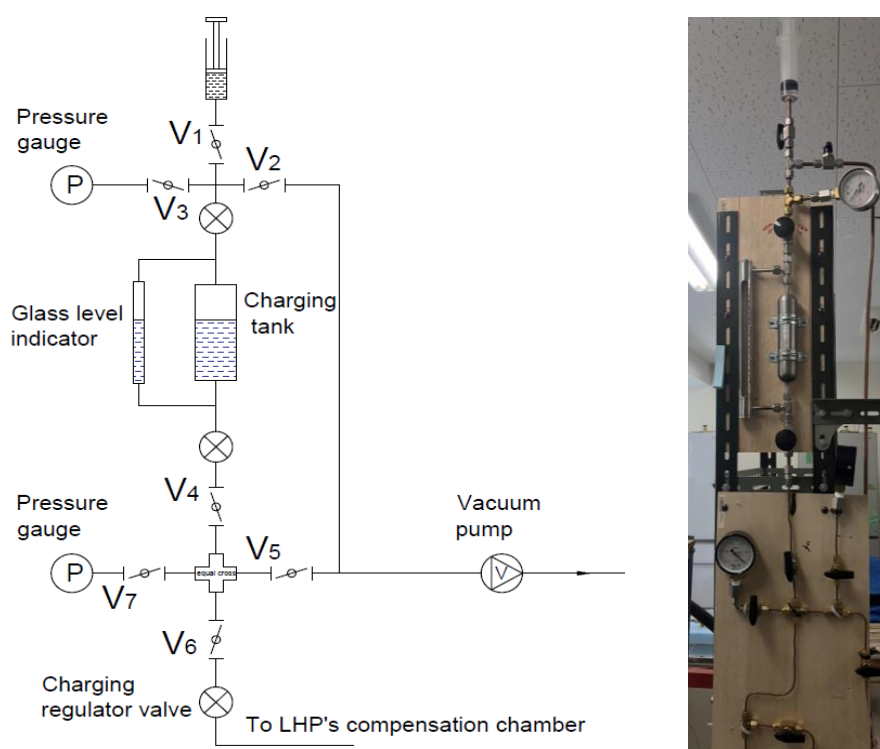


Figure 2.10: Charging and vacuum system for LHP experiment

Figure 2.10 explains the vacuum and charging system of the LHP. The first step is closing the valve V_1 , then vacuuming the whole volume of the charging system and LHP by the ULVAC GLD-051 pump. The vacuum duration was almost longer than 1 day. The next step is to disconnect the LHP and the charging tank by closing the valve V_2 , V_5 , V_6 , opening the valve V_1 to make the working fluid from the syringe flow down into the charging tank. The working fluid can enter the charging tank due to the difference between atmosphere pressure above the syringe and the vacuum pressure inside the tank. The valve V_1 was closed after finishing this step. To eliminate the non-condensable gas dissolved in the working fluid, the charging tank was heated to boil the liquid inside and vacuum again. This vacuum procedure was conducted by the closing and opening the valve V_3 and the regulating valve above the charging tank

alternatively to avoid the liquid flow into the vacuum pump. Finally, the valve V6 was opened for working fluid flow into the LHP. The amount of working fluid charged to the LHP was adjusted by the charging regulator valve and observing the changing of liquid level on the glass level indicator. Distilled water (Kanto Chemical Co.) and ethanol (99.5% - Kishida Chemical Co.) were used as working fluids in this study.

2.4 THERMOCOUPLES USED IN THE EXPERIMENT

In this study, the values of temperature obtained in this experiment was calculated from the voltage generated by the thermocouples. The function between temperature and voltage was established for each thermocouple by the calibration which was conducted in the range of temperature from 5°C to 85°C and the Pt 100 thermometer was used as the standard source.

Table 2.4: Thermocouple functions

	$T(^{\circ}\text{C}) = A(\text{mV})^3 + B(\text{mV})^2 + C(\text{mV}) + D$				Position	Type
	A	B	C	D		
T ₁	0.050505	-0.54679	25.96917	0.079023	Heating block	K
T ₂	0.04212	-0.49325	25.8464	0.091384	Heating block	K
T ₃	0.046446	-0.52175	25.95336	0.055325	Heating block	K
T ₄	0.047415	-0.58635	26.45013	0.031727	Evaporator base	K
T _{eo}	0.058322	-0.6219	26.40351	0.078046	Outlet of evaporator	K
T _{ci}	0.054046	-0.60576	26.4029	0.081788	Inlet of condenser	K
T _{co}	0.051309	-0.59833	26.42314	0.069116	Outlet of condenser	K
T _{cci}	0.060671	-0.62339	26.38473	0.0830122	Inlet of compensation chamber	K
T _{wa-i}	0.061386	-0.64182	26.44933	0.088756	Cooling water inlet	K
T _{wa-o}	0.058055	-0.62227	26.41918	0.086077	Cooling water outlet	K
T _a	0.050787	-0.58618	26.37563	0.079356	Ambient temperature	K
T _{cw1} to T _{cw5}	0.03162	-0.6989	25.7212	0.018629	Outer wall of the condenser tube	T

Table 2.5: Temperature difference estimating

	$\Delta T = dT/dV * \Delta V = (3A(\text{mV})^2 + 2*B*(\text{mV}) + C) * \Delta V$			Position
	3A	2B	C	
ΔT_{12}	0.151515	-1.09358	25.96917	Different between T ₁ and T ₂
	0.12636	-0.9865	25.8464	
ΔT_{23}	0.12636	-0.9865	25.8464	Different between T ₂ and T ₃
	0.139338	-1.0435	25.95336	
ΔT_{13}	0.151515	-1.09358	25.96917	Different between T ₁ and T ₃
	0.139338	-1.0435	25.95336	
ΔT_{wa}	0.184158	-1.28364	26.44933	Different between T _{wa-i} and T _{wa-o}
	0.174165	-1.24454	26.41918	

The calibration results are shown in the appendix C

2.5 OTHER EQUIPMENT AND MEASUREMENT DEVICES

In addition, there are other devices and measuring instrument used in the experiment that are demonstrated in the table 2.6

Table 2.6: Specification of other equipment and measurement devices

No	Device	Model	Specification
1	Cartridge heater	WATLOW G1J31	ϕ 9.42 x 38.1 mm Q = 150 W; T _{max} = 760°C
2	Voltage slider	YAMABASHI MVS - 520	Input: 100V 56/60 Hz Voltage output: 0 – 130V Resolution: 0.6 V Current output: 5.2 A Capacity: 0.52 KVA
3	Data acquisition	KEITHLEY 2701	No. of input channel: 80 No. of slot” 2 DC voltage: 100 nV – 1000 V; Resolution: 1 μ V Communication: ethernet
4	Pressure transducer	SENSEZ HBV-300kPa	Input: 0 – 300kPa abs Output: 1 – 5 DVC Uncertainty: \pm 0.5% FS (Nonlinear: \pm 0.5% FS)
5	Mass flowmeter	MASSMAX 7150K	Compact version Nominal flow 100 kg/h; Maximum: 130 kg/h Current output: 4-20mA DC Error: \pm 0.13 % of reading
6	Digital power meter	YOKOGAWA WT230	
7	Vacuum pumps	ULVAC GLD – 051	Ultimate pressure: 6.7 Pa
8	Constant temp. circulator	ADVANTEC LV 400	

REFERENCES

- [1] Y. F. Maydanik, M. A. Chernysheva, and V. G. Pastukhov, “Review: Loop heat pipes with flat evaporators,” *Appl. Therm. Eng.*, vol. 67, no. 1–2, pp. 294–307, 2014.
- [2] A. J. G. Yunus A. Cengel, *Heat and Mass Transfer; Fundamental & Application*, Fifth edit. Mc Graw Hill, 2014.
- [3] SMC Coporation, Sinter metal element (EB/ES Series) [cited 2017 Nov. 27th].

Chapter 3

Experimental Investigation on LHP Performance Under Gravity-Assisted Condition - The First Pattern of Evaporator

In this chapter, the setup and the results from the experiment of the LHP with the first pattern of evaporator when working at gravity assisted condition are presented. The LHP was accompanied with the stainless-steel sintering wick, and working fluid was water. The results including

- Startup progress of LHP at various heating power
- Evaluating the cooling capacity and thermal performance of the LHP through the values of heater temperatures, LHP operating temperatures and thermal resistance on the range of heating power.
- Cooling performance of the LHP after turning the heaters off.
- Obtaining the relation between heat flux and evaporator heat transfer coefficient (HTC). From this result, the assumption about the various boiling heat transfer characteristics inside the evaporator corresponding to different ranges of operating heat flux was constructed.

3.1 INTRODUCTION

In recent decades, the rapid developments in telecommunication and information technology led to the dramatic changes in the data center industry. One of the most changes is the gain of generated heat power and heat flux because of the increment of the components installed on one chip. While in the 1960s, there were about one thousand elements functioning on one chip, it is predicted that this number can reach 20 billion for the 1-cm² size chip 2020 [1]. It limits the utilization the present cooling methods such as air cooling or 1-phase cooling because of low cooling capacity. In addition, the existent of various new social networks, cloud computing technologies, the number of data centers increases years after years. For examples, it was recorded that in the United States, the number of data centers increased from 432 to 2094 units during the period 1998-2010 [2]. As a result, there is the increased demand for electricity energy to operate these systems. Also mentioned in [2], in 2010 electrical energy consumed by data centers took 1.3% of total global using, and annual increment was predicted as high as 15 to 20%. However, around 33% of them was used by the mechanical equipment functioning inside the thermal management systems or become useless energy [3]. In consequence, requirements of an effective modern cooling methodology are not only keeping the electronics operating stably under the safety temperature but also making them friendly with the environment by reduced electricity energy consumption.

From the above points, loop heat pipe (LHP), a novel catalog of the heat pipe, can be one of potential candidates. In comparison with a normal heat pipe, LHP can transfer heat with the lower thermal resistance through the further distance because the liquid and vapor lines are separated together and there is no wick or capillary structure requested on the whole length of the liquid line, so reducing the total pressure drop along the loop [4]. The working fluid is circulated between evaporator and condenser by capillary forced or gravity force, so there is no work input to operate the pump or compressor as in the case of other two-phase cooling methods. It means that the both of electricity consumption and operating cost can be reduced while the lifespan and reliable operation become higher due to the reduction of mechanical components. When applied in the fields such as cooling the processors of the high-performance computer or data center on earth, it is possible to arrange the position of the condenser to be higher than evaporator; as the result, heat transfer capacity of LHP can be increased significantly more than in the case of horizontal or anti-gravity operating condition.

Therefore, studying on the LHP operating under gravity assisted condition or loop thermosyphon has taken attention from different research groups. Ji Li et al [5] conducted an experiment to investigate the startup and stable operation of LHP with a square-flat evaporator and grooved-sintered copper wick. From the measuring and observation results, they proposed two modes, boiling trigger mode and evaporation trigger mode to explain the different startup behavior of LHP for different heat loads. To more understand the effect of inventory on LHP performance, the research group of J. Xu et al [6] made the flat cooper LHP with evaporator's cover made from polycarbonate. They made the conclusion that large inventory can prevent heat leak through the wick body but cause high-frequency temperature oscillation during startup as well as during operation period. One of the most recent studies was conducted by G. Zhou et al that focused on the two-phase flow characteristics of LHP with flat evaporator [7]. Their observation and measuring results show that boiling incipience depends slightly on the heat loads and nucleate boiling as well as thin film evaporation are the two-main heat transfer mechanisms inside their evaporator. Moreover, there are other studies on the wickless LHP or loop thermosyphon. Most of these studies try to modify the evaporator or change the working fluid to improve cooling capacity. A. Suzuki et al [8] introduced a LHP that applies the JEST (Jet Explosion Stream Technology) technology to enhance the heat transfer in the evaporator. In the studies conducted by C. Kondou et al [9] and H. He et al [10], the heat transfer in the evaporator can be enhanced if the wettability characteristics of the boiling surface is modified appropriately. Indicated in [9], the super-hydrophilic surface could enhance the evaporator heat transfer when working fluid is volatile fluids such as R134a, R1234Ze(D), R1234Ze(E). However, in the cases that working fluid is water, a mixed-wettability surface is suggested to eliminate the negative effect due to the boiling of water under sub-atmosphere pressure [10].

Although there are numerous studies on loop thermosyphon or LHP operating with the favorable gravitational condition, it still requires more research to simplify the structure of LHP, particularly evaporator to make the LHP become the commercialization state as normal heat pipe. In this study, a copper LHP with sintered stainless-steel wick was manufactured and investigated its thermal performance during startup, stable operational period as well as cooling performance under zero – heating power when functioning under gravity assisted condition. The different design of the present evaporator is the crossing groove or fin array was machined on the inner surface of the evaporator as shown in Fig. 3.2(a). This design can avoid machining the vapor grooves on the wick surface that can damage or change the surface characteristics of

the wick. Besides, it also guarantees the sufficient space for evaporation as well as paths for vapor flow out easily, so prevent vapor forming inside the wick. The evaporator lid is made of polycarbonate to observe the state of compensation chamber; therefore, water is selected as working fluid because of low operational pressure. Our experimental result indicate that this simple design of evaporator can satisfy the heat power generated from the future electronic device. Moreover, in this study, we assumed a theory of boiling heat transfer to explain the various performance of the evaporator with different heat flux values.

3.2 EXPERIMENTAL SETUP

Table 3.1: Main parameters of LHP

Heating block	
Material	Copper
Mass, kg	4.36
Evaporator body	
Material	Copper
Length, mm	80
Width, mm	70
Height, mm	24.5
Active area, mm ²	60 x 45
Fin geometry	
Cross area, mm ²	2 x 2
Height, mm	1.5
Fin pitch, mm	4
Wick structure [11]	
Material	SUS 316L
Opening, μm	63
Void ratio, %	36 – 48
Bulk volume, mm ³	50 x 41 x 5
Vapor line	
OD/ID, mm	6.35/4.35
Length, mm	800
Condenser line	
OD/ID, mm	6.35/4.35
Length, mm	600
Liquid line	
OD/ID, mm	3.2/1.7
Length, mm	1300

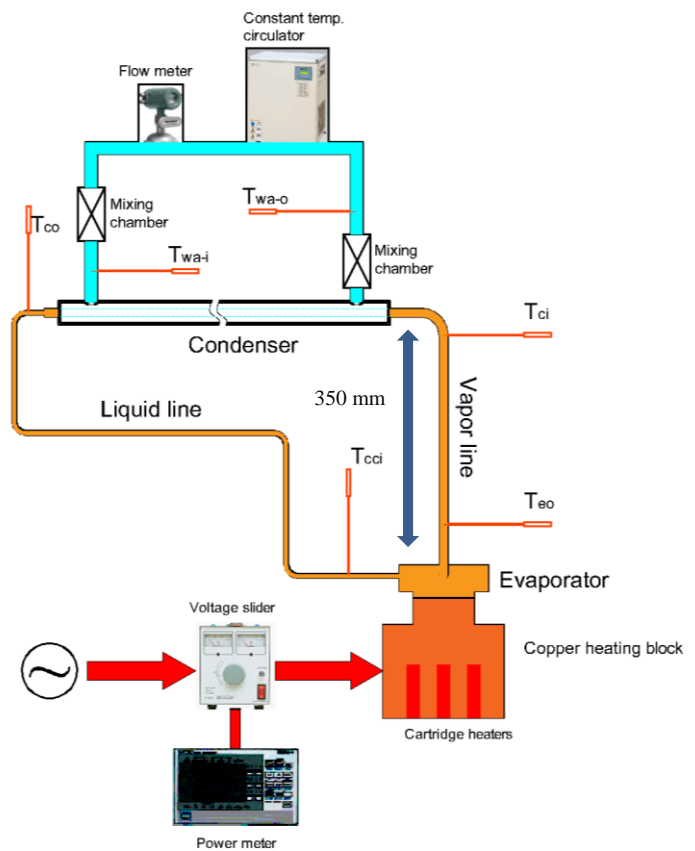
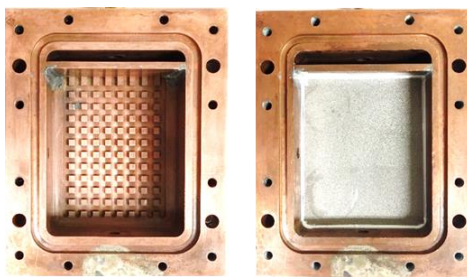
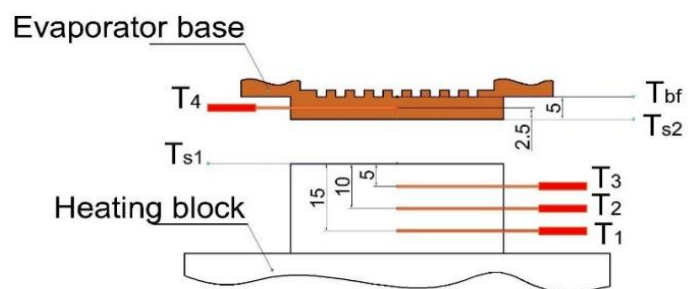


Figure 3.1: Schematic diagram of experiment setup



(a)



(b)

Figure 3.2: a) Geometry of the inner surface the evaporator b) Temperature gradient measurement

The schematic diagram of experiment is described in Fig. 3.1, and table 3.1 lists the main specifications of the LHP. In this experiment, the condenser was located 350 mm higher than the elevation of the evaporator. The evaporator was heated by four cartridge heaters installed inside the copper heating block. The condenser was cooled by water. In this experiment, the cooling water was maintained at the mass flow rate around 27 kg/h and inlet temperature of 27.5°C. Heating power supplied to the evaporator was adjusted and observed by the volt slider

and the digital power meter. To minimize thermal contact resistance, besides the simple screw locking system, a thin thermal grease layer was filled to the interface between evaporator and heating block. Four thermocouples T_{eo} , T_{ci} , T_{co} , T_{cci} were inserted directly at four distinguish positions of LHP that are outlet of evaporator, inlet of condenser, outlet of condenser and inlet of compensation chamber respectively. They detect the temperature distribution inside the LHP, so the characteristics of circulation as well as phase distribution can be evaluated. For accessing the accurate values of heating power and heat flux supplied to the evaporator, three thermocouples T_1 , T_2 , T_3 were installed as shown in Fig. 3.2(b) to measure the temperature gradient caused by the heat flux and the temperature on the top surface of heating block T_{s1} . Thermocouple T_4 was inserted in the evaporator base to estimate the temperature at the evaporator's bottom surface T_{s2} and temperature at the base of the fin T_{bf} . The temperature difference and mass flow rate of cooling water measured from two thermocouple T_{wa-i} , T_{wa-o} and mass flow meter could help in determining the heat released at the condenser. The ambient temperature was kept around 25°C during the experiment. Table 3.2 lists the uncertainty values of the mas flow meter and thermocouples (obtained from the calibration process in which Pt100 thermometer (Chino Co. Model – R900-F25AT) was the used as the standard source)

Table 3.2: Uncertainty values

	Uncertainty
T_1, T_2, T_3	$\pm 0.06^\circ\text{C}$
T_4	$\pm 0.07^\circ\text{C}$
T_{eo} ,	$\pm 0.06^\circ\text{C}$
T_{ci} ,	$\pm 0.06^\circ\text{C}$
T_{co}, T_{cci}	$\pm 0.1^\circ\text{C}$
T_{wa-i} ,	$\pm 0.1^\circ\text{C}$
T_{wa-o}	$\pm 0.06^\circ\text{C}$
T_a	$\pm 0.16^\circ\text{C}$
Mass flow meter	0.18% of reading



Figure 3.3: The real setup of the experiment

3.3 DATA REDUCTION

From the measured values of T_1 , T_2 , T_3 , heat flux q and heat flow rate Q supplied to the evaporator can be determined

$$q = \frac{1}{3} \left(k \frac{\Delta T_{12}}{\delta_1} + k \frac{\Delta T_{23}}{\delta_1} + k \frac{\Delta T_{13}}{2\delta_1} \right) \quad (3.1)$$

$$Q = qA \quad (3.2)$$

Where

$$\delta_1 = 5 \text{ mm}; A = 27 \text{ cm}^2$$

And temperature on the top surface of heating block T_{s1} and bottom surface of evaporator T_{s2}

$$T_{s1} = \frac{1}{3} \left[\left(T_1 - \frac{3(q\delta_1)}{k} \right) + \left(T_2 - \frac{2(q\delta_1)}{k} \right) + \left(T_3 - \frac{(q\delta_1)}{k} \right) \right] \quad (3.3)$$

$$T_{s2} = T_4 + \frac{q\delta_2}{k}; \text{ where } \delta_2 = 2.5 \text{ mm} \quad (3.4)$$

Total thermal resistance R_t , evaporator thermal resistance R_e , condenser thermal resistance R_c and thermal contact resistance R_{ct}

$$R_t = \frac{T_{s1} - T_{wa-i}}{qA} \quad (3.5)$$

$$R_e = \frac{T_{s2} - T_{eo}}{qA} \quad (3.6)$$

$$R_c = \frac{T_{ci} - T_{wa-i}}{Q_c} \quad (3.7)$$

With Q_c is the heat released from the condenser

$$Q_c = m_{wa} c_p (T_{wa-o} - T_{wa-i}) \quad (3.8)$$

$$R_{ct} = \frac{T_{s1} - T_{s2}}{Q} \quad (3.9)$$

The evaporator HTC h_e

$$h_e = \frac{q}{T_{bf} - T_{eo}} \quad (3.10)$$

In the Eq. 3.10, T_{eo} was considered as saturated temperature of vapor in the evaporator. As being described in Fig. 3.2(b), T_{bf} is temperature at the base of the fins or the surface of the groove which can be estimated by the below equation

$$T_{bf} = T_4 - \frac{q\delta_2}{k} \quad (3.11)$$

Appendix D-1 displays the thermal balance between heating power Q and heat released from the condenser Q_c , and appendix D-2 demonstrates temperature gradient measured in the whole range of heating power. Difference between the heat supplied and heat released from the condenser was not more than 10 percent. Uncertainty values of the parameters estimated from experiment such as heat flux q , temperature T_{sl} , total thermal resistance R_t , thermal contact resistance R_{ct} and evaporator HTC h_e is shown in appendix E-1. When heating power is higher than 150 W, uncertainty of R_t and h_e are smaller than 10% and 25% respectively.

3.4 RESULTS AND DISCUSSIONS

3.4.1 Startup characteristics of the LHP

Startup of LHP is complicated but attractive phenomenon that was mentioned in almost LHP studies. The duration and behavior of LHP including changes of temperature, pressure or phase distribution are the parameters paid the most attention at the startup procedure. Because of passive heat transport device, the LHP's startup depends on various conditions such as heating power or heat flux, thermal mass of evaporator and heat source, working fluid, filling ratio, operating orientation etc. The first result in this chapter discusses the startup behavior of this LHP under gravity assisted condition at different heating power.

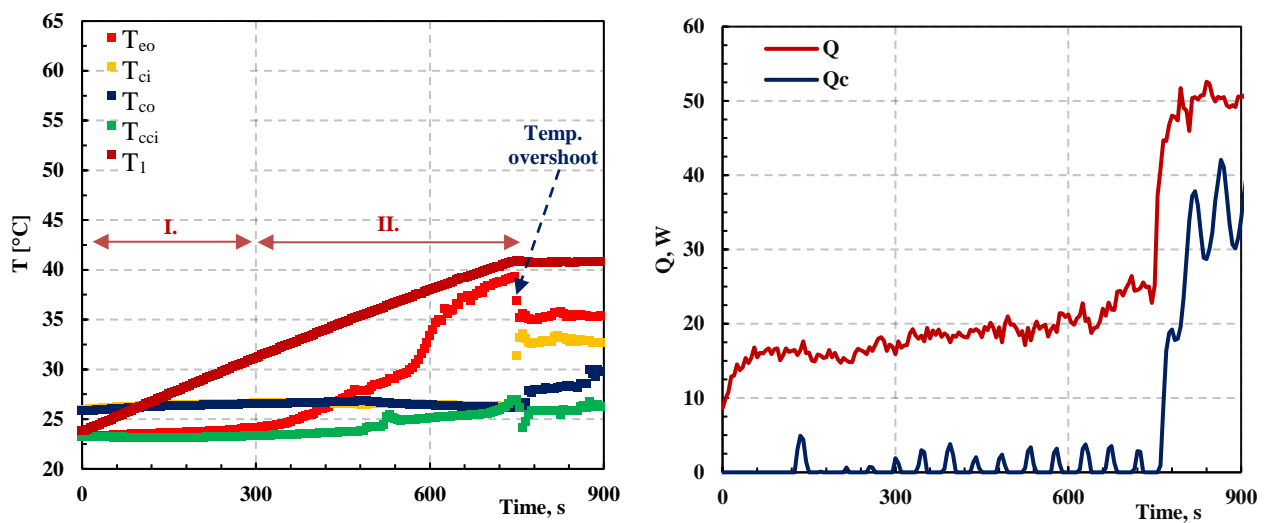


Figure 3.4: Startup of the LHP at heating power of 50 W

a) Changing of temperatures; b) Heat supplied to evaporator and heat released from condenser

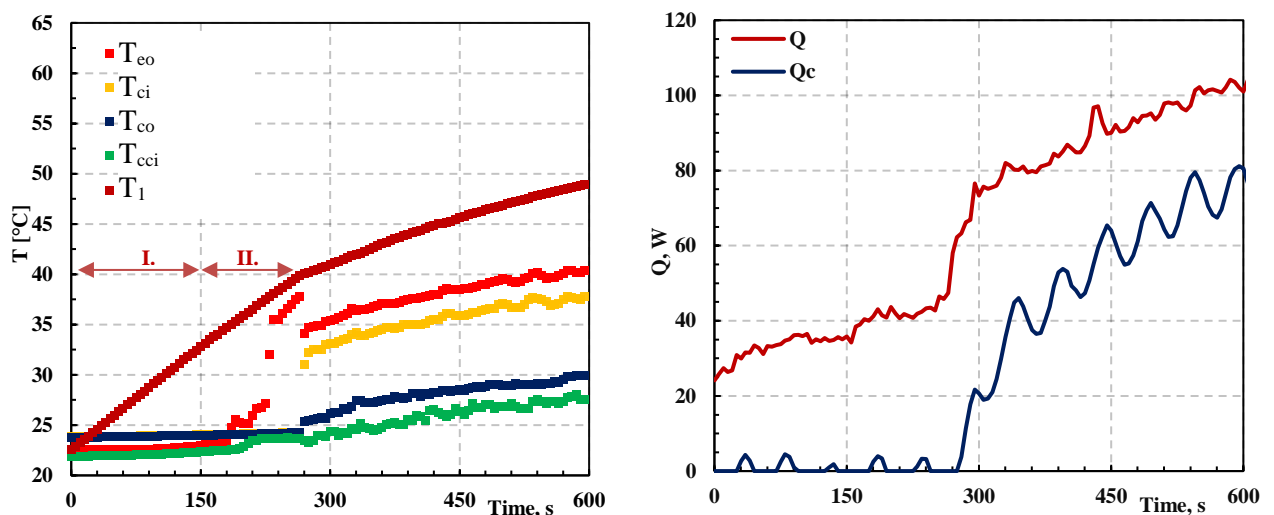


Figure 3.5: Startup of the LHP at heating power of 125 W

a) Changing of temperatures; b) Heat supplied to evaporator and heat released from condenser

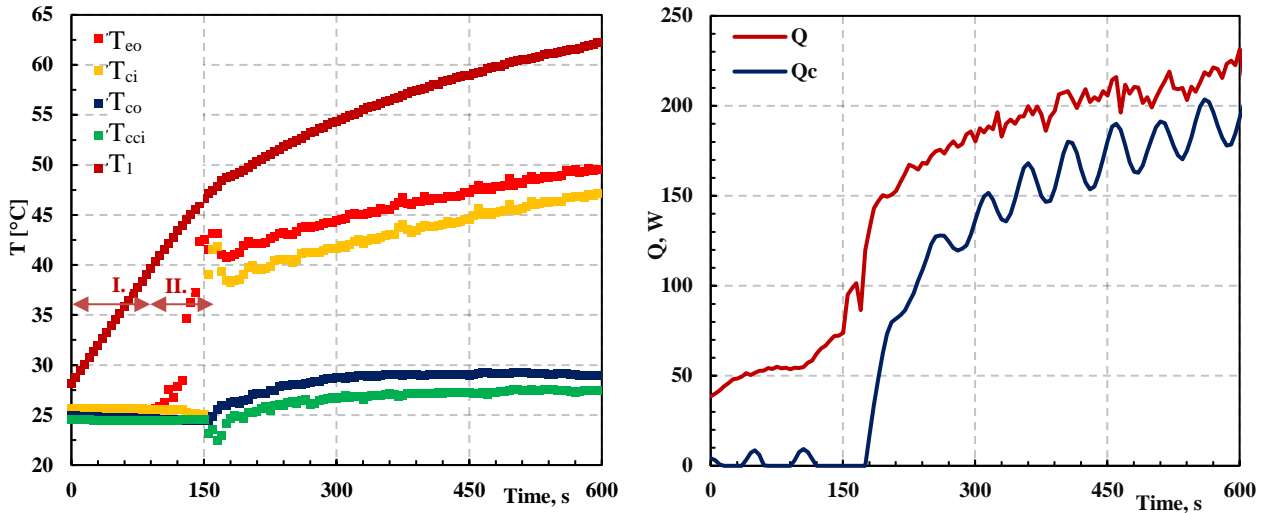


Figure 3.6: Startup of the LHP at heating power of 270 W

a) Changing of temperatures; b) Heat supplied to evaporator and heat released from condenser

The startup characteristics of this LHP were investigated at various operating heating power such as 50 W, 125 W, and 270 W through the changing of temperatures, the heat flowing to the evaporator and heat released from the condenser with time. In general, the duration of startup reduced with the magnitude of heating power. It took around 12 mins for the startup at 50 W while at the heating power of 270 W, the startup finished after 2.5 min. From the changing of temperatures measured at different locations of the LHP, the startup process can be divided into two stages at all values of heating power. In the first stage, in the all cases of heating power, it was observed that only temperature T_1 increased with time, the temperatures at four positions of LHP almost had the same values and were not different to the initial state values although heat was supplied continuously. These obtained data demonstrate that the LHP does not operate during the first stage of startup or there was no heat transferred from the heater to cooling water by the LHP. Almost heat is changed into sensitive heat to increase the temperature of the heating block and the evaporator body; therefore, thermal mass of the heating block and evaporator could be considered as the reason caused this stage to happen.

In the second stage, there was a rise of temperature T_{eo} . The ending of the second stage was recognized at the time when temperature T_{ci} suddenly jumped to the value of T_{eo} while T_{eo} reached close to temperature of the heater. At that moment, it was also observed that the temperature T_{co} and T_{cci} raised up slightly while heat released from the condenser could be detected. It indicates at that moment the hot vapor can enter the condenser and become liquid, then return the compensation chamber or circulation totally happened. However, the process of this stage at different heating power has some difference. The temperature T_{eo} increased

slowly at the heating power of 50 W, but there was the fast growth of this temperature at heating power of 120 W and 270 W. In addition, at the end of startup period, the presence of temperature overshoot of T_{eo} was observed. The overshoot's magnitude reduced with the increase of heating power. These results can be explained by the phase distribution and boiling mechanism. Because of gravity-assisted condition, at the initial state the vapor grooves, vapor collector and lower part of vapor line are flooded with liquid phase that makes vapor to be generated and flow out the evaporator more difficultly. Particularly under heating power at 50 W, the slow increase of T_{eo} can be understood that subcooled boiling inside the evaporator at this stage. This is also the reason that caused the temperature overshoot happen. When heating power increases, the combination of high evaporation rate and reduction of the liquid phase in the vapor line makes the duration of second stage and magnitude of temperature overshoot reduce significantly; consequently, the LHP can startup faster.

3.4.2 Cooling capacity and thermal performance of LHP

a) Cooling capacity

In this experiment, if the temperature T_{s1} on the top surface of the heating block is assumed as operating temperature of electronics, the cooling capacity of an LHP can be defined as the heating power that this LHP can take out the heater and keep the operating temperature of electronics or T_{s1} below the safety limitation that is normally recommended to be 85°C to assure of reliable and effective operation of processor [3]. The cooling capacity of an LHP is not a constant value but it depends on some parameters such as temperature of heat sink, method of condenser cooling, ambient temperature as well as the degradation with time. This LHP can be considered as the fresh LHP, and its condenser was cooled by water whose inlet temperature and mass flow rate were setup at 27.5°C and 27 kg/h. The ambient temperature was maintained around 25°C.

Figure 3.7 shows the dependence of temperature T_{s1} , T_{s2} (Fig. 3.2(b)) corresponding the temperatures at the top surface of heater and evaporator's bottom surface on heating power. This experiment was conducted in the range of heating power from 50 to 520 W. Although the experiment of LHP at 35 W was conducted, the LHP could not startup successfully under this heating power. The largest value 520 W of heating power in this experiment was the capacity of the volt slider. From the above definition, when this LHP was used to cool the electronic device, its cooling capacity was around 350 W. This value of cooling capacity was decided basing upon the operating limitation temperature of the electronic devices, not due to the

operation limitation such as capillary limitation, dry out limitation, etc. Although in the experiment, the evaporator was fixed to the heating block by screws and thermal grease of which purpose is used to improve the contact quality, the effect of thermal contact resistance cannot eliminate totally. At the low heating power, the temperature difference was little, and its value increased with the heating power. The thermal contact resistance could cause the temperature difference to be around 5°C when LHP operated at the heating power of 520 W. Therefore, thermal contact resistance is also one of factors need to be paid more attention to improve the cooling capacity of the LHP.

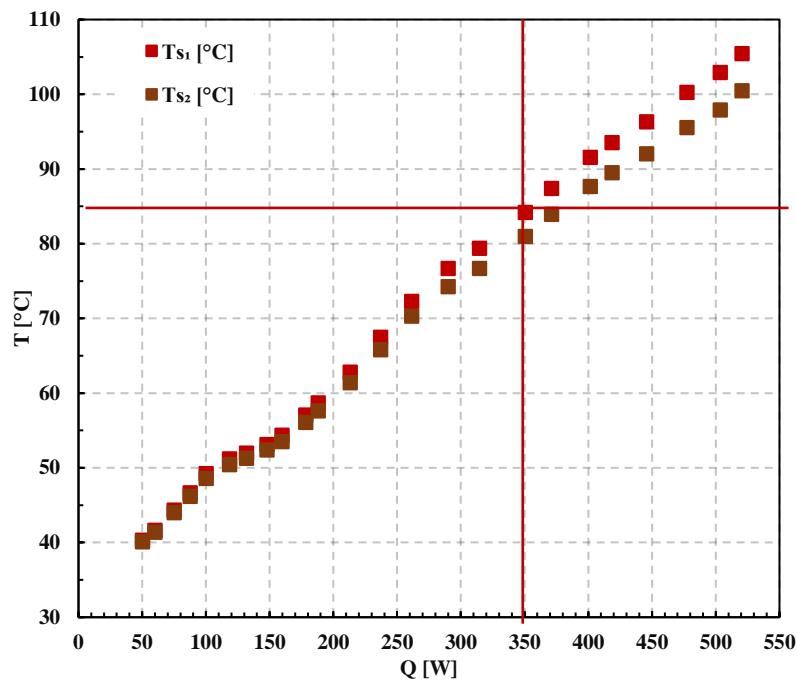
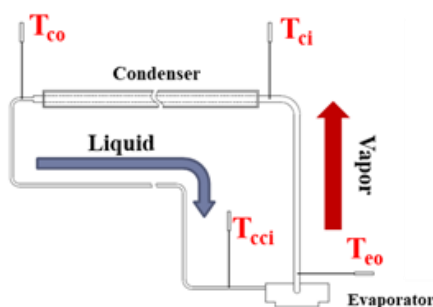


Figure 3.7: Changing of temperatures T_{s1} T_{s2} on the heating power

b) Thermal performance of the LHP

Figure 3.8 demonstrates the temperatures of working fluid at different positions along the LHP's body when heating power was maintained at 90 W, 160 W, 300 W, 350 W, 475 W, and 520 W.



T_{eo} : Temperature at the outlet of the evaporator;
 T_{ci} : Temperature at the inlet of the condenser
 T_{co} : Temperature at the outlet of the condenser;
 T_{cci} : Temperature at the inlet of the compensation chamber

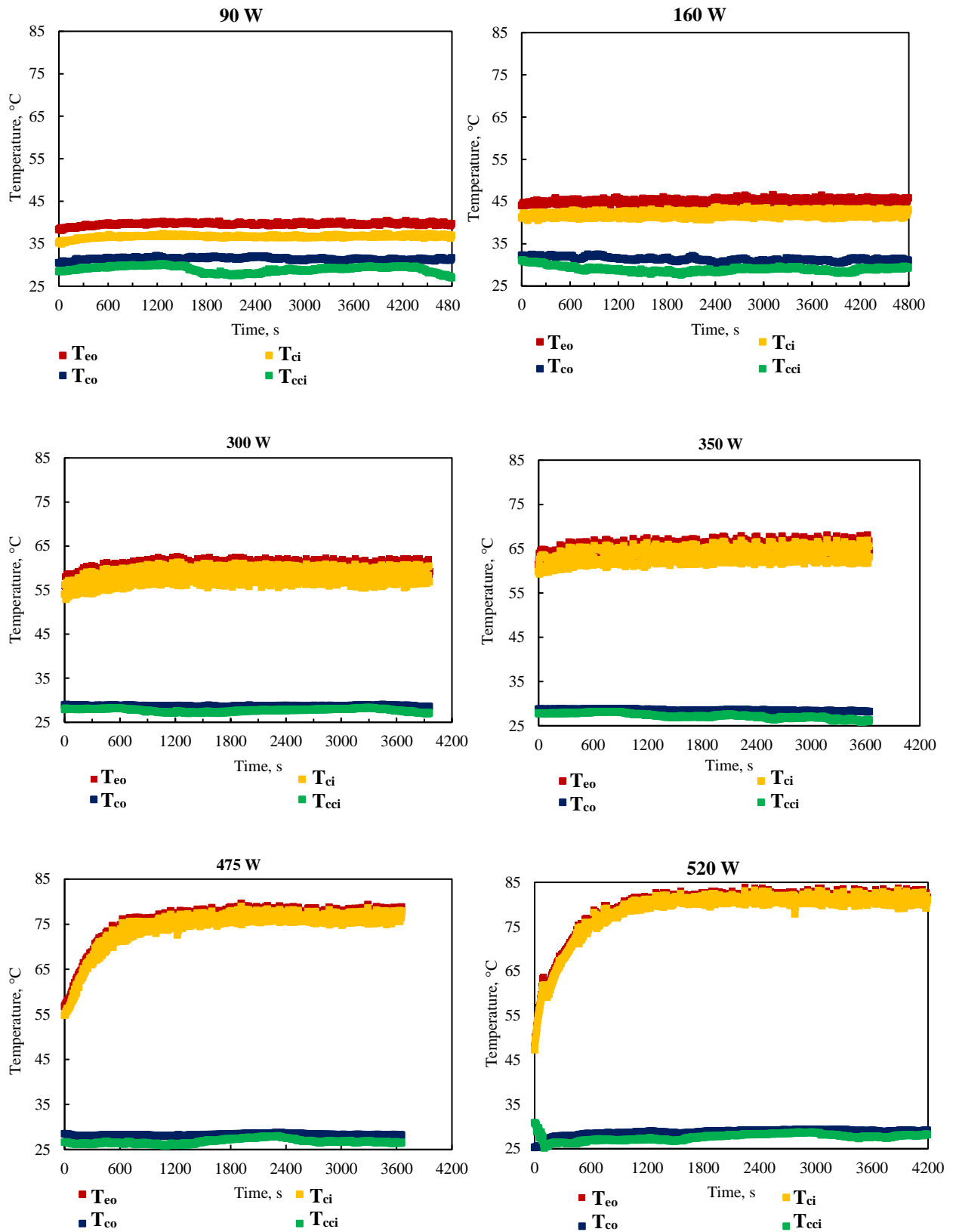


Figure 3.8: Temperature of working fluid at different positions along LHP's body collected during the operating period

From the graphs shown in Fig. 3.8, it is sure that the LHP can maintain the stable operation, or the circulation of working fluid happened well inside the LHP. This conclusion can be withdrawn from the significant difference between T_{eo} , T_{ci} with T_{co} and T_{cci} and the result that temperature T_{cci} was a little less than T_{co} . However, the LHP also performed some distinguished behaviors when heating power was adjusted at different magnitudes. With the heating power at 90 W and 160 W, there were the difference between T_{eo} and T_{ci} , but the values of these two temperatures could be considered as constant. When the heating power were turn into 300 W and 350 W, the temperature difference of T_{eo} and T_{ci} became less, but they behaved the high-frequency and small-amplitude oscillation. The values of T_{eo} and T_{ci} distributed uniformly around the mean value with the amplitude around 2 to 2.5°C. At the heating power of 475 W and 520 W, the temperatures T_{eo} and T_{ci} were closed together while the oscillation became weaker. In addition, the stable operation of LHP at 520 W shows that this value of heating power is not the boiling or capillary limitation of this LHP. The temperature distribution inside the LHP in the whole range of operating heating power was demonstrated in Fig. 3.9.

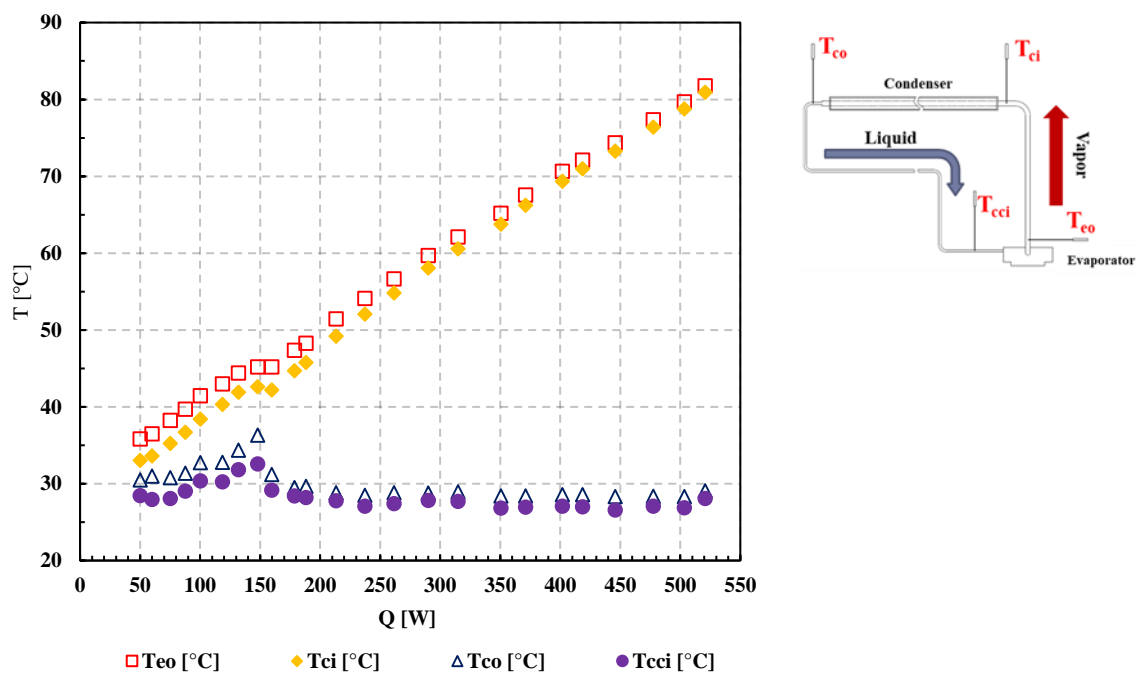


Figure 3.9: Temperature distribution inside the loop heat pipe at various heating power from 50 to 520 W

The change of LHP's total thermal resistance R_t and LHP components' thermal resistance including evaporator thermal resistance R_e , condenser thermal resistance R_c and thermal contact resistance R_{ct} on the heating power is shown in Fig. 3.10.

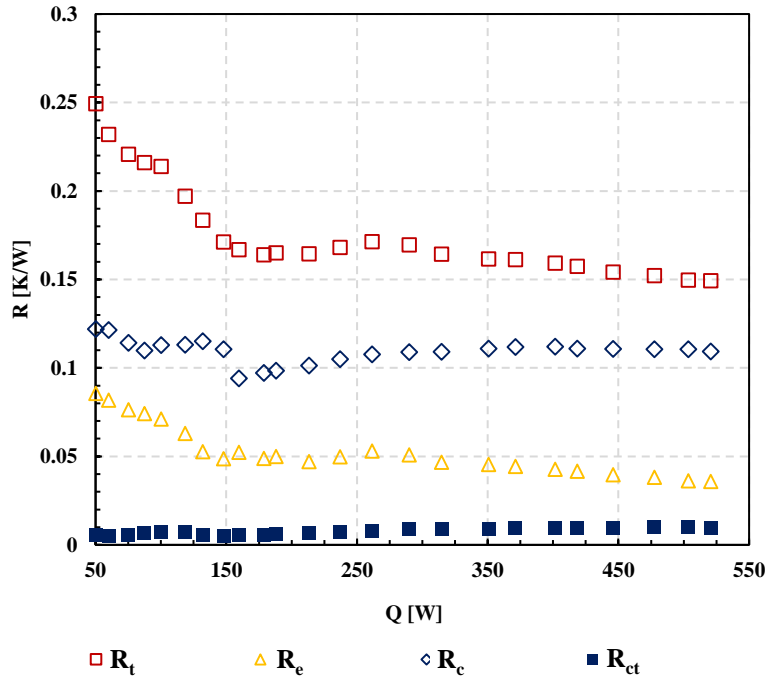


Figure 3.10: Changing of different thermal resistances on heating power

R_t : total thermal resistance; R_e evaporator thermal resistance;
 R_c : condenser thermal resistance; R_{ct} : thermal contact resistance

In general, the total thermal resistance R_t and the evaporator resistance R_e reduced with the increase of heating power; however, the significant reduction occurred almost in the range of heating power from 50 to 150 W. It can be explained because it is difficult for vapor to be generated and depart from the inner surface of evaporator when the boiling of water happens under low heating power and vacuum condition. Besides, the liquid flooding situation of evaporator at the initial stage also contributes to these results. The minimum value of R_t and R_e was 0.149 K/W and 0.0036 K/W when the heating power had the value at 520 W. On the contrary, the condenser thermal resistance R_c was almost constant at different values of heating power, but it contributed more than other components in the total thermal resistance of the LHP. In addition, this experiment also determined the thermal contact resistance R_{ct} between the bottom of evaporator and top of heating block. With the present fixing method, R_{ct} had the average value at 0.007 K/W and changed in the range of 0.005 to 0.01 K/W. This resistance can be ignored at low heating power, but for the high heat dissipated devices, it is necessary to pay more attention to eliminate its influence.

3.4.3 The evaporator HTC and assumption about boiling heat transfer phenomenon inside the evaporator

Figure 3.11 displays the changing of evaporator HTC h_e on the heat flux and Fig. 3.12 does the change of heat flux with excess temperature ($T_{bf} - T_{eo}$). To evaluate the heat transfer performance of this evaporator with the bare surface, the results obtained from the experiment was compared with the calculational values that was estimated from the Rohsenow equation (Eq. 3.12) whose obtained results can be in error by $\pm 30\%$ for excess temperature for a given heat transfer rate [12].

$$q = \mu_l h_{fg} \left[\frac{g(\rho_l - \rho_v)}{\sigma} \right]^{\frac{1}{2}} \left[\frac{c_p(T_s - T_{sat})}{C_{sf} h_{fg} Pr_l^n} \right]^3 \quad (3.12)$$

Where

- q : value of heat flux, W/m^2
- μ_l : viscosity of the liquid, $kg/(m \cdot s)$
- h_{fg} : latent heat, J/kg
- g : gravitational acceleration, m/s^2
- ρ_l : density of liquid phase, kg/m^3
- ρ_v : density of vapor phase, kg/m^3
- σ : surface tension, N/m
- c_{pl} : specific heat of the liquid, $J/kg \cdot K$
- T_s : surface temperature of the heater, $^{\circ}C$
- T_{sat} : saturation temperature of the liquid, $^{\circ}C$
- C_{sf} : experimental constant that depends on surface-fluid combination
- Pr_l : Prandtl number of the liquid
- n : experimental constant that depends on the fluid

In the Rohsenow equation, the value of heat flux was input to find out the excess temperature and evaporator HTC. Values of n and C_{sf} were selected at 1 and 0.013 respectively. The properties of saturation liquid and vapor were obtained from the temperature at the outlet of the evaporator T_{eo} that is considered as the saturation temperature of vapor by the REFPROP Version 9.1.

Figure 3.11 displays the relation between evaporator HTC and heat flux supplied to the evaporator, while the change of excess temperature due to the heat flux was shown in Fig. 3.12.

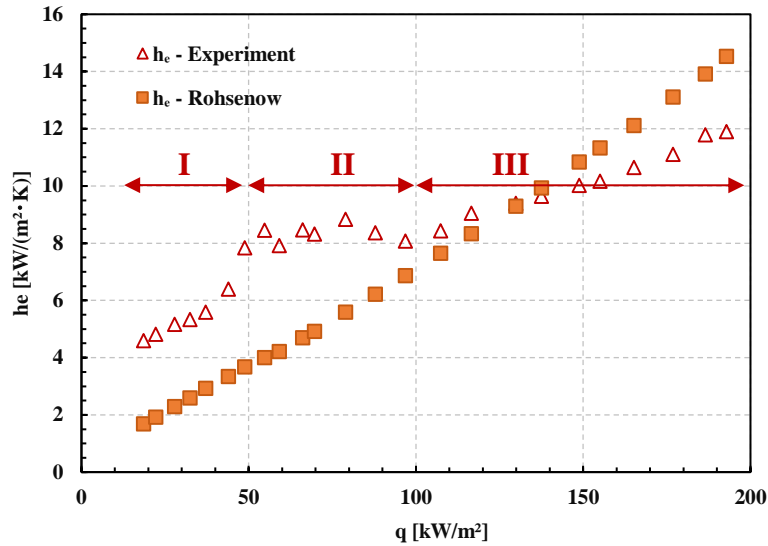


Figure 3.11: Effect of heat flux on the evaporator HTC

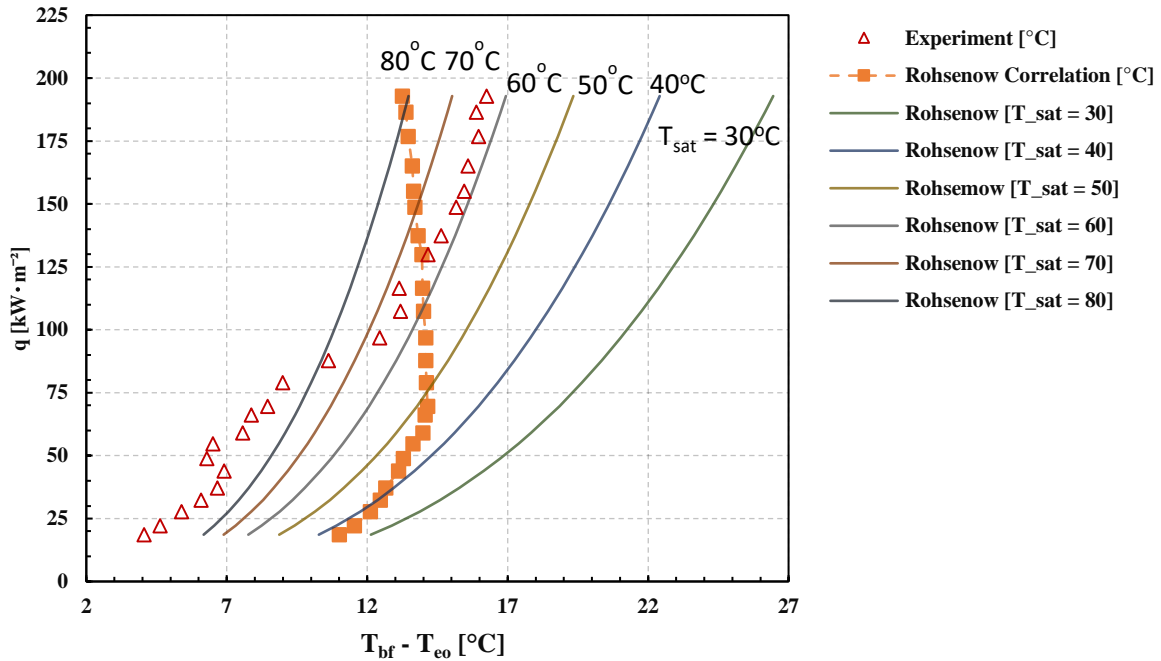


Figure 3.12: Relation between heat flux and excess temperature

In general, both of evaporator HTC obtained from experiment and Rohsenow correlation almost increased with the heat flux. However, while the calculational results raised up nearly linearly with the flux, the experimental results show that the effect of heat flux on the evaporator HTC could be classified into three regions. Firstly, when heat flux was smaller than 50 kW/m^2 , the relation between evaporator HTC h_e and heat flux was almost linear. In the range of heat flux from 50 kW/m^2 to 100 kW/m^2 , the values of h_e was nearly constant or changed slightly with the change of heat flux. Continuing increasing heat flux made the relation

become linear again. In addition, the experimental results were only higher than calculational results when heat flux is lower than 100 kW/m^2 .

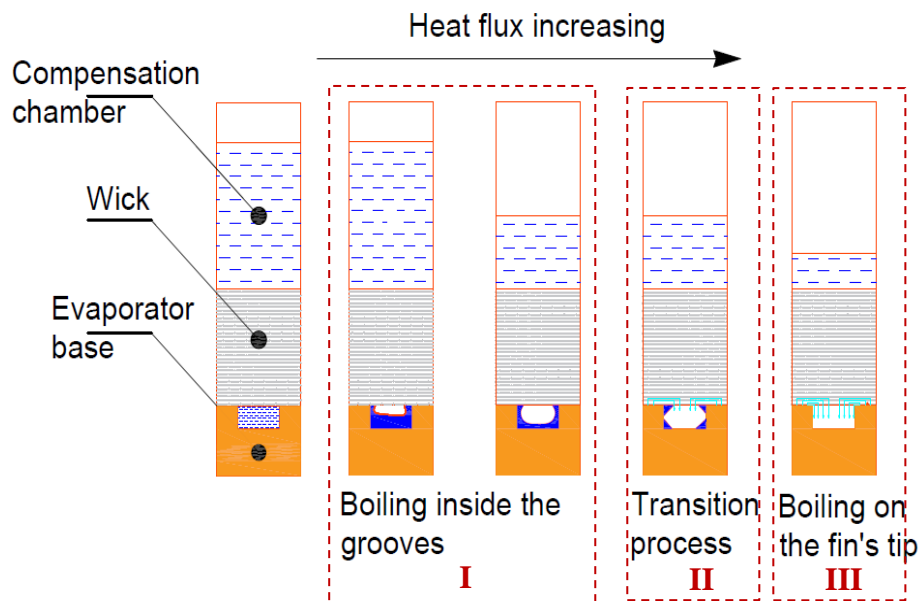


Figure 3.13: Assumption of boiling phenomenon under different magnitude of heat flux

To explain the about results, an assumption about boiling heat transfer described in Fig. 3.13 was supposed. Under low heat flux condition, the combination between small evaporation rate and the liquid flooding the vapor grooves that makes vapor flow out evaporator difficultly. This is also the reason which causes evaporator thermal resistance R_e as well as total resistance R_t to be larger in this situation. When increasing heat load, there is less liquid existing at the vapor grooves, the L-V interface area becomes larger that helps vapor escape evaporator more easily. On the other hand, when compared with the results from Rohsenow correlation, the experimental results had the higher values. It can be explained because the array of fins on the inner surface of evaporator increases the heat transfer area from the solid base to the liquid; as a result, enhancing the HTC under this situation. When heat flux is more than 50 kW/m^2 , less liquid existing inside the grooves causes the L-V interface surface insufficient with heat input; therefore, a fraction of heat input will serve for boiling inside the grooves, the rest fraction must transfer through the fins to make boiling happen on contact surface between the fins and wick body, but this boiling now was not too active. It explains why within this range of heat flux the evaporator HTC was almost constant with heat flux. Keeping on increasing heat flux more than 100 kW/m^2 , nuclear boiling will happen efficiently on the fin's tip surface; hence, evaporator HTC h_e increased proportionally with heat flux again. On the contrary, within this range of heat flux, the results obtained from Rohsenow correlation became higher than

experiment. From the above assumption, when heat flux was higher than 100 kW/m^2 , the boiling happens almost on the tip surface of the fins. It means that the height of the fins may cause the evaporator thermal resistance increase. Besides, the change of boiling from inside the grooves to on the contact surface tip of the fins also reduces the area for boiling. Two above explanations can be the reasons why the evaporator HTC determined from experiment had the smaller values than from correlation in the range of heat flux being larger than 100 kW/m^2 . In summary, under small heat flux, the L-V interface presents inside vapor grooves and expands its area with heat flux value. Keeping heat flux increasing can clear all liquid inside vapor grooves and cause the liquid-vapor interface to move to the contact surface between wick and evaporator body. The above results also show that it is necessary to conduct the study on finding the optimal size of the fin to improve the performance of the evaporator when functioning under high heat flux situation.

3.4.4 Cooling performance of LHP after turning off the heater

Because LHP is a passive heat transport device, its performance after shutting down the electronic device is also the important factor that need to be investigated. It is necessary to sure that the LHP can cool the electronic device to the normal temperature as fast as possible despite no heating power.

This experiment was carried out after the stable operation of LHP at. Fig. 3.13 displays the change of temperature T_l , T_{eo} , T_{ci} , T_{co} , T_{cci} after turning heaters off. It took about 15 minutes to reduce the T_l from 102°C to 37°C , then value of T_l almost constant. The cooling rate reduced with time. During the first five minutes, the average cooling rate was around $8.12^\circ\text{C/minute}$ and decreased to 3.83°C during the next five minutes and finally was $1.15^\circ\text{C/minutes}$. When T_l had value 37.6°C , T_{ci} dropped suddenly far from T_{eo} or the circulation stopped. T_{eo} did not reduce, that indicates the evaporation still happened, but the heat released from heater was not strong enough to maintain the circulation.

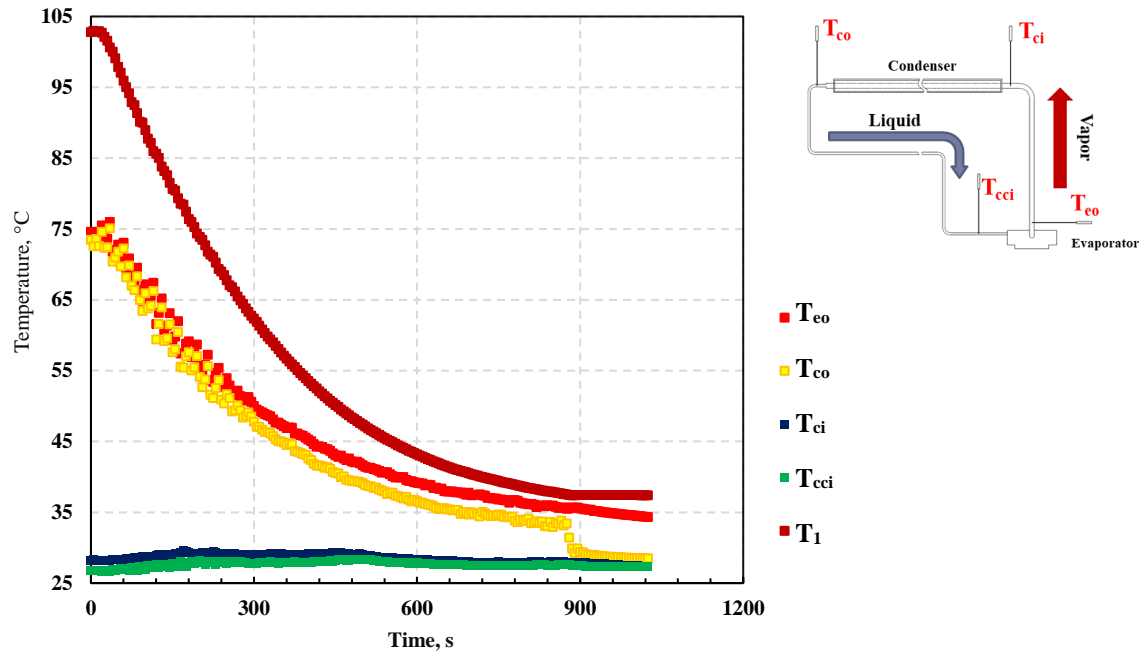


Figure 3.14: Cooling performance of the LHP after turning off the heaters

3.5 CONCLUSION

In this study, an LHP with flat-rectangular evaporator was manufactured and investigated performance under gravity assisted condition in the range of heating power from 50 W to 520 W. Time for the present LHP to startup reduced from 12 mins to 2.5 mins when heating power increased from 50 W to 270 W. The flooding situation at the vapor line can be the reason that causes the startup to be longer and the appearance of temperature overshoot at the end of startup under low heating power condition.

The present LHP could maintain temperature on top surface of the heating block below 85°C, which is the commonly suggested limitation value for the safe and effective operation, when heating power was smaller than 350 W. Besides, it kept the stable operational performance on the whole range of heating power without the sign of dry-out inside evaporator.

In general, both of total thermal resistance R_t and thermal resistance of evaporator R_e became smaller with the increasing of heat load. Consequently, R_t and R_e had the minimum values 0.149K/W and 0.0036 K/W respectively when heating power was at 520 W. The thermal contact resistance R_{ct} had maximum value 0.01 K/W.

In addition, an assumption of boiling heat transfer was introduced in this study for explaining the change of the evaporator heat transfer coefficient of the present LHP with heat flux. At small heat flux, the L-V interface forms inside vapor grooves and gains its surface area with

heat flux. When heat flux has value more than 100 kW/m^2 , it presents at the contact surface between fin and wick body. Evaporator heat transfer coefficient h_e was almost constant with heat flux during transition process, where heat flux is from 50 kW/m^2 to 100 kW/m^2 .

With the 4.36-kg copper heating block, under no heating power condition, it took about 15 minutes to reduce the temperature T_j inside the heating block from 102°C to 37°C with the max cooling rate that was 8.12°C/min in the first five minutes of cooling period.

REFERENCES

- [1] S. M. Sohel Murshed and C. A. Nieto de Castro, "A critical review of traditional and emerging techniques and fluids for electronics cooling," *Renew. Sustain. Energy Rev.*, vol. 78, no. March 2016, pp. 821–833, 2017.
- [2] K. Ebrahimi, G. F. Jones, and A. S. Fleischer, "A review of data center cooling technology , operating conditions and the corresponding low-grade waste heat recovery opportunities," *Renew. Sustain. Energy Rev.*, vol. 31, pp. 622–638, 2014.
- [3] A. C. Kheirabadi and D. Groulx, "Cooling of server electronics: A design review of existing technology," *Appl. Therm. Eng.*, vol. 105, pp. 622–638, 2016.
- [4] Y. F. Maydanik, "Loop heat pipes," vol. 25, pp. 635–657, 2005.
- [5] J. Li, D. Wang, and G. P. Peterson, "Experimental studies on a high performance compact loop heat pipe with a square flat evaporator," *Appl. Therm. Eng.*, vol. 30, no. 6–7, pp. 741–752, 2010.
- [6] J. Xu, Z. Wang, H. Xu, and L. Zhang, "Experimental research on the heat performance of a flat copper-water loop heat pipe with different inventories," *Exp. Therm. Fluid Sci.*, vol. 84, pp. 110–119, 2017.
- [7] G. Zhou and J. Li, "International Journal of Heat and Mass Transfer Two-phase flow characteristics of a high performance loop heat pipe with flat evaporator under gravity," vol. 117, pp. 1063–1074, 2018.
- [8] A. SUZUKI, K. SATO, Y. KOITO, and T. TOMIMURA, "Prototype Experiment on Cooling Performance of a JEST-type Loop Heat Pipe," *4th World Conf. Appl. Sci. Eng. Technol.*, no. October, pp. 24–27, 2015.
- [9] C. Kondou, S. Umemoto, S. Koyama, and Y. Mitooka, "Improving the heat dissipation performance of a looped thermosyphon using low-GWP volatile fluids R1234ze(Z) and R1234ze(E) with a super-hydrophilic boiling surface," *Appl. Therm. Eng.*, vol. 118, pp. 147–158, 2017.
- [10] H. He, K. Furusato, M. Yamada, B. Shen, and S. Hidaka, "Efficiency enhancement of a loop thermosyphon on a mixed-wettability evaporator surface," *Appl. Therm. Eng.*, vol. 123, pp. 1245–1254, 2017.

- [11] SMC Coporation, Sinter metal element (EB/ES Series), pp. 103–118 [cited 2017 Nov. 27th]
- [12] A. J. G. Yunus A. Cengel, *Heat and Mass Transfer; Fundamental & Application*, Fifth edit. Mc Graw Hill, 2014.

Chapter 4

Experimental Investigation on LHP Performance Under Gravity-Assisted Condition with Different Working Fluids – The Second Pattern of Evaporator

This chapter introduces the experiment of the LHP that utilized the second pattern of the evaporator equipped with the stainless-steel sintered wick. The new pattern was designed to remove some disadvantage of the first design, especially the ability that vapor collector connect to compensation chamber. The results of this experiment are the comparison of the performance of the LHP functioning with two different working fluids that were water and ethanol (C₂H₅OH). The results in this experiment also confirmed the assumption introduced in the chapter 3 and implement the effect of convection heat transfer mechanism on the performance of the evaporator. The detail results including

- Evaluating the cooling capacity of water LHP and ethanol LHP.
- Comparison the thermal performance of LHP when working with water and ethanol through the temperature distribution inside the LHP.
- Comparison the values of total thermal resistance, evaporator thermal resistance and condenser thermal resistance.
- Obtain the evaporator HTC of water LHP and ethanol LHP. In this study, the evaporator HTC was estimated from both of temperature T_{e0} and T_{e-sat} that obtained from the pressure values measured at outlet of evaporator. These results were used to confirm the assumption of boiling phenomenon introduced in chapter 3.

4.1 INTRODUCTION

Because of passive operating characteristics, LHP's performance is influenced by various factors such as the selection of working fluid, filling ratio, wick geometric and thermal properties, cooling and ambient condition, geometric designs of the component [1]. Despite that, the selection of working fluid can be one of the most important parameters because the appropriate working fluid can improve the heat transfer processes in the evaporator and condenser of the LHP or minimize the pressure loss caused by the circulation, so increase the cooling capability. There are many criteria for selecting a working fluid such as the compatibility with LHP's material, good thermal stability, wettability characteristic, suitable operating pressure, high Merit number ($\sigma\rho_l h_{fg}/\mu$), and etc. [2]. In addition, the fluid working in the LHP should also have the high value of derivative dP/dT for the ensuring the LHP start up and operation. Therefore, it is difficult to find out the working fluid that can satisfied all above requirements, but it is important to understand the way that the working fluids effect on performance of not only the LHPs but also each components belonging to the LHP; so, it is possible to find out the appropriate design that can balance the advantage and disadvantage points of each working fluid used in the LHP.

In this study, water and ethanol were selected as the working fluid of LHP. Until now, water has been considered as one of the common working fluids of heat pipe and loop heat pipe due to its advance thermal properties such as high latent heat, high surface tension, low operating pressure, high liquid thermal conductivity, nontoxic fluid. On other hand, there are some disadvantages relating to the thermal properties of water including wettability, high freezing point, small value of derivative (dP/dT). Therefore, this experiment also investigated the thermal performances of LHP charged with ethanol, the fluid has the low freezing point (-114.1°C), larger value of derivative dP/dT , especially the good wettability characteristics. The experiment with two working fluids also aims to confirm the assumption of boiling heat transfer characteristics happening in this kind of evaporator that was mentioned in the chapter 3.

4.2 EXPERIMENTAL SETUP

Table 4.1: Main parameters of LHP

Heating block	
Material	Copper
Mass, kg	4.36
Evaporator base	
Material	Copper
Length x Width x Height, mm	80 x 70 x 8
Active area, mm ²	60 x 45
Evaporator body	
Material	Stainless steel
Length x Width x Height, mm	80 x 70 x 23
Fin geometry	
Cross area, mm ²	2 x 2
Height, mm	1.5
Fin pitch, mm	4
Wick structure [3]	
Material	SUS316
Opening, μm	63
Void ratio, % (measured)	42
Bulk volume, mm ³	50 x 41 x 5
Compensation chamber	
Length x Width x Height, mm	40 x 31 x 18
Vapor line	
OD/ID, mm	6.35/4.35
Length, mm	725
Condenser line	
OD/ID, mm	6.35/4.35
Length, mm	600
Liquid line	
OD/ID, mm	6.35/4.35
Length, mm	110
OD/ID, mm	3.2/1.7
Length, mm	1200
Working fluid amount (ml)	
Ethanol	36
Water	34.5

Table 4.2: Uncertainty values

	Uncertainty
T_1, T_2, T_3	$\pm 0.06^\circ\text{C}$
T_4	$\pm 0.07^\circ\text{C}$
T_{eo}	$\pm 0.06^\circ\text{C}$
T_{ci}	$\pm 0.06^\circ\text{C}$
T_{co}, T_{cci}	$\pm 0.1^\circ\text{C}$
T_{wa-i}	$\pm 0.1^\circ\text{C}$
T_{wa-o}	$\pm 0.06^\circ\text{C}$
T_a	$\pm 0.16^\circ\text{C}$
T_{cw}	$\pm 0.1^\circ\text{C}$
Pressure transducer	$\pm 1.5 \text{ kPa}$
Mass flow meter	0.18% of reading

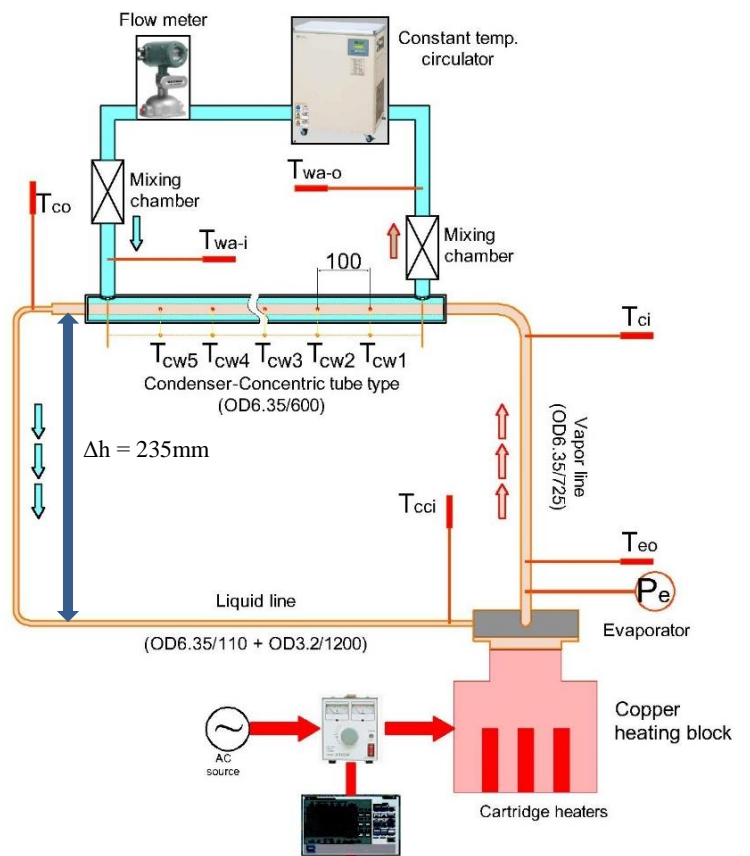


Figure 4.1: Schematic diagram of experiment

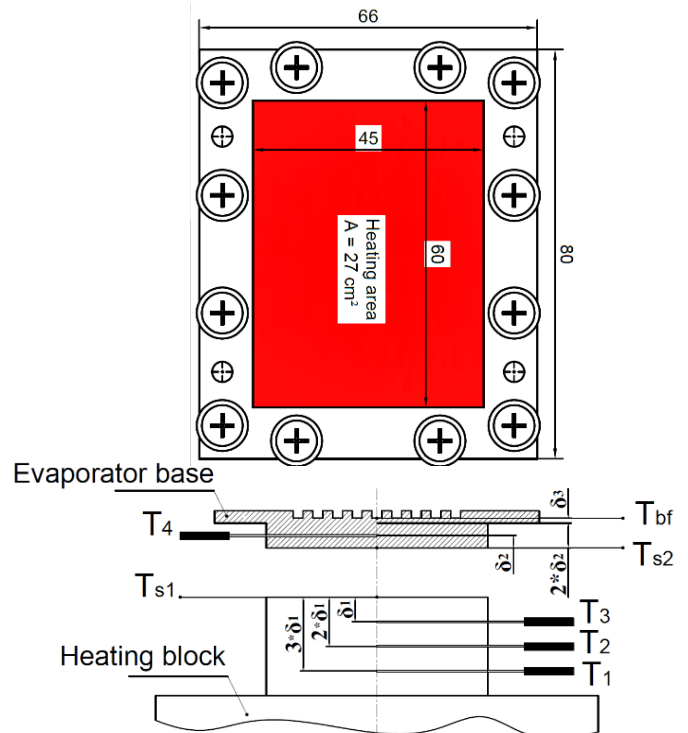


Figure 4.2: Temperature gradient measurement

Figure 4.1 and table 4.1 show the setup of experiment and the main specification of the LHP in this chapter. The assembly and different parts of the evaporator are described in Fig 4.3. Although the way of assembling was changed, the fins or crossing grooves machined on the inner surface of this evaporator has the same geometry and dimension as one belonging to the previous evaporator. The measurement of the temperature of the working fluid inside the LHP and the methods estimating the heating power supplied to the evaporator, the temperatures at the top surface of heating block and bottom surface of evaporator T_{s1} and T_{s2} , at the base fin T_{bf} , and the heat released from the condenser were like the methods used in the experiment introduced in the chapter 3. Moreover, there was a pressure transducer installed at the outlet of the evaporator to detect the pressure of vapor. Five T-type thermocouples including T_{cw1} to T_{cw5} were fixed on the outer wall of condenser to find out the temperature distribution when LHP operated. However, in this experiment the elevation difference between the evaporator and condenser had value at 235 mm. The cooling water was adjusted at the mass flow rate of 35 kg/h and inlet temperature at 25°C.

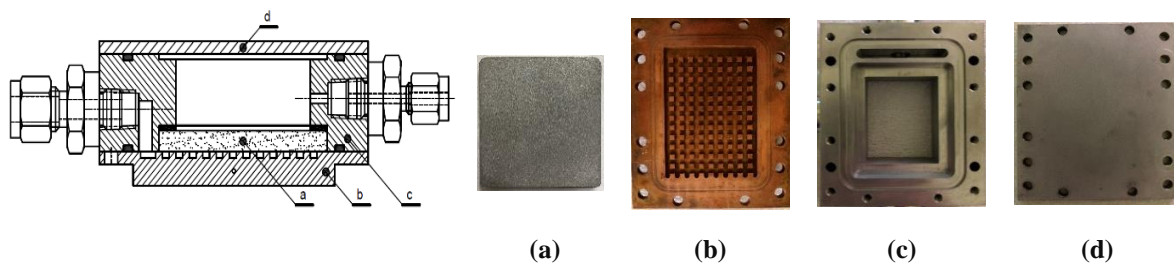


Figure 4.3: Evaporator structure (a) Stainless steel sintered wick (b) The copper base of evaporator (c) The stainless steel body of evaporator (d) The stainless steel cover



Figure 4.4: Real setup of experiment before insulating the evaporator

4.3 DATA REDUCTION

From Fig. 4.2, the values of heat flux q and heat flow rate Q flowing from the heating block to the evaporator can be estimated as follows

$$q = \frac{1}{3} \left(k \frac{\Delta T_{12}}{\delta_1} + k \frac{\Delta T_{23}}{\delta_1} + k \frac{\Delta T_{13}}{2\delta_1} \right) \quad (4.1)$$

$$Q = qA \quad (4.2)$$

Where

- $\delta_1 = 5$ mm, distance between the thermocouples T_1, T_2, T_3
- $A = 27$ cm²

Hence, temperature at the top surface of heating block T_{s1} could be estimated

$$T_{s1} = \frac{1}{3} \left[\left(T_1 - \frac{3(q\delta_1)}{k} \right) + \left(T_2 - \frac{2(q\delta_1)}{k} \right) + \left(T_3 - \frac{(q\delta_1)}{k} \right) \right] \quad (4.3)$$

In combination with the temperature measured by thermocouple T_4 , temperature at the bottom surface of evaporator T_{s2} can be determined

$$T_{s2} = T_4 + \frac{q\delta_2}{k} \quad (4.4)$$

Where $\delta_2 = 2.5$ mm

The values of total thermal resistance R_t , evaporator thermal resistance R_e , condenser thermal resistance R_c , and thermal contact resistance R_{ct} could be estimated by the following equations

$$R_t = \frac{T_{s1} - T_{wa-i}}{Q} \quad (4.5)$$

$$R_e = \frac{T_{s2} - T_{eo}}{Q} \quad (4.6)$$

$$R_c = \frac{T_{ci} - T_{wa-i}}{Q} \quad (4.7)$$

$$R_{ct} = \frac{T_{s1} - T_{s2}}{Q} \quad (4.8)$$

Because vapor flows at high velocity and the vapor pipe was insulated well, the process vapor flowing from outlet of evaporator to inlet of condenser can be recognized as adiabatic process, and temperature difference between T_{eo} and T_{ci} is not noticeable; therefore

$$R_t = R_e + R_c + R_{ct} \quad (4.9)$$

Different with chapter 3, the evaporator HTC obtained from this experiment were determined from two correlations. The first one h_{e-T} was estimated from temperature T_{eo} measured at the outlet of evaporator as mentioned in chapter 3, and the other h_{e-P} was calculated from the saturation temperature T_{sat-P} known from the vapor pressure P_e by REFPROP Ver. 9.1.

$$h_{e-T} = \frac{q}{T_{bf} - T_{eo}} \quad (4.10)$$

$$h_{e-P} = \frac{q}{T_{bf} - T_{sat-P}} \quad (4.11)$$

This method could detect the state of vapor existing at the outlet of evaporator could be saturated vapor or superheated vapor.

T_{bf} in the Eq (4.10) and Eq (4.11), as shown in Fig. 4.2, is temperature at the base of the fins that can be estimated by Eq (4.12)

$$T_{bf} = T_4 - q \left(\frac{\delta_2}{k} + \frac{A\delta_3}{kA'} \right) \quad (4.12)$$

Where $A = 27 \text{ cm}^2$, $A' = 52.8 \text{ cm}^2$, $\delta_3 = 1 \text{ mm}$

A , A' , δ_2 , δ_3 are the dimensions displayed in Fig 4.2

- $A = 27 \text{ cm}^2$, active area of the evaporator
- $A' = 52.8 \text{ cm}^2$, the area determined from the outer dimension of the evaporator
- $\delta_2 = 2.5 \text{ mm}$; $\delta_3 = 1 \text{ mm}$

Appendix D-3 displays the thermal balancing between the heating power and the heat released from the condenser. The relative differences in all experiments of water LHP and ethanol LHP were not higher than 10%. Appendix D-4 presents the temperature gradient corresponding each values of heating power. Following the methodology introduced by Robert J. Moffat [4], uncertainty values of the parameters such as heat flux q , temperature T_{sl} , total thermal resistance R_{ct} , evaporator HTC h_{e-T} and h_{e-P} is shown in appendix E-2 and appendix E-3. When heating power is higher than 150 W, uncertainty values of R_t in the experiments of water LHP and ethanol LHP is not more than 10%.

4.4 RESULTS & DISCUSSIONS

4.4.1 Cooling capacity and performances of water LHP and ethanol LHP

a) Cooling capacity of LHP

In this study, the LHP was charged with ethanol and water respectively. The cooling capacity of LHPs was determined at the conditions that LHPs could be regarded as the fresh LHPs and condenser was cooled by water of which mass flow rate and inlet temperature was adjusted at 35 kg/h and 25°C respectively. The room temperature was maintained around 25°C.

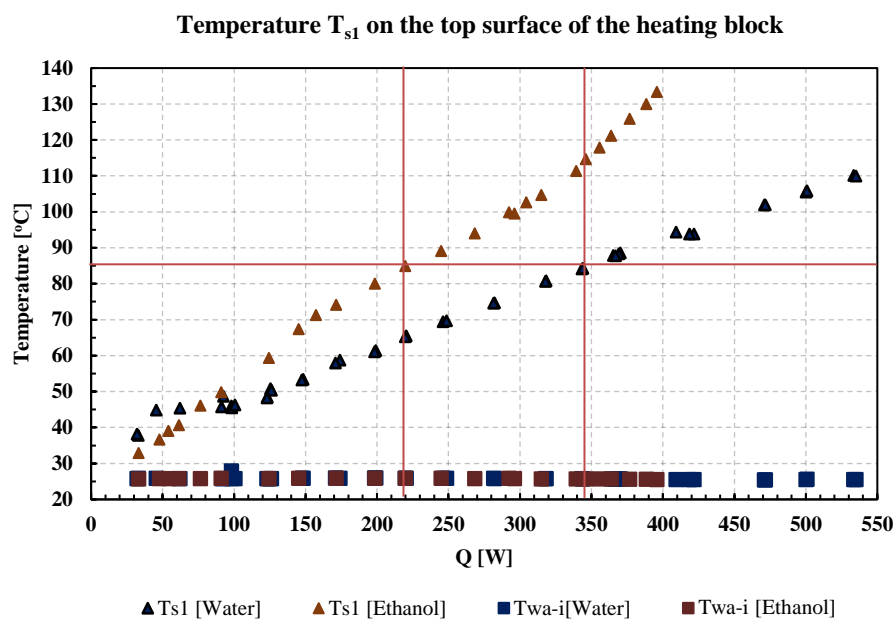


Figure 4.5: Temperature T_{s1} at different heating power in the experiments of water LHP and ethanol LHP

Figure 4.5 displays values of temperature on the top surface of the heating block T_{s1} when it was cooled by ethanol LHP and water LHP respectively. It is sure to affirm that temperatures of cooling water at inlet of condenser were maintained constant in different experiments of water LHP and ethanol LHP. As the whole, water LHP had the better performance than ethanol LHP except for the range of heating power below 90 W. The water LHP could maintain the temperature T_{s1} not to be more than 110°C when the heaters generated heat at the rate from 33 W to 530 W, but in the experiment of ethanol LHP, this temperature reached 133°C at the heating power of 395 W only. The ethanol LHP functioned better than the water LHP when heat generated at the rate smaller than 75 W. With the definition of cooling capacity of electronics cooling device mentioned in chapter 3, the ethanol LHP could keep temperature T_{s1} under 85°C when transferring heat at the rate lower than 220 W; on the other hand, the water LHP could satisfy this condition when transferring heat at the rate of 350 W from the heating block to the cooling water. Although there were some little changes in experiment setup (the

elevation difference between the evaporator and condenser), design of the evaporator as well as condenser cooling condition comparing with the experiment introduced in chapter 3, cooling capacity of water LHP obtained from two experiments were not significantly different.

b) Thermal performance of LHP

Thermal performance or the characteristics of the circulation of working fluid inside the LHP can be evaluated through the temperatures of working fluid that were measured at different positions such as outlet of evaporator T_{eo} , inlet of condenser T_{ci} , outlet of condenser T_{co} and inlet of compensation chamber T_{cci} .

The values of temperatures shown in Fig. 4.6 & Fig. 4.7 indicate that although the ethanol LHP could not function at the heating power that is as high as the water LHP could, the operation and fluid circulation of ethanol LHP seems to be more stable than in the case of water LHP. This conclusion can be made from the results that in the range of heating from 150 W to 275 W, the average temperature of water returning the CC T_{cci} was higher than temperature of water flowing out the condenser T_{co} . In the ethanol LHP experiment, the values of T_{co} were equal to T_{cci} at each heating power conditions. In addition, from Fig. 4.6, the temperature T_{cci} in the water LHP also behaved the complex fluctuations with various amplitudes. These measured data indicate that between the inlet of CC and the position of thermocouple T_{cci} there was the fluctuated movement of the L-V interface. The fluctuation of T_{cci} also caused the temperature T_{ci} , T_{eo} and T_4 to oscillate; however, the oscillation of T_4 was not noticeable and could be regarded as stable operation. The magnitude and the effect of T_{cci} fluctuation on the vibration of T_4 , T_{eo} and T_{ci} become weaker when heat supplied to the evaporator increases. In the experiment of ethanol LHP, there was no appearance of oscillation of T_{cci} (Fig. 4.9)

However, in the experiment of water LHP, working fluid flowing out of the condenser had temperatures that was not different noticeably with the inlet temperature of cooling water, but this difference became larger with heating power in the case of ethanol LHP. This result shows that the cooling characteristic of the condenser operating with ethanol was less effective than one with water. It is one of the reasons that make the ethanol LHP could not working as powerfully as the water LHP could.

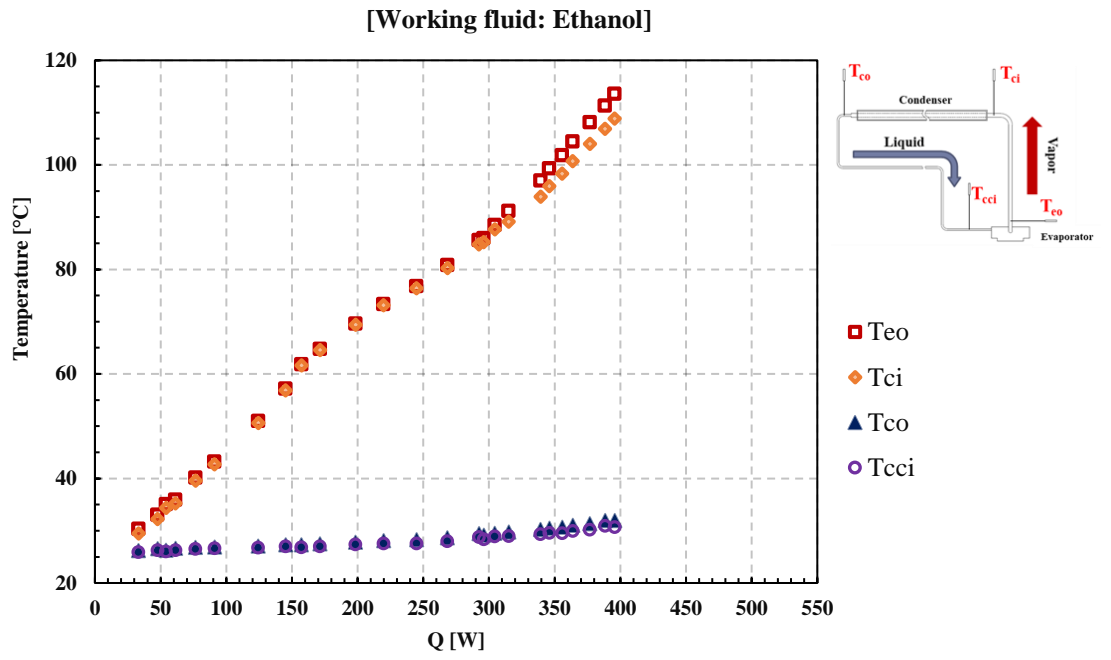


Figure 4.6: Temperature distribution of working fluid inside the ethanol LHP

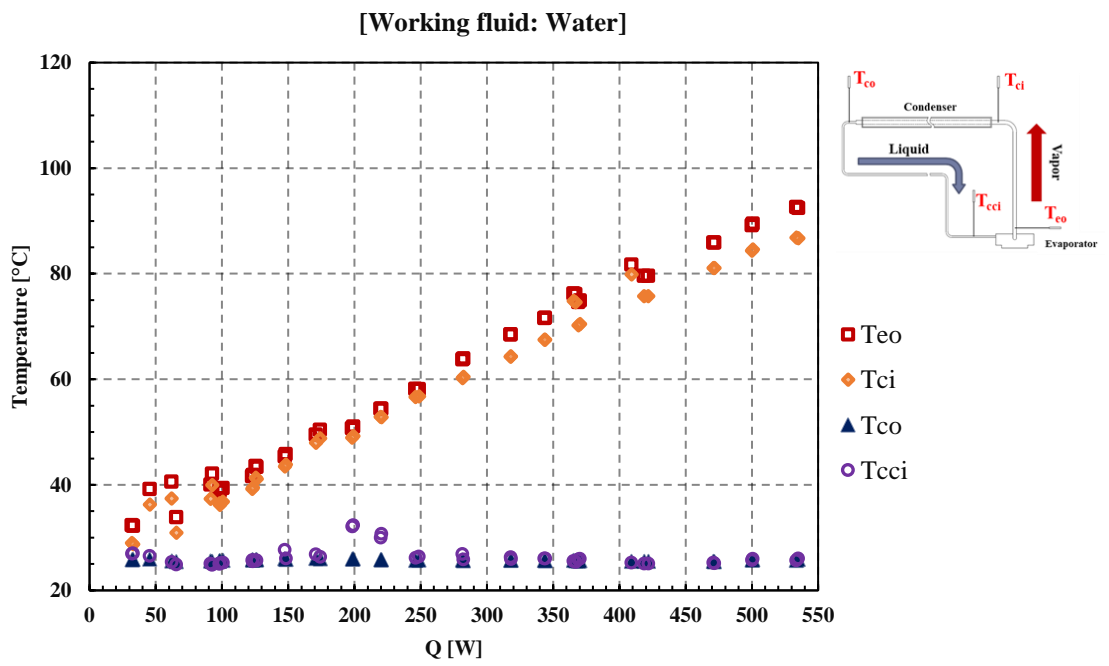


Figure 4.7: Temperature distribution of working fluid inside the water LHP

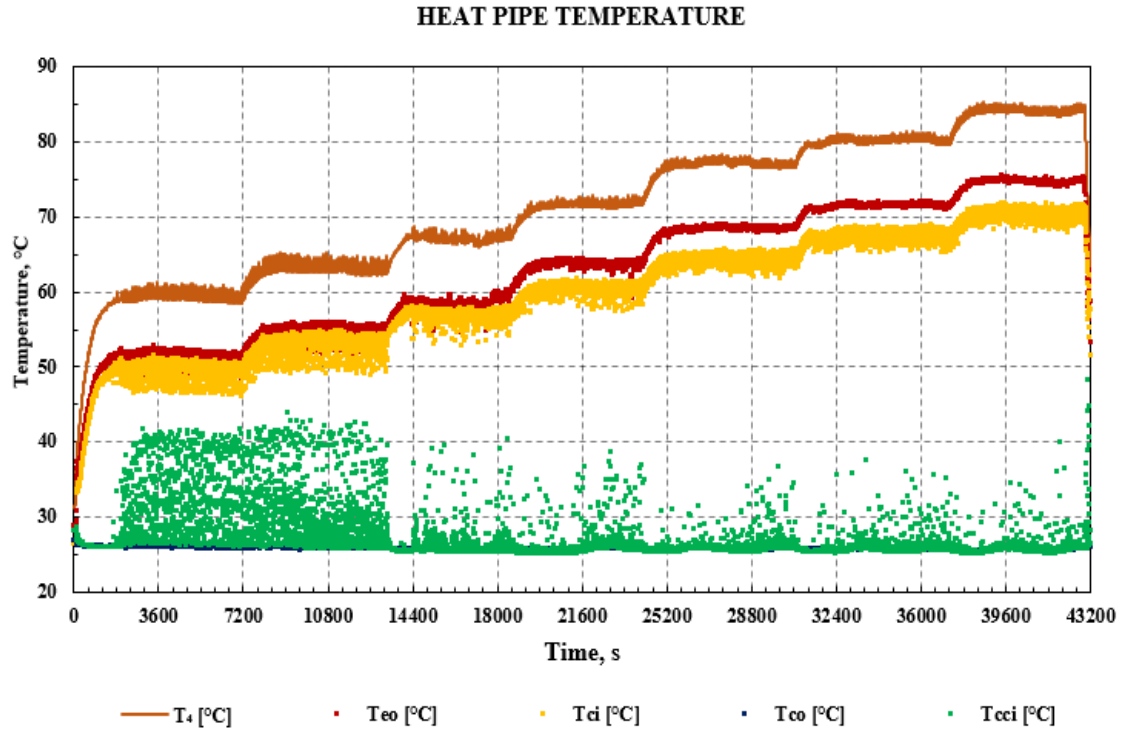


Figure 4.8: Temperature distribution inside the water LHP (from 200 to 350 W, interval: 25 W)

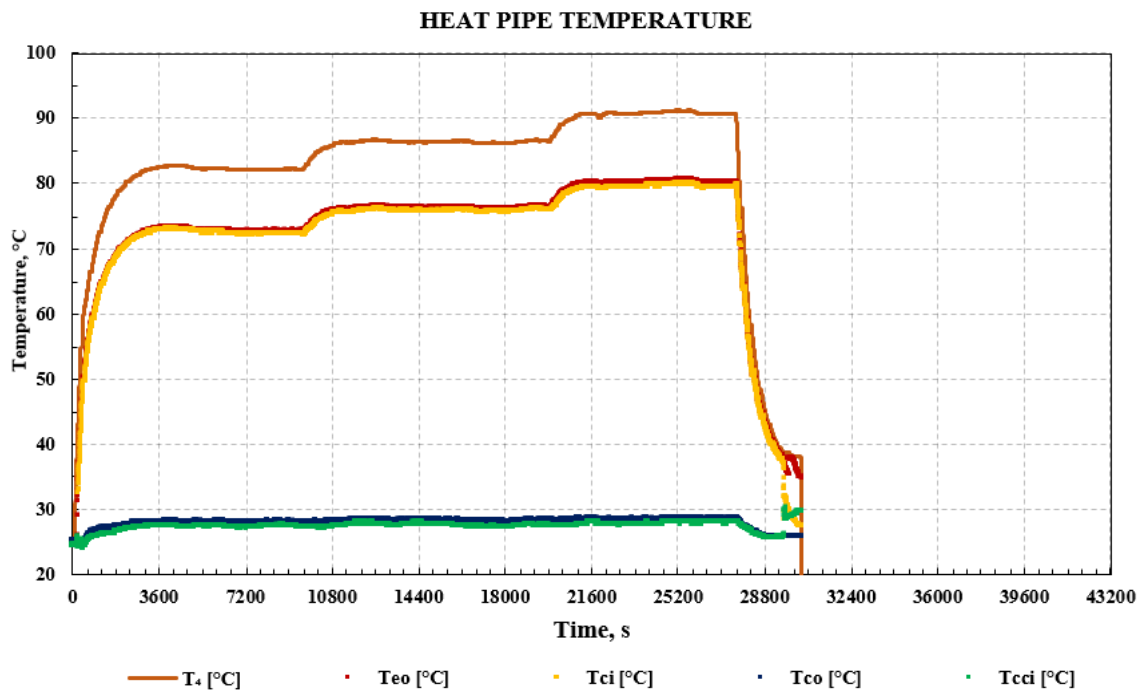
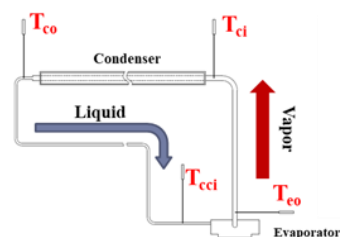


Figure 4.9: Temperature distribution inside the ethanol LHP (from 200 to 250 W, interval: 25 W)



T_4 : temperature at the base of the evaporator
 T_{eo} : Temperature at the outlet of the evaporator
 T_{ci} : Temperature at the inlet of the condenser
 T_{co} : Temperature at the outlet of the condenser

4.4.2 Thermal resistances comparison

This section compares total thermal resistance R_t , thermal resistances of evaporator R_e , condenser thermal resistance R_c and contact thermal resistance R_{ct} obtained from experiments of ethanol LHP and water LHP.

a) The change of total thermal resistance with heating power

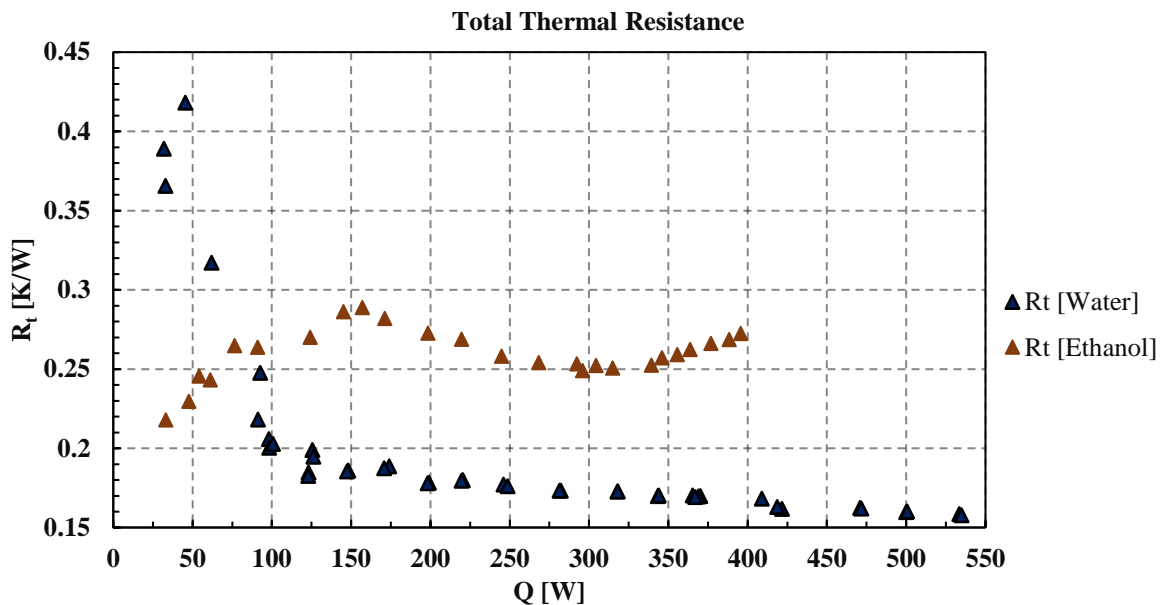


Figure 4.10: Total thermal resistance of water and ethanol LHP varied with heating power

Figure 4.10 displays how the total thermal resistance R_t of the water and ethanol LHP varies with values of heating power. It agrees with the previous discussion that the water LHP operated better than ethanol LHP when heating power supplied to the evaporator was more than 90 W. With the water LHP, values of R_t changed within the tendency that becomes smaller with the increase of heating power, especially it reduced significantly from 0.418 to 0.2 K/W when heat supplied to the evaporator increased from 30 to 100 W. At the heating power of 535 W, this thermal resistance had the value of 0.159 K/W. This value was slightly higher than minimum value of R_t 0.149 K/W obtained in the experiment of chapter 3. On the other hand, the change of total thermal resistance R_t with heating power gotten from the ethanol LHP was not like what behaved in the experiment of water LHP. Only in the range of heat power from 150 to 300 W, values of R_t reduced with the increasing of heating power, while it almost raised up under the rest operating conditions. The ethanol LHP had the minimum value of R_t at 0.218 K/W when functioning at the heating power of 33W. The following sections will explain

more detail about the differences in performance of each LHP's components when working with ethanol and water.

b) The change of the evaporator thermal resistances with heating power

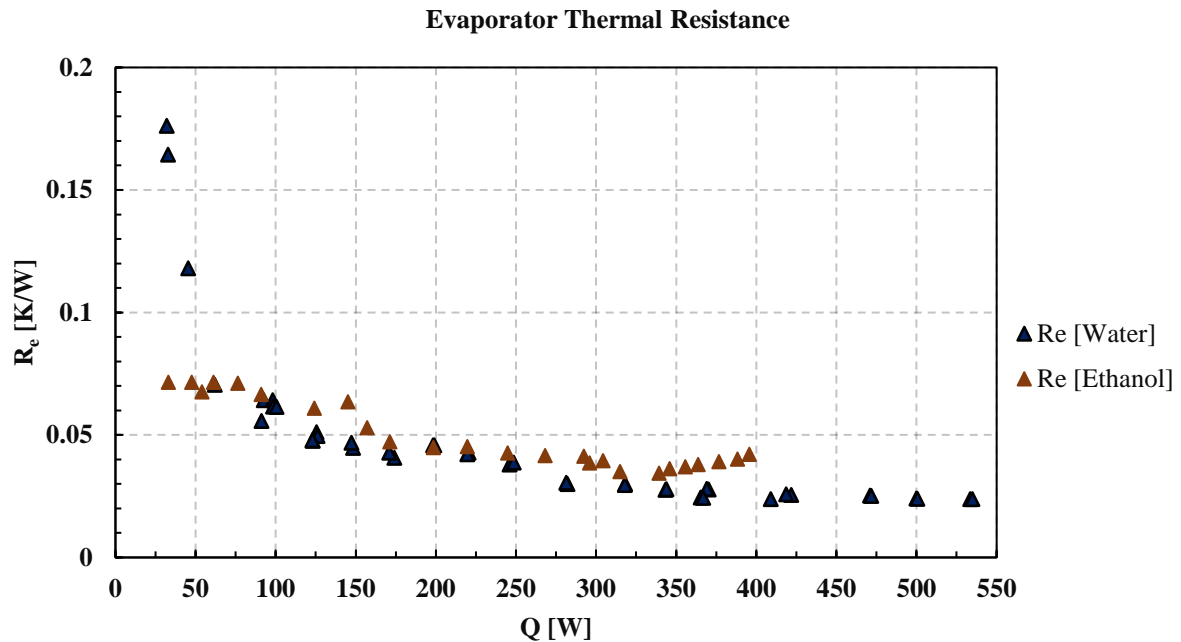


Figure 4.11: Changing of evaporator thermal resistance on heating power in the experiments of water and ethanol LHP

The variation of evaporator thermal resistance R_e with heating power values in the experiment of water and ethanol LHP is displayed in Fig 4.11. Generally, the evaporator behaved almost same characteristics when operating with water and ethanol. In the range of heating power from 90 to 300 W, there was no notable difference in both of values and changing tendency of thermal resistance values between the evaporators functioning with water and ethanol. In this region, the higher heating power is generated from the heaters, the smaller values of evaporator thermal resistance become. However, there were still some distinct behaviors happening. The evaporator operating with ethanol performed more effectively than one with water when heating power was not higher than 90 W. Further, in the range that heating power was higher than 300 W, when raising up the supplied heat, the ethanol evaporator increased its thermal resistance while thermal resistance of water evaporator continued decreasing little. Besides, observing the Fig. 4.10 and 4.11, it can be concluded that in the case of ethanol LHP, performance of the evaporator affects weakly on total performance of the LHP, particularly in the range of heating power from 33 to 150 W. On the other hand, with the water LHP, the high

thermal resistance of the evaporator contributes significantly to the total thermal resistance of LHP when heating power was less than 90 W.

c) The change of the condenser thermal resistances with heating power

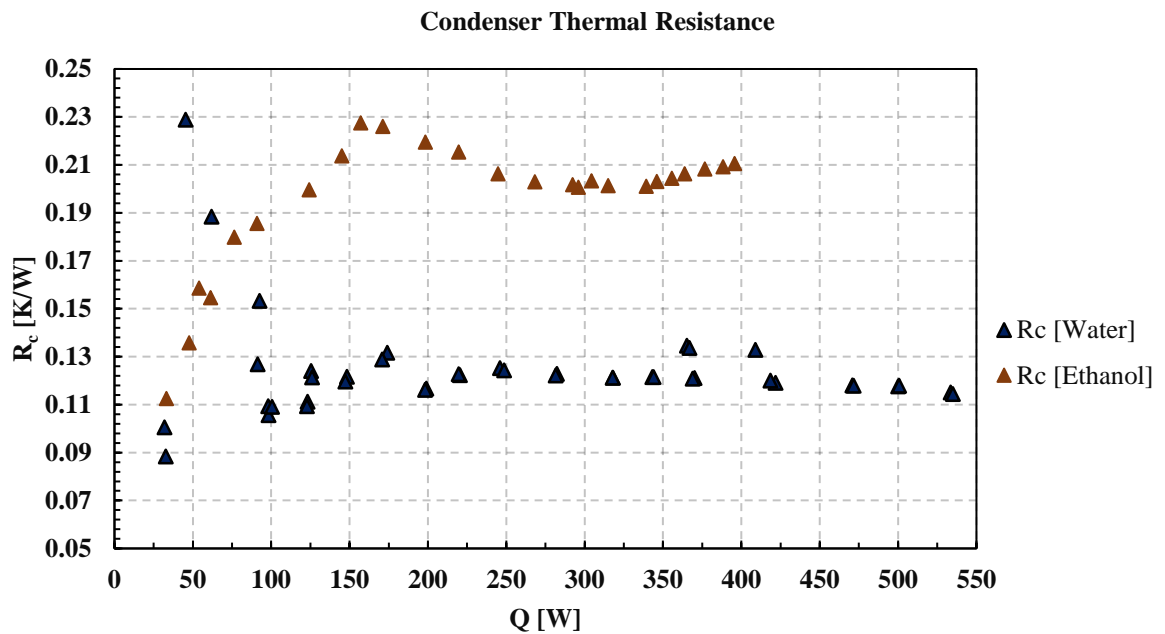


Figure 4.12: Changing of condenser thermal resistance on heating power in the experiments of water and ethanol LHP

The effect of heating power on the condenser working in ethanol LHP and water LHP is presented by Fig 4.12. Comparing with Fig 4.10, it can be concluded that thermal performances of LHPs are dominated strongly by the heat transfer process at the condenser, especially in the case of LHP charged with ethanol. The high thermal resistance existing at the condenser of the ethanol LHP can be recognized as the main reason causing the cooling capacity of this LHP to be lower than water LHP. Moreover, the tendencies that the condenser thermal resistance varied with the heating power were clearly different between the cases that water and ethanol were charged to the LHP. With the water LHP, values of R_c reduced strongly within the low heating power region, then became almost constant in the high heating power range, but the thermal resistance of the condenser belonging to ethanol LHP raised up when heating power was increased. The difference in the thermal properties of water and ethanol can be used to explain this result. Basing upon the Chato correlation (Eq (4.13)) [5], because water has higher latent heat and liquid thermal conductivity, at the same rate of heat released from condenser the thickness of ethanol liquid condensing must be more than in the case of water, and this layer becomes the resistance preventing the heat transfer process from the vapor to cooling

water. Moreover, the low vapor density of water that makes vapor velocity higher is also another reason that explain why the condenser working with water had the lower thermal resistance.

Condensation HTC estimated by Chato correlation

$$\bar{h}_c = 0.555 \left[\frac{g \rho_l (\rho_l - \rho_v) k_l^3 h'_{fg}}{\mu_l (T_{sat} - T_s) D} \right] \quad (4.13)$$

Where: $h'_{fg} = h_{fg} + \frac{3}{8} c_{p,l} (T_{sat} - T_s)$ (4.14)

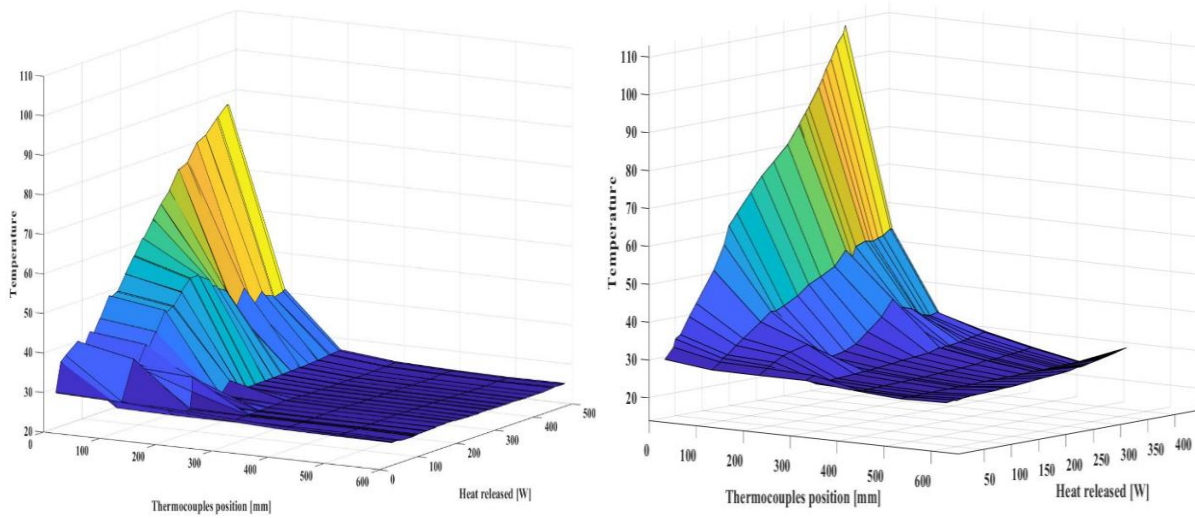


Figure 4.13: Temperature distribution on the outer wall of condenser (a) water LHP (b) ethanol LHP

Thermocouples' positions:

0 mm (inlet of condenser): T_{ci} , 100 mm: T_{cw1} , 200 mm: T_{cw2} , 300 mm: T_{cw3} , 400 mm: T_{cw4} , 500mm: T_{cw5} ,
600 mm (outlet of condenser): T_{co}

In this experiment, five T-types thermocouples from T_{cw1} to T_{cw5} were fixed on the outer wall of condenser to detect the temperature distribution along the length of the condenser. The distance between two thermocouples was 100 mm. Measured values obtained from these thermocouples are shown in Fig. 4.11. The condenser working with water had the shorter two-phase flow region or the heat transfer area for condensation being smaller than one working with ethanol. However, at the low heat power condition, condensation process of water also took half of the condenser's length; consequently, the pressure loss becomes higher which can increase both the pressure and saturation temperature of vapor before entering the condenser. Therefore, the condensation thermal resistance of condenser operating with water would be higher under these heating power conditions.

d) Thermal contact resistance

Although both the evaporator's bottom and the top surface of heating block are the flat surfaces, and a thin layer of thermal conductivity grease was used to minimize the thermal resistance caused by contact condition, it is impossible to ignore this resistance. From the temperature gradient measured by three thermocouples T_1 , T_2 and T_3 and the temperature T_4 measured at the evaporator base, it is possible to estimate the thermal contact resistance.

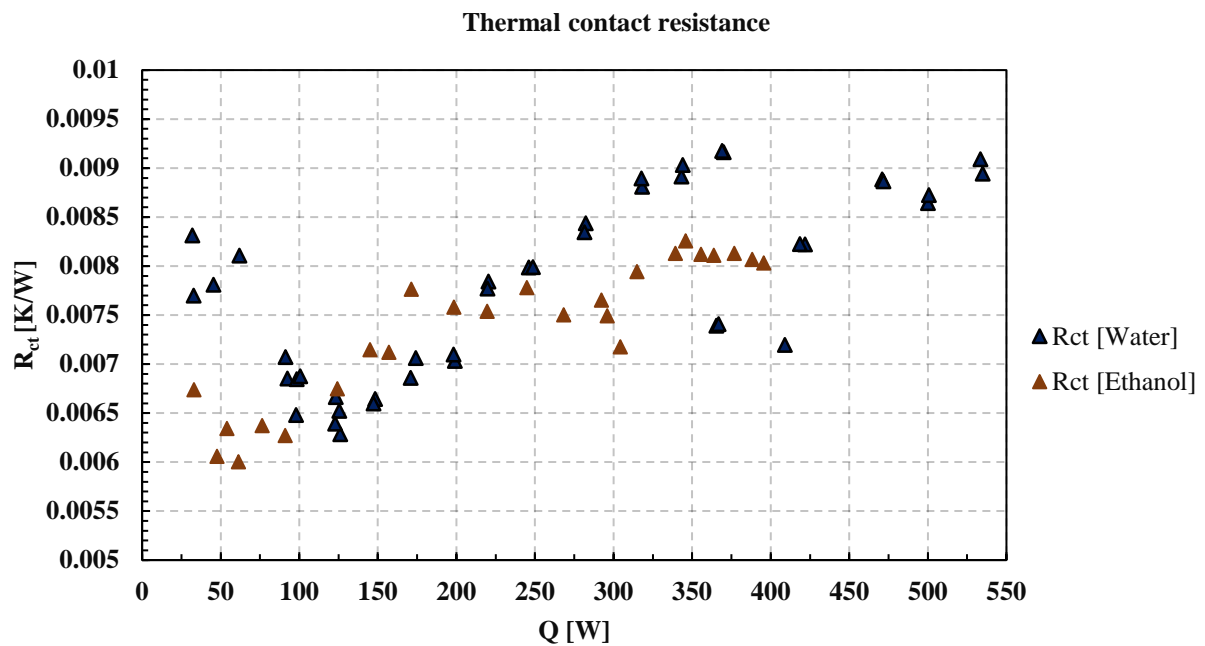


Figure 4.14: Thermal contact resistance

The results in Fig 4.14 shows that values of thermal contact resistance R_{ct} at various heating power conditions in both of experiments of water LHP and ethanol LHP were not notably different and mostly changed in the range from 0.006 K/W to 0.0092 K/W. Although the experiment of ethanol LHP and water LHP were conducted separately, the R_{ct} in two cases had almost same value or this thermal resistance had the same effect on the cooling capacity of ethanol and water LHP. These results also agreed with the thermal contact resistance obtained in chapter 3.

4.4.3 Evaporator heat transfer coefficient and the boiling characteristics of evaporator operating with water and ethanol

In this study, the evaporator HTC was estimated from the temperature T_{eo} of vapor at the outlet of the evaporator and the saturation temperature T_{sat-P} obtained from the pressure of the vapor measured by the pressure transducer installed in front of thermocouple T_{eo} .

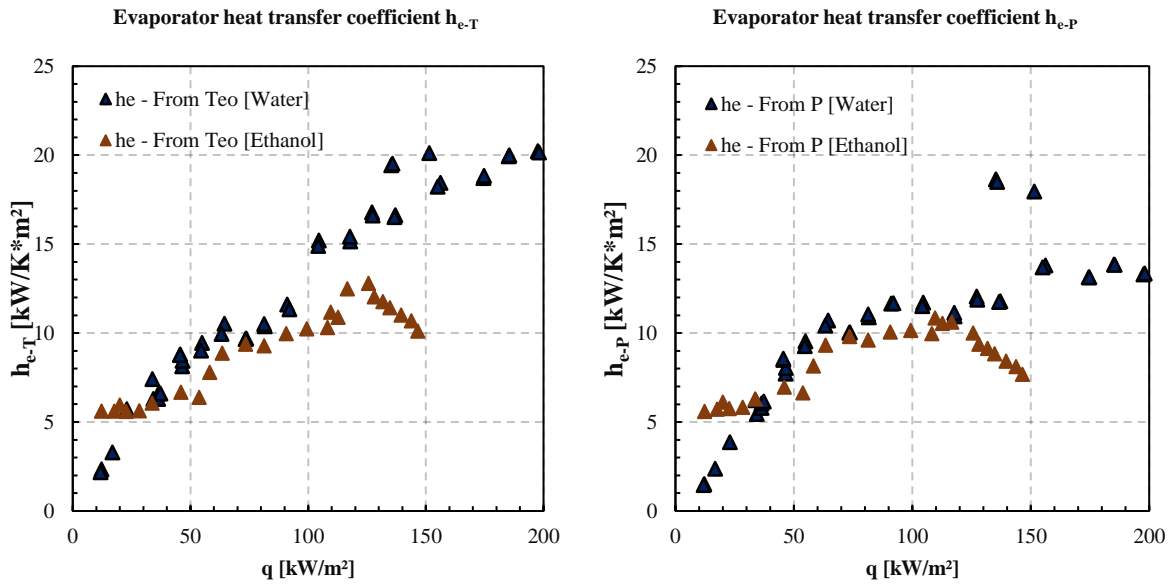


Figure 4.15: Evaporator HTC in the in the experiments of water and ethanol LHP

- a) Estimated from temperature at the outlet of evaporator T_{eo}
- b) Estimated from saturated temperature T_{sat-P}

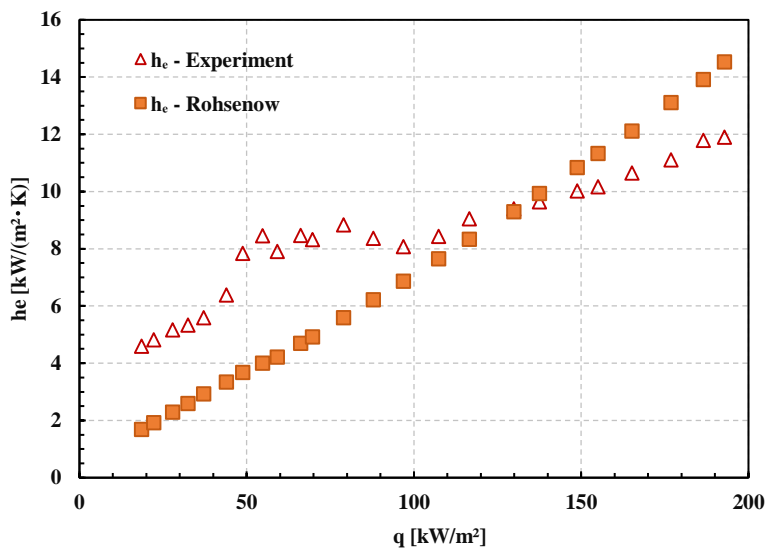


Figure 4.16: Evaporator HTC in the in the experiment introduced in chapter 3 (water is working fluid)

In the range of heat flux lower than 100 kW/m^2 , there was no notable difference between the results determined by the two Eq (4.10) & (4.11) in both experiments of water and ethanol LHP. It indicates that vapor flows out the evaporator almost existed at the saturated state without superheated process. When heat flux was increased to be higher than 100 kW/m^2 , evaporator HTC obtained from T_{eo} was higher than values calculated from saturation temperature T_{sat-P} . The difference in these results shows that the vapor might be superheated before leaving the evaporator. The heat for superheated progress can be came from the surround

area of the fins and the groove's surface where do not contact with the wick's body. From this explanation, it can be withdrawn that with this design of evaporator when the heat flux is higher than 100 kW/m^2 , the working fluid almost boiled on the fin's tip surface or the interface between the wick and the fins. This result confirms the assumption of boiling characteristics in this evaporator that was introduced in previous chapter.

Comparing the evaporator HTC in the experiments of water and ethanol LHP, the evaporator operating with ethanol had the higher heat transfer coefficient when the heat flux was smaller than 30 kW/m^2 . The high surface tension of water could make the formation and growing of the bubble more difficult under small heat flux condition; consequently, it requested the higher excess temperature for the boiling to happen. In the range of 30 to 100 kW/m^2 heat flux, the evaporator HTC of water LHP was higher than values of ethanol LHP a little. The noticeable difference occurred when the value of heat flux was higher than 100 kW/m^2 . Because the heat transfer coefficient calculated from Eq (4.10) does not consider the superheated process, the performance of the evaporator should be discussed based upon the results shown in Fig. 4.13(b). When functioning under this condition, the evaporator HTC in the experiment of water LHP increased little with the increment of heat flux, but this parameter reduced in the case of ethanol LHP. The reason for dissimilar performance can be revealed by the assumption described in Fig. 4.17.

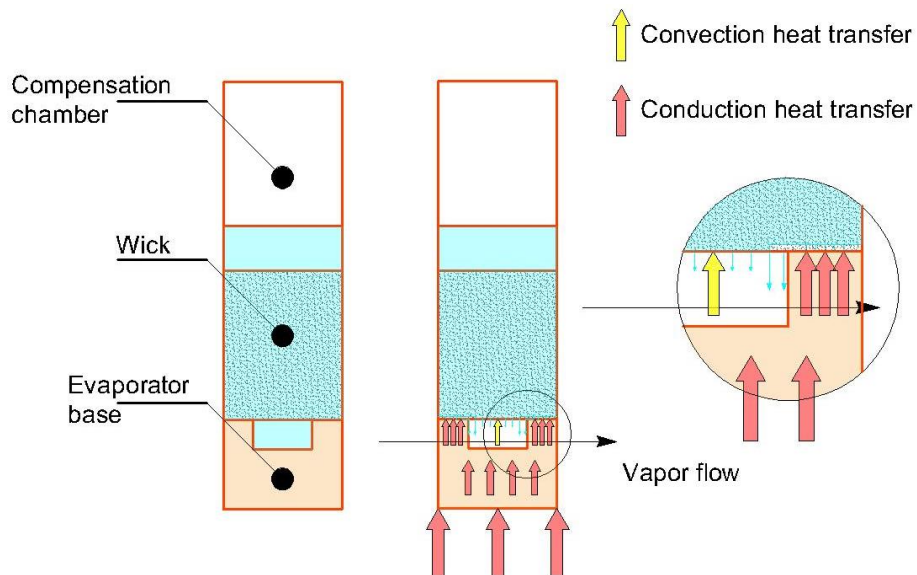


Figure 4.17: Assumption about boiling heat transfer mechanism under condition that heat flux is higher than 100 kW/m^2

As mentioned in the above discussion, when heat flux is larger than 100 kW/m^2 , the boiling almost happens at the surface where the wick and the fins contact together. Because of this characteristic, the evaporator HTC will be influenced by some disadvantage sides such as the heat flux on the fin's tip became higher, and a thin layer of vapor that may form on the tip surface of the fin makes the liquid more difficult in receiving heat for evaporation. Particularly, in the case of ethanol because of the small surface tension, it cannot create the menisci having enough area for evaporation process as the liquid having high surface tension like water can do. Consequently, the ethanol vapor layer will be thicker and excess temperature becomes higher. Furthermore, the convection heat transfer is also an aspect that should be focused. Although almost heat had to flow through the fin to the liquid in the wick by conduction, there is some heat transferred to the wick by convection and radiation as displayed in Fig. 4.17. This mechanism of heat transfer can improve the boiling characteristic by promoting the boiling happening on the non-contact surface of the wick. It means that the wick surface can be utilized effectively for the boiling, so the “boiling load” on the contact surfaces could be reduced. If the effect of radiation is regarded to be similar, the difference in convection heat transfer when water and ethanol were working fluid contributes to make the evaporator behave differently. Because ethanol has the higher product of $(h_{fg}\rho_v)$ than water, at the same heat flux, vapor velocity flow through the groove will be slower than the water vapor (Eq. 4.15). As the results, the promotion of boiling by the convection in the case of ethanol is weaker than water. The above assumption explains why under the condition that heat flux was more than 100 kW/m^2 , the evaporator heat transfer coefficient in the experiment of water LHP increased slightly with the increment of heat flux while this parameter reduced in the ethanol LHP's experiment.

Velocity of vapor flowing in the vapor removal channel

$$\omega_v = \frac{Q}{A_v h_{fg} \rho_v} \quad (4.15)$$

4.5 CONCLUSION

In this study, LHP with the second pattern of evaporator was fabricated and investigated its performances when working with two different fluids including water and ethanol. All of experiments were conducted under the same condenser cooling condition. The experimental results demonstrate that as a whole, the water LHP had the better cooling performance than ethanol LHP except for the range of heat power lower than 90 W. The water LHP could maintain the temperature at the top surface of the heating block smaller than 85°C when operating under heat power of 350 W; on the other hand, the ethanol LHP could satisfy this

condition when the heat power was around 220 W only. Among various components of thermal resistance, the condenser thermal resistance was the component that dominates most on the LHP's performance, especially in the case of the ethanol LHP. For the water LHP, at the low heat power operating condition, the evaporator thermal resistance also contributed significantly to the total thermal resistance of the LHP because of the high surface tension characteristic that could make the formation and growing process of the bubble difficult. In addition, the results of the evaporator heat transfer coefficient obtained from the experiments of water and ethanol LHP in this study also confirmed for the assumption of boiling heat transfer characteristics that presented in the previous study. Moreover, the assumption about the effect of convection heat transfer mechanism on the boiling heat transfer when heat flux was more than 100 kW/m² was also considered in this study to explain the difference in changing evaporator HTC with heat flux when LHP was charged with water and ethanol.

REFERENCES

- [1] S. Launay, V. Sartre, and J. Bonjour, "Parametric analysis of loop heat pipe operation : a literature review," vol. 46, pp. 621–636, 2007.
- [2] R. M. David Reay, Peter Kew, *Heat Pipe Theory, Design, and Applications*, Sixth Edit. 2014.
- [3] SMC Coporation, Sinter metal element (EB/ES Series), pp. 103–118 [cited 2017 Nov. 27th]
- [4] R. J. Moffat, "Describing the uncertainties in experimental results," *Exp. Therm. Fluid Sci.*, vol. 1, no. 1, pp. 3–17, 1988.
- [5] D. P. Incropera, Frank P., DeWitt, *Fundamentals of heat and mass transfer*. Hoboken, NJ : John Wiley & Sons, 2007.

Chapter 5

LHP Performance Under Horizontal Orientation – The First Pattern of Evaporator

In this chapter, thermal performance of LHP with the first pattern of the evaporator operating under horizontal orientation with various operating conditions such as different heating powers and temperatures of cooling water was investigated by experiment. The evaporator was equipped with the stainless-steel sintered wick, and water was charged to the LHP. When LHP's condenser was cooled by water at 28.5°C, the LHP could operate in the range of heating power from 10 to 94 W and maintained the temperature on the top surface of the heating block T_{sl} lower than 100°C; however, the LHP demonstrated the weak oscillating behavior of T_{cci} as well as serious long startup progress under heat load at 10 W. Experimental results also show that the total thermal resistance R_t obtained when LHP was cooled by water at 36.5°C and 28.5°C had the same values, and were smaller than the case that cooling water was set at 18.5°C. It can be explained because when functioning at horizontal orientation, the performance of LHP will be dominated by the pressure in the CC P_{cc} more than the temperature of cooling water. On the contrary, when cooled by water at 36.5°C, LHP cannot operate stably under heat load at 90 W due to hotter liquid returns to compensation chamber and reduce the wick cooling effect when comparing with the other cases.

5.1 INTRODUCTION

LHP, a passive two-phase flow heat transport device, was developed firstly by Gerasimov and Maydanik in 1972[1]. Due to owning the advantage features that are high heat transport capacity, flexible characteristics, none work consumption for circulation of working fluid, LHP was quickly used in thermal management systems belonging to the spacecraft or satellites such as AURA (2004), ICESat (from 2003 to 2010), SWIFT (2004), etc...[2]. Moreover, LHP now is also considered as one of the potential solutions that can satisfy the cooling demand of the electronics working on the earth such as processors in data center [3], the high-power IGBT elements [4], or the LED light [5]. However, until now the situation of LHP application has not reached the commercial state as the conventional heat pipe does. Maybe only the company Calyos [6] that has been created in 2012 in Belgium (Europe) develops the LHP for electronics cooling. One of the reasons can be the complicated structure of the evaporator, especially the capillary structure. In the normal LHP, it is often to see the vapor grooves machined on the wick surface that causes the possibility of error become higher, and the changing of characteristics of wick surface such as number of pore and pore size, roughness, wettability. The study of H. Li et al [7] shows that when the wick surface was machined by the lathing method, the influence of lathing on the wick was not only on the machined surface but also the neighboring area. The machined surface is tearing and most of pore will be blocked. In the study of S.C. Wu et al [8], the cylindrical nickel sintered wick was damaged when they tried to increase the number of grooves from eight to sixteen. As a result, the cost of fabricating will be higher, and the economic competition of the LHP is no longer attractive. Consequently, simplifying the structure of the LHP's evaporator is one of the important features that make the LHP become more popular in the market. Therefore, the design of the flat – rectangular evaporator with the crossing grooves machine on the inner wall was proposed in this study.

The results obtained in previous chapters demonstrate that the LHP with the evaporators designed by our group can satisfied the cooling requirement for the electronics such as the processor functioning in the data center when operating under gravity assisted condition. This LHPs can take the heat generated from the heater at the rate of 350 W (12.9 W/cm^2) and keep the temperature on the top surface of the heating block not over 85°C while the condenser was cooled by the water at the temperature from 25°C to 28.5°C . This chapter continues investigating the thermal performance of the LHP with the first pattern of evaporator when functioning horizontally or evaporator was installed at the same elevation with the condenser.

The experiment also found out the effect of the inlet temperature of cooling water on the LHP's performance.

5.2 EXPERIMENTAL SETUP & DATA REDUCTION

5.2.1 Experimental setup

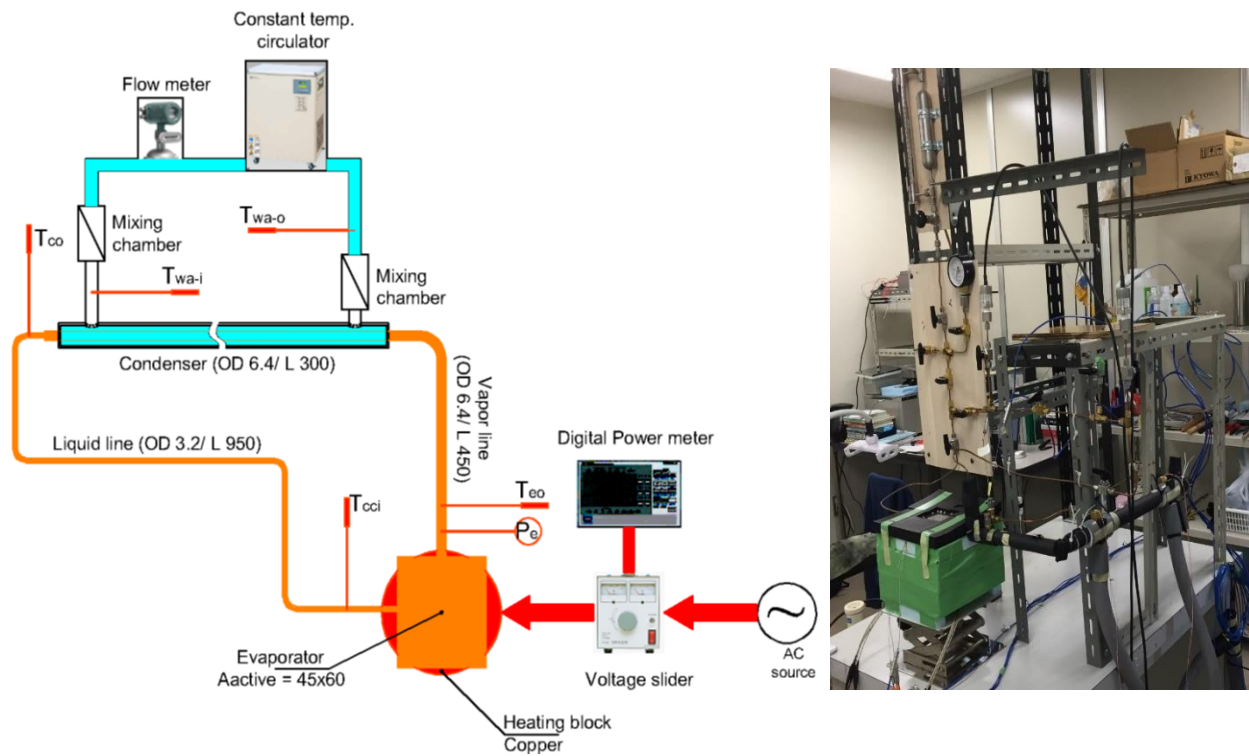


Figure 5.1: Schematic of experiment and the real setup

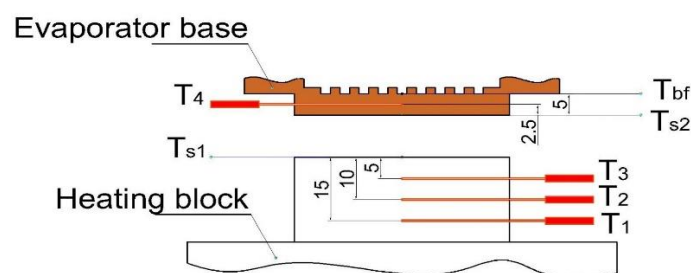


Figure 5.2: Temperature gradient measurement

Figure 5.1 demonstrates the schematic of experiment with the dimensions of vapor line, condenser and the liquid line. The experiment had similar setup to one mentioned in chapter 3 and 4 except the evaporator and the condenser were installed at the same elevation. The heating power supplied to the evaporator were adjusted by the voltage slider and the digital power meter. The condenser was cooled by water whose mass flow rate and inlet temperature were

controlled by the constant temperature circulator. However, because of operation under horizontal orientation, the heat transfer capacity of the LHP could reduce significantly, so the condenser length of this LHP was 300 mm instead of 600 mm as in the case of operation under gravity assisted condition. Similarly, three thermocouples T_1 , T_2 , T_3 were used to measure the heating power and the heat flux flowing from the heating block to the evaporator as well as the temperature on the top surface of the heating block T_{s1} . Combination with the value of temperature T_4 , it was possible to estimate temperature at the bottom surface of the evaporator T_{s2} and temperature at the base of the fins T_{bf} . Along the LHP body, there were three thermocouples inserted directly at the three different positions such as outlet of evaporator T_{eo} , outlet of condenser T_{ci} and inlet of compensation chamber T_{cci} . Heat released from the condenser was calculated from the mass flow rate and temperature different of cooling water measured by the mass flowmeter and two thermocouples T_{wa-i} and T_{wa-o} .

In this experiment, cooling water was adjusted at the mass flow rate at 30 kg/h and the inlet temperature T_{wa-i} was changed at various values including 18.5°C, 28.5°C and 36.5°C.

5.2.2 Data reduction

Heat flux q and heat flow rate Q flowing through the heating surface to active area A (27 cm²) of evaporator

$$Q = qA = \frac{1}{3} \left[k \left(\frac{T_1 - T_2}{\delta_1} \right) + k \left(\frac{T_2 - T_3}{\delta_1} \right) + k \left(\frac{T_1 - T_3}{2\delta_1} \right) \right] A \quad (5.1)$$

Temperatures at the top surface of the heating block T_{s1} and bottom face of evaporator T_{s2} (Fig. 5.2)

$$T_{s1} = \frac{1}{3} \left\{ \left(T_1 - 3 \frac{q\delta_1}{k} \right) + \left(T_2 - 2 \frac{q\delta_1}{k} \right) + \left(T_3 - \frac{q\delta_1}{k} \right) \right\} \quad (5.2)$$

$$T_{s2} = T_4 + \frac{q\delta_2}{k} \quad (5.3)$$

Total thermal resistance R_t and evaporator thermal resistance R_e

$$R_t = \frac{T_{s1} - T_{wa-i}}{Q} \quad (5.4)$$

$$R_e = \frac{T_{s2} - T_{eo}}{Q} \quad (5.5)$$

The evaporator HTC h_e

$$h_e = \frac{q}{T_{bf} - T_{eo}} \quad (5.6)$$

In the Eq. (5.6), T_{eo} was considered as saturation temperature of vapor in the evaporator. As being described in Fig. 5.2, T_{bf} is the temperature at the base of the fins or the surface of the groove which can be estimated by the below equation

$$T_{bf} = T_4 - \frac{q\delta_2}{k} \quad (5.7)$$

5.3 RESULTS AND DISCUSSIONS

5.3.1 Performance of LHP when cooled by water at 28.5°C

a) Startup of the LHP

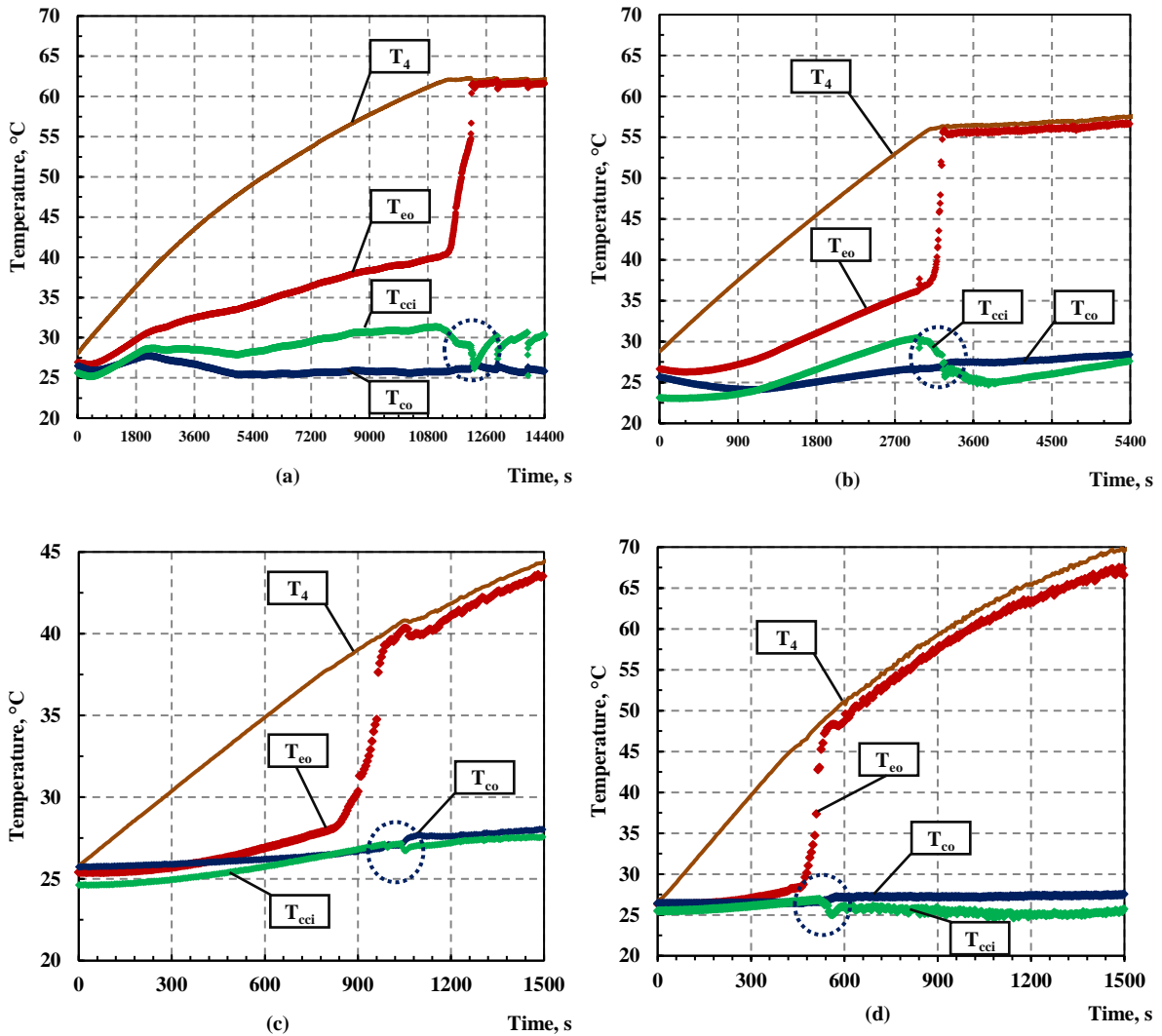


Figure 5.3: Startup progresses of LHP at different heating power a) 10 W; b) 20 W; c) 30 W; d) 90 W

T_4 : temperature at the base of the evaporator; T_{eo} : temperature at the outlet of the evaporator

T_{co} : temperature at the outlet of condenser; T_{cci} : temperature at the inlet of compensation chamber

Figure 5.3 demonstrates the startup of the LHP at various heating power including 10 W, 20 W, 30 W and 90 W respectively. In this experiment, there was no thermocouple locating at the inlet of the condenser. The ending of startup process could be recognized through the signs such as temperature T_{eo} suddenly increasing close to T_4 and temperature T_{cci} becoming slightly smaller than T_{co} . These signals indicate that vapor was generated and entered the condenser, at the same time the liquid condensed and returned the compensation chamber, caused the change in temperature of T_{cci} . The LHP could startup at very low heating power input such as 10 W or 20 W that it was impossible for the LHP operating under gravity condition mentioned in chapter 3. It can be explained because the horizontal orientation makes less liquid collect at the outlet of evaporator than in the case that the condenser is above the evaporator. The LHP operating at 10 W and 20 W could achieve the stable operation after accomplishing the startup; however, under heating power at 30 W and 90 W, the LHP had to continue to adjust the flow rate of working fluid to balance with the heating power input despite of shorter startup durations. Additionally, there was a noticeable increase of temperature T_{cci} the startup at low heating load such as 10 W and 20 W. This result is explained due to combination of flooding situation in the evaporator and the small heating power causes vapor to be form difficultly during startup period, so heat tend to transfer through the wick to the CC and make the temperature T_{cci} become higher.

b) Thermal performance of the LHP

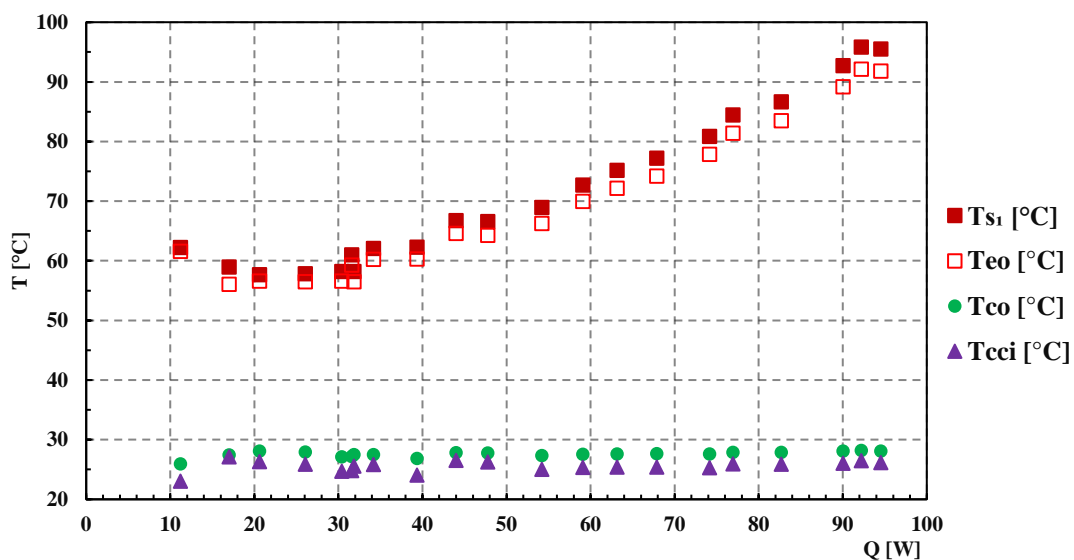


Figure 5.4: Temperature T_{s1} and temperatures of working fluid in the LHP varied with heating power
 T_{s1} : temperature at the top surface of the heating block; T_{eo} : temperature at the outlet of the evaporator
 T_{co} : temperature at the outlet of condenser; T_{cci} : temperature at the inlet of compensation chamber

When operating horizontally, the cooling capacity of the LHP degraded significantly. The temperature T_{sl} on the top surface of the heating block could exist at the value lower than 85°C when the heat generated from the heater was not over 80 W only. In addition, when the heating power reached 95 W , temperature T_{sl} and T_{eo} almost higher than 91°C . Under this condition, the heater should be turn off to avoid the formation of the polycarbonate lid as well as the silicone adhesive used inside the evaporator. However, through the values of temperature T_{eo} , T_{co} and T_{cci} , it could be concluded that the circulation of working fluid in the LHP was stable in the range of heating power from 10 W to 94 W .

Moreover, the experimental results also demonstrate that the tendency T_{sl} and T_{eo} changing varied with the ranges of heating power. In the range of heating power from 10 to 30 W , the temperatures T_{sl} and T_{eo} reduced with the increase of heating power, then they became higher when the heat power supplied to the evaporator was raised up. This behavior of the LHP could be clarified in the Fig. 5.6 which displays the value of LHP total thermal resistance R_t at various heating power values. It reduced dramatically in the ranges of heating power from 10 W to 30 W , then slightly reduced from 35 to 55 W , and operating under constant thermal conductivity mode when heating power belonging the range from 55 to 94 W . The minimum value of R_t was around 0.7 K/W when heating power was at 94 W (3.48 W/cm^2). In addition, the results displayed in Fig. 5.5 also clarify that the evaporator thermal resistance R_e took only the small fraction of the total thermal resistance R_t of the LHP.

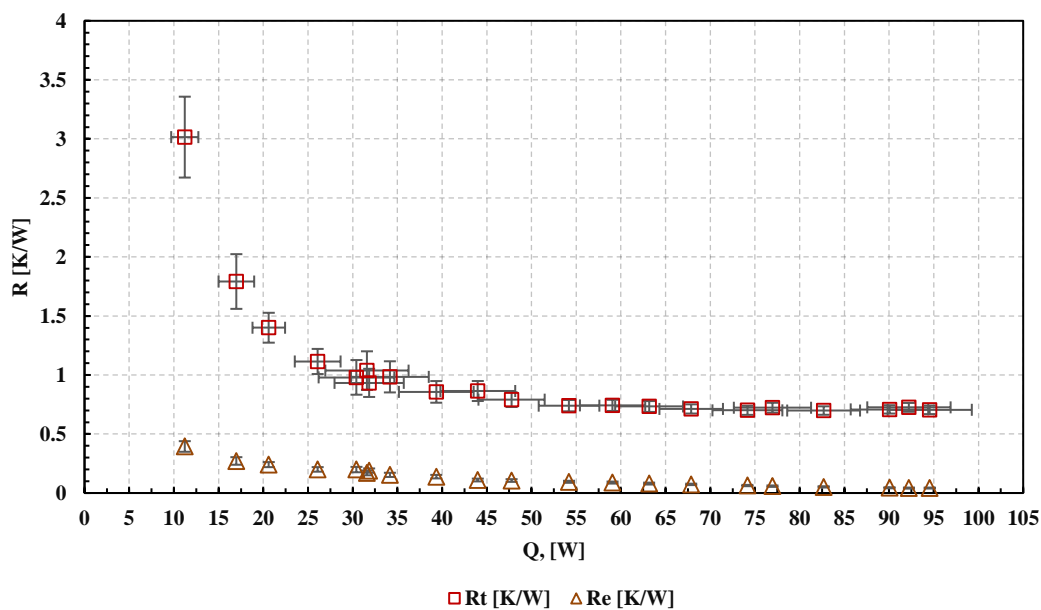


Figure 5.5: Total thermal resistance R_t and evaporator thermal resistance R_e

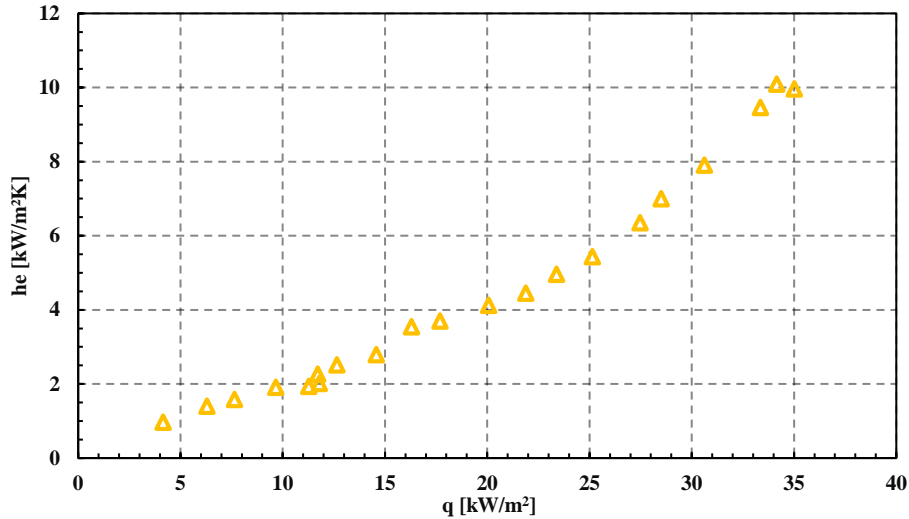


Figure 5.6: Evaporator heat transfer coefficient h_e

As shown in Fig. 5.6, the evaporator HTC h_e almost increased proportionally with the heat flux. Moreover, comparing to the evaporator HTC determined in the chapter 3, the value of h_e in the case of horizontal orientation seems to be higher in the same range of heat flux from 20 kW/m² to 35 kW/m². It can be explained because in the horizontal case the boiling happens at the higher temperature or higher pressure and less liquid collecting at the outlet of evaporator; as a result, vapor is generated and departed from the evaporation section easier.

5.3.2 LHP's performance under different cooling conditions

In this experiment, the performance of the LHP was investigated in the experiments in which the temperature of cooling water at the inlet of condenser T_{wa-i} was setup at three different values such as 18.5°C, 28.5°C and 36.5°C while mass flow rate of cooling water was kept at the same value at 30 kg/h.

The loop heat pipe will operate well in the case that the following condition can be satisfied

- Capillary condition: the capillary pressure created by the boiling of working fluid on the surface of the sintering wick is larger than total pressure drop when working fluid circulating around the loop.

$$\Delta p_{ca} > \Delta p_{vl} + \Delta p_c + \Delta p_{ll} + \Delta p_{wk} + \Delta p_g \quad (5.8)$$

- However, the condensed liquid can enter the compensation chamber if the total pressure at the inlet of compensation chamber P_{cci} is larger than the pressure inside the compensation chamber P_{cc} or

$$P_{cc} \leq P_{cci} \leftrightarrow P_{cc} \leq P_{co} - (\Delta p_{ll} + \Delta p_g) \quad (5.9)$$

- With the LHP works horizontally, $\Delta p_g = 0$, therefore:

$$P_{co} \geq P_{cc} + \Delta p_{ll} \quad (5.10)$$

It means that the condensation pressure of working fluid is decided by not only the cooling condition but also the pressure P_{cc} inside the CC. However, the pressure in the CC depends on many parameters such as the wick properties, working fluid properties, evaporator material and even the ambient condition. Therefore, in this experiment despite the inlet temperature of cooling water was reduced, due to the pressure of P_{cc} that makes the condensation cannot happen at lower temperature, and results in increasing thermal resistance existing at the condenser. In this case, the cooler cooling water helps only in subcooling the liquid before entering the compensation chamber.

5.4 CONCLUSION

When LHP's condenser was cooled by water at 28.5°C, this LHP can operate stably in the range of heat load from 10 W to 94 W while temperature at the top surface of heating block is lower than 100°C.

Total thermal resistances of LHP when cooled by water at the temperature of 28.5°C and 36.5°C are nearly equal under each heating powers. Nevertheless, R_t became higher when the temperature of cooling water reduces to 18.5°C. It could be explained because the LHP performance in this case is dominated by the pressure inside the compensation chamber P_{cc} more than the inlet temperature of cooling water.

These results indicate that LHP can function efficiently with natural water without cooled in advance. It means that it is possible to cut down electricity consumption by the chiller system when using LHP to cool electronics devices.

REFERENCES

- [1] R. M. David Reay, Peter Kew, *Heat Pipe Theory, Design, and Applications*, Sixth Edit. 2014.
- [2] Jentung Ku(Nasa/Goddard Space Flight Center), “Introduction to Loop Heat Pipes,” 2015.
- [3] J. Li, D. Wang, and G. P. Peterson, “Development of a robust miniature loop heat pipe for high power chip cooling,” *Proc. ASME Micro/Nanoscale Heat Mass Transf. Int. Conf. 2009, MNHMT2009*, vol. 3, no. November, 2010.
- [4] L. Vasiliev *et al.*, “International Journal of Heat and Mass Transfer Loop heat pipe for cooling of high-power electronic components,” *Int. J. Heat Mass Transf.*, vol. 52, no. 1–2, pp. 301–308, 2009.
- [5] B. J. Huang, Y. H. Chuang, and P. E. Yang, “Low-cost manufacturing of loop heat pipe for commercial applications,” *Appl. Therm. Eng.*, vol. 126, pp. 1091–1097, 2017.
- [6] “Calyos.” [Online]. Available: <https://www.calyos-tm.com/>. [Accessed: 07-Jan-2019].
- [7] H. Li, Z. C. Liu, B. Bin Chen, W. Liu, C. Li, and J. Yang, “Development of biporous wicks for flat-plate loop heat pipe,” *Exp. Therm. Fluid Sci.*, vol. 37, pp. 91–97, 2012.
- [8] S. C. Wu, D. Wang, J. H. Gao, Z. Y. Huang, and Y. M. Chen, “Effect of the number of grooves on a wick’s surface on the heat transfer performance of loop heat pipe,” *Appl. Therm. Eng.*, vol. 71, no. 1, pp. 371–377, 2014.

Chapter 6

Oscillating Behavior of the LHP When Operating Under Overcharged Condition

This chapter introduces the results of the experimental study on the performance of loop heat pipe (LHP) with the first pattern of evaporator when functioning under overcharged conditions. This LHP was charged with water and operated under horizontal orientation. The results demonstrate that the amount of working fluid affects strongly on the thermal performance of the LHP such as startup process, stable characteristics, and thermal resistance. The LHP started up at the higher temperature and performed more oscillating behavior when charged with more working fluid. In addition, based upon the change of temperatures at different positions of the LHP, an assumption about the phase distribution inside LHP was introduced to explain the oscillation behavior of the LHP.

6.1 INTRODUCTION

One of the important characteristics of the LHP used to cool the electronic devices is the reliability and stable characteristics. However, if the LHP functions under an unsuitable condition or the design parameters are inappropriate, it will behave the oscillating characteristics that reduce the lifespan or even damage the electronics due to the wide change in operating temperature. Therefore, besides studying on the stable characteristics and the methods improving the heat transfer capacity of LHP, it is important to understand the oscillating characteristics of the LHP as well as the reasons for eliminating this behaviour in the future designs. Ku et al [1] suggested a theory to explain the low frequency, high amplitude oscillation in LHP by analysing the experimental data from Rodriguez study. They supposed that there is the relation between the temperature oscillation and the range of the vapor front movement inside the condenser. They also indicated that the combination of the large thermal mass attached to evaporator, low heat power input and the sink temperature that is lower than ambient temperature can cause and maintain this kind of oscillation. Moreover, from the study on miniature – ammonia LHP of S.V. Vershinin et al [2], not only the cooling condition but also the amount of working fluid and orientation can be recognized as the causes of temperature operation, especially in the case of shortage working fluid. In the experimental study of Nagano et al [3], when the heat sink temperature was held at 10°C, the effect of the amount of working fluid on the performance and start-up characteristics of cylindrical LHP was evaluated. Their results showed that under-charged caused the start-up failure while operation of LHP became less stable under over-charged condition. From the experiment of J. Xu et al [4], it was found that when the LHP operated under gravity assisted condition, oscillation behaviour existed in both of low and high inventories under low heat input power. However, in the case of the high inventory, the heat leak through the copper sintered wick could be reduced, and LHP operated stably when higher heat input power was supplied to evaporator.

Therefore, it is necessary to study more on the influence of the amount of charged working fluid on the oscillation behaviour of the LHP. In this chapter, an LHP with the flat-rectangular evaporator was fabricated, and the experiment investigating its performance under different charging ratio (CR) was conducted. Firstly, the LHP was charged with 28.5 ml water (CR about 61%), then the amount of working fluid was reduced step by step by the charging and vacuum system. Moreover, an assumption about the movement of L-V interfaces in liquid and vapor lines was introduced to explain the behaviour of the LHP under different inventories condition.

6.2 EXPERIMENTAL SETUP & DATA REDUCTION

6.2.1 Experimental setup and charging system

a) Experimental setup

Table 6.1 and 6.2 list the main specifications as well as volumes of different sections of the LHP while the schematic diagram of the experiment is described in Fig. 6.1. The methods of heating the evaporator and cooling the condenser were like one mentioned in chapter 3, 4, 5. Accurate value of heating power supplied to evaporator and temperature on the top surface of the heating block T_{s1} were also determined from the data obtained from three 0.5 mm-diameter thermocouples T_1, T_2, T_3 inserted in the heating block. Four thermocouples including $T_{eo}, T_{ci}, T_{co}, T_{cci}$ were attached directly to the LHP at different positions such as outlet of evaporator, inlet of condenser, outlet of condenser and inlet of compensation chamber (CC) respectively to investigate the temperature of working fluid inside the LHP. The absolute pressure of vapor at outlet of evaporator and compensation chamber were also measured by the pressure transducers. In this experiment, cooling water was controlled at the mass flow rate of 35 kg/h and inlet temperature at 28.5°C by the constant temperature circulator device. During the experiment, the room temperature was kept around 26°C.

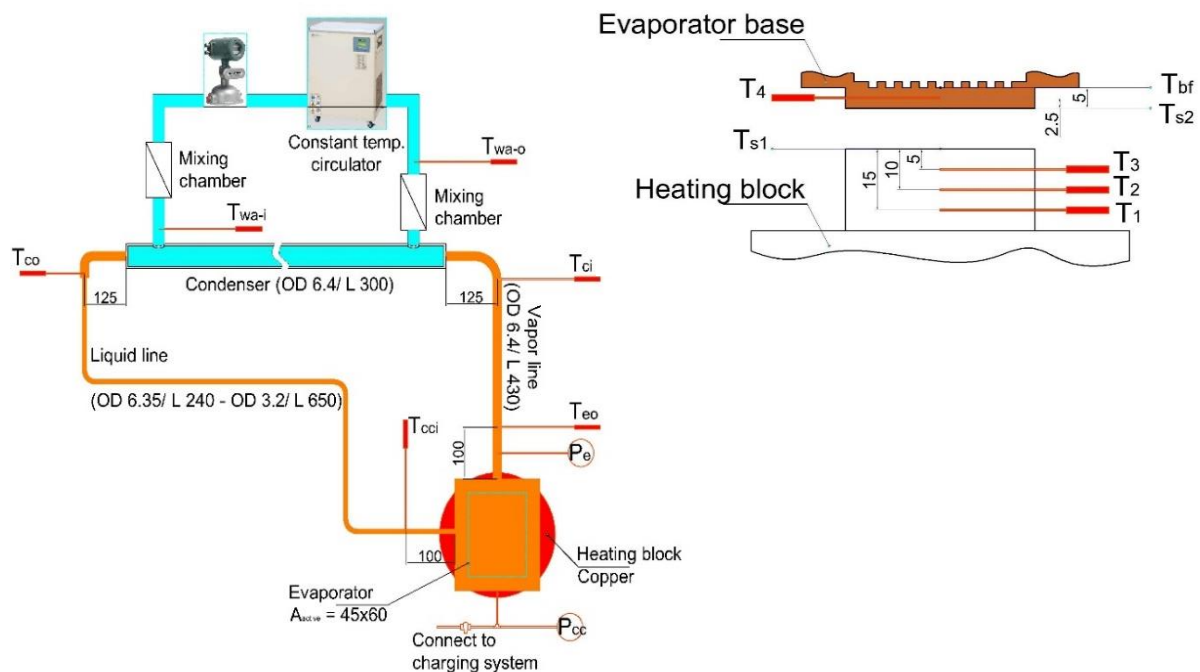


Figure 6.1: Schematic diagram of experimental setup

Table 6.1: Main specifications of the LHP

Evaporator (Including CC)	
Length, mm	80
Width, mm	70
Height, mm	24.5
Active area, mm ²	60 x 45
Fin geometry	
Cross area, mm ²	2 x 2
Height, mm	1.5
Fin pitch, mm	4
Wick structure [5]	
Pore radius, μm	63
Porosity, %	36 – 48
Bulk volume, mm ³	50 x 41 x 5
Vapor line	
Length, mm	430
OD/ID, mm	6.35/4.35
Condenser	
Length, mm	300
OD/ID, mm	6.35/4.35
Liquid line (1/4" and 1/8" tube)	
Length, mm	240
OD/ID, mm	6.35/4.35
Length, mm	650
OD/ID, mm	3.2/1.7
Copper heating block	
Mass, kg	4.36

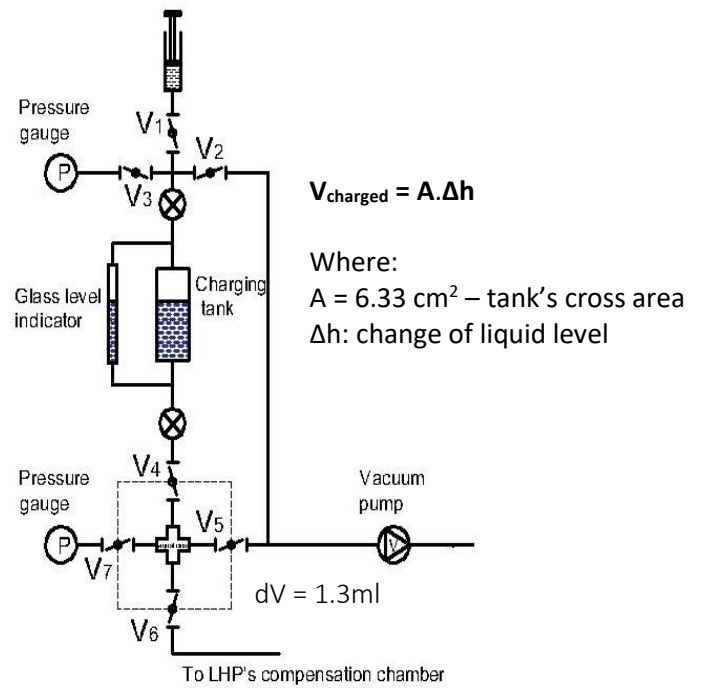


Figure 6.2: Vacuum and charging system

Table 6.2: Volumes of different sections of the LHP*

Vapor groove	1.9 ml
Vapor collector	2.2 ml
Compensation chamber	21.5 ml
Wick's pore volume	4.9 ml
Vapor line	6.4 ml
Condenser	4.5 ml
Liquid line	5 ml
Total volume	46.4 ml

* The internal volume was determined from the dimensions of the components

b) Charging system and charging procedure

The vacuum and charging system of LHP is described in Fig. 6.2. Firstly, all the valves except valve V_1 were opened for vacuum the total internal volume of LHP and charging system by the ULVAC GLD – 051 vacuum pump of which ultimate pressure is 6.7 Pa. Then, the valves V_2 , V_4 , V_5 were closed for charging purified water from the cylinder to the charging tank. After this step, valve V_2 was opened to vacuum the charging tank again to guarantee the vacuum pressure inside

the tank as well as eliminate the dissolved air. When vacuum pressure was satisfied, only valves V_4 and V_6 were opened to charge water into the LHP. The amount of charged water was controlled by the regulating valve installed above the valve V_4 and the glass level indicator. Within this methodology, the uncertainty is about 6.5% of charging amount which was estimated from the uncertainties of the cross area of the charging tank A (5%) and the change of liquid level demonstrated by the glass level indicator (1 mm).

For reducing the amount of water inside the LHP after charging, the volume dV between the valves V_4, V_5, V_6, V_7 was vacuumed firstly. Then the valve V_6 was opened and closed immediately while the valve V_5 was being closed. Because of the different pressure, water inside the LHP will flow into the space dV . The amount of water flowing out the LHP was assumed at liquid phase and have the same volume as dV (1.3 ml). Finally, the valve V_5 was opened for the vacuum pump to vaporize the water out of dV .

6.2.2 Data reduction

Heat flux q and heat flow rate Q flowing through the heating surface to active area A (27 cm²) of evaporator

$$q = \frac{1}{3} \left[k \left(\frac{T_1 - T_2}{\delta_1} \right) + k \left(\frac{T_2 - T_3}{\delta_1} \right) + k \left(\frac{T_1 - T_3}{2\delta_1} \right) \right] \quad (6.1)$$

$$Q = qA \quad (6.2)$$

Heater surface temperature T_{s1}

$$T_{s1} = \frac{1}{3} \left\{ \left(T_1 - 3 \frac{q\delta}{k} \right) + \left(T_2 - 2 \frac{q\delta}{k} \right) + \left(T_3 - \frac{q\delta}{k} \right) \right\} \quad (6.3)$$

Total thermal resistance R_t

$$R_t = \frac{T_{s1} - T_{wa-i}}{Q} \quad (6.4)$$

Moreover, from the measured values of pressure at the outlet of evaporator P_e and CC P_{cc} , saturation temperature of vapor at outlet of evaporator T_{e-sat} and in the CC T_{cc-sat} can be determined by using the REFPROP version 9.1.

6.3 RESULTS & DISCUSSIONS

6.3.1 Performance of LHP when charged with 28.5 ml water (CR was 61%)

Figure 6.3 demonstrates the performance of LHP added with 28.5 ml water. At the initial period, the saturated temperature T_{e-sat} was higher than the temperature T_4 because of the existent of non-condensable gas inside the LHP. During the period when heating power was controlled at 50W, there was no sign indicating circulation of working fluid or the startup of the LHP. The unceasing increase of the T_{e-sat} or the raise of the pressure of vapor at outlet of the evaporator with temperature T_4 proved that the vapor was generated continuously during the heating process; however, it could not flow through vapor line to enter the condenser due to the presence of too much liquid inside the vapor line. This explanation can be drawn from the large difference between T_{e-sat} and T_{eo} . In addition, another sign indicating overcharged condition is that there are no suddenly increment of temperature at inlet of compensation chamber T_{cci} despite the increase of P_{cc} , or the liquid line was also filled with liquid. The above explanations is displayed in Fig. 6.4. Although the experiment was continued at heating power at 75 W to boost the evaporation rate, there was no improvement in the LHP's performance or the sign of circulation. The heaters must be turned off when T_4 achieved the value 100°C to avoid the deformation of polycarbonate lid. Therefore, in the next section, the amount of charged water inside the LHP would be reduced and the performance of LHP under the new inventory would be investigated.

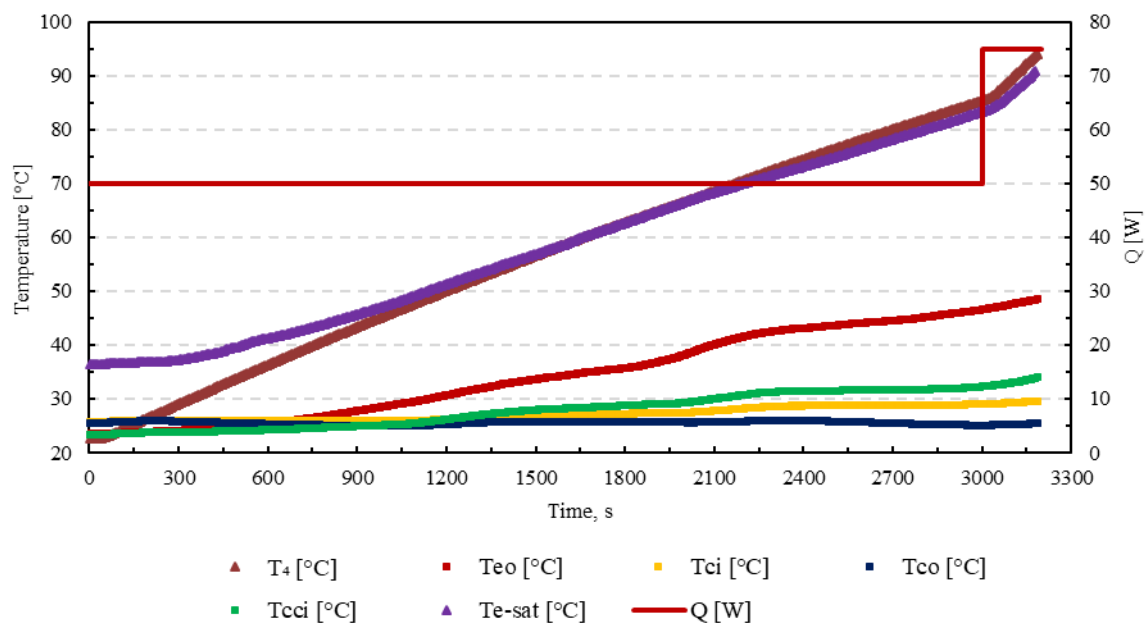


Figure 6.3: Temperature in the base of evaporator T_4 and temperatures at different positions of LHP (CR was 61%)

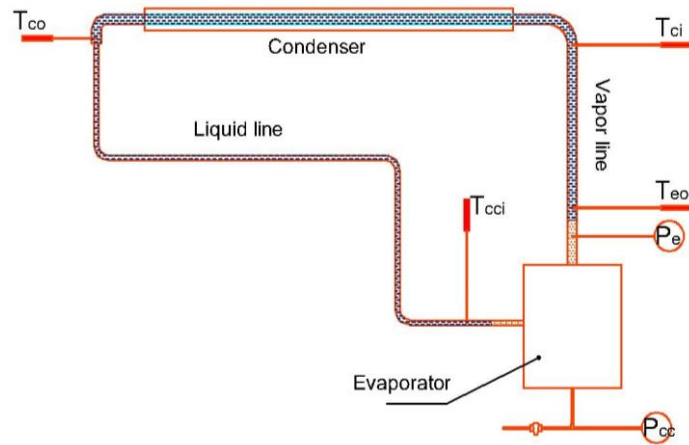


Figure 6.4: Assumption of phase distribution when LHP operating at CR was 61%

6.3.2 Thermal performance of LHP after the first-time reducing amount of charged water (CR = 58.7%)

The amount of charged water was reduced by the method mentioned in section 6.2.1. The procedure was conducted one time, so the amount of water taken out was assumed to be the same volume with dV (1.3ml). The new CR was around 58.7%. Fig 6.5 demonstrates the LHP's performance under the heating power of 45 W.

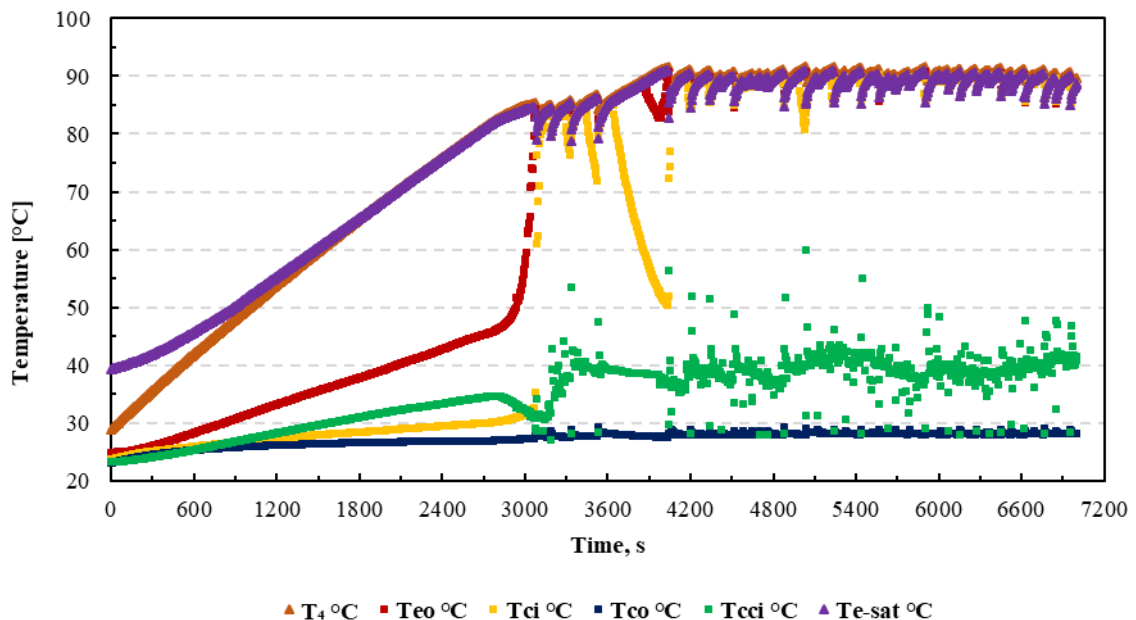


Figure 6.5: Temperature in the base of evaporator T_4 and temperatures at different positions of LHP after the first time of reducing amount of charged water (heating power at 45 W – CR was around 58.7%)

The startup of the LHP under this condition had some similar characteristics to previous one such as the large gap between T_{e-sat} and T_{eo} and T_{e-sat} being higher than T_4 at the begin of

experiment because of the existent of the non-condensable gas. After heating, because the partial pressure of non-condensable gas became smaller when compared with the pressure of vapor, so its influence could be negligible. Moreover, when T_4 increased to the value 85°C , the working fluid inside the LHP began to circulate. After circulation happened, T_{eo} and T_{ci} were equal together and behaved the low amplitude, high-frequency oscillation. These results point out that there was no presence of liquid phase inside the vapor line while the low amplitude, high-frequency oscillation could be caused by the fluctuating movement of the liquid-vapor interface inside the condenser section. Moreover, T_{cci} being higher than T_{co} indicated that the liquid-vapor interface existed not only in the condenser but also in the liquid line. When the interface in the condenser moved forward to the liquid line, the cool liquid could return the CC and make T_{cci} decrease to T_{co} . At this moment, the interface in the liquid line disappeared. The return of cool liquid reduced the temperature and pressure in the CC, and this led to the drop of P_e and the reduction of T_{eo} and T_4 . However, the lower-pressure vapor could not keep the liquid-vapor interface in the condenser stable, the liquid phase would move forward to the vapor line until P_e recovered again. As a result, T_{eo} and T_4 increased with the gain of P_e while T_{cci} became higher than T_{co} because of the invasion of vapor to the liquid line or the reappearance of phase interface in the liquid line. When the pressure P_e was strong enough, vapor could force the condensed liquid to return the CC again, and the above-mentioned phenomenon would happen repeatedly

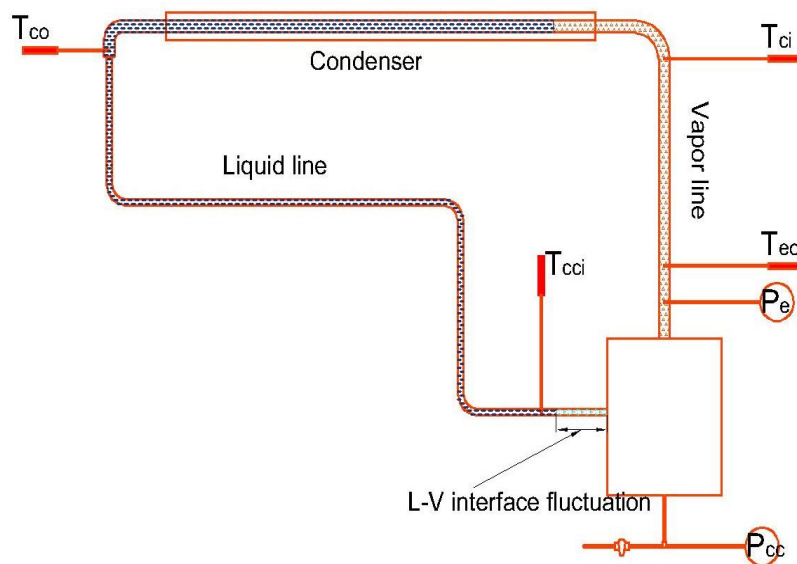


Figure 6.6: Phase distribution when LHP operating at the heating power at 45 W and CR was around 58.7%. The L-V interface fluctuation in the liquid line caused the oscillation of T_{cci} , T_{eo} and T_{ci}

Figure 6.7 shows the performance of LHP at the heating power of 25 W after the circulation happened successfully. The oscillating behavior became high amplitude, low-frequency, especially oscillation of the temperature at inlet of the condenser T_{ci} . Different with the case of heating power at 45 W, T_{ci} dropped down far from T_{eo} . These results happened because low heating power caused the smaller evaporation rate and the more presence of liquid phase inside the LHP. Besides, based on the changes of T_{eo} , T_{ci} , T_{co} and T_{cci} , an explanation about phase distribution inside the LHP under this condition can be introduced as follows.

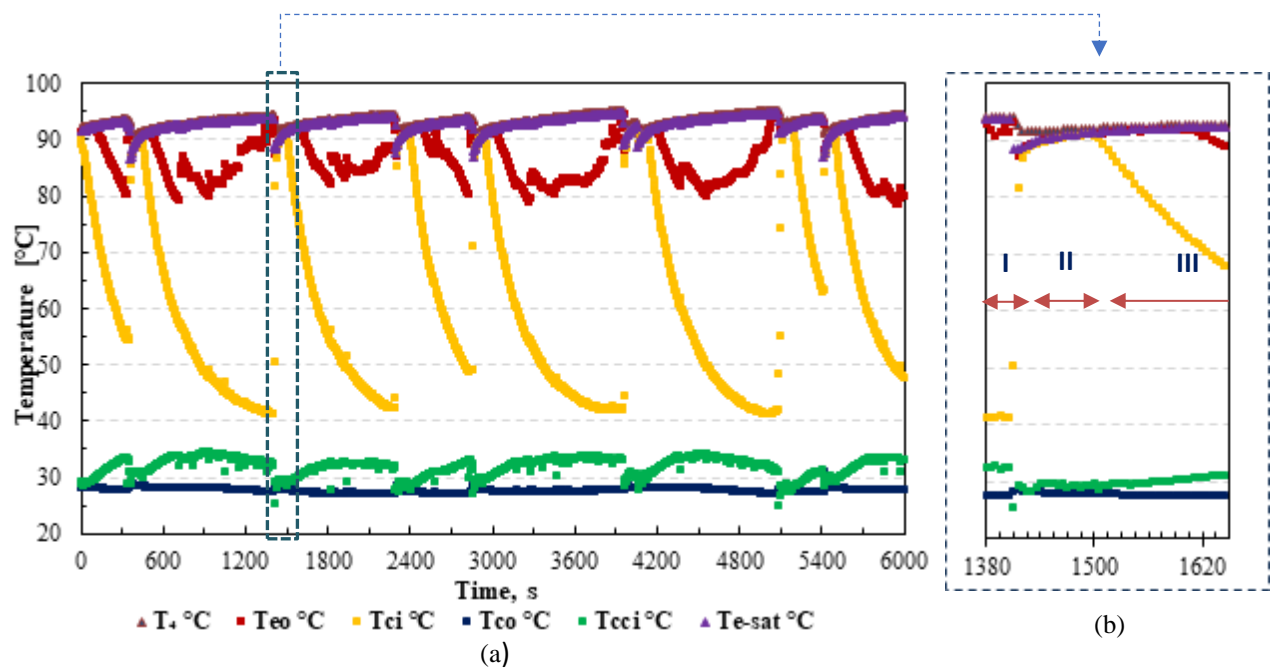


Figure 6.7: Temperature in the base of evaporator T_4 and temperatures at different positions of LHP after the first time of reducing amount of charged water (heating power at 25 W – CR was around 58.7%)

Before the occurrence of circulation, state I – Fig 6.7(b), the measured results such as T_{eo} equalling T_{e-sat} , T_{ci} being smaller than T_{eo} about 50°C while T_{cci} being higher than T_{co} indicate that there were two liquid-vapor interfaces existing in the vapor and liquid line. The first interface located between the positions of the thermocouples T_{eo} and T_{ci} and another existed near the inlet of the CC. When the pressure of vapor P_e became strong sufficiently, it forced liquid flow out the vapor line to return the CC of the evaporator. As a result, the LHP switched on, state II – Fig. 6.7(b), and heat could be transported quickly, T_{ci} suddenly increased to value of T_{eo} or the liquid-vapor interface moved forward to the condenser section. Simultaneously, the interface inside the liquid line disappeared and temperature T_{cci} dropped to T_{co} . However, the circulation could not be maintained for long time, both of T_{eo} and T_{ci} reduced, especially T_{ci} while T_{cci} became higher than T_{co} . At the begin of state III – Fig 6.7(b), the pressure P_e also

suddenly decreased due to the quickly expansion of vapor's volume inside the vapor line, and the reduction of P_{cc} due to returning of cool liquid; hence, the low-pressure P_e could not maintain the interface inside the condenser, but this interface invaded back to the vapor line or the liquid phase inside the vapor line increased. It is the reason why T_{ci} dropped quickly. In addition, the combination of low heating power condition and more liquid phase existing inside the vapor grooves of evaporator made the evaporation happen more difficulty; as a result, the reduction of T_{eo} occurred, and heat leak through the wick structure increased or T_{cci} increased. When the amount of liquid inside vapor grooves reduced, vapor flowed out vapor line or T_{eo} increased again. The increment of vapor amount in vapor line led to the recover of pressure until it was strong enough to force all of liquid out of vapor line and return the CC or circulation happened again. The same phenomenon as explanation will repeat again. The above explanation could be summarized by the Fig 6.8.

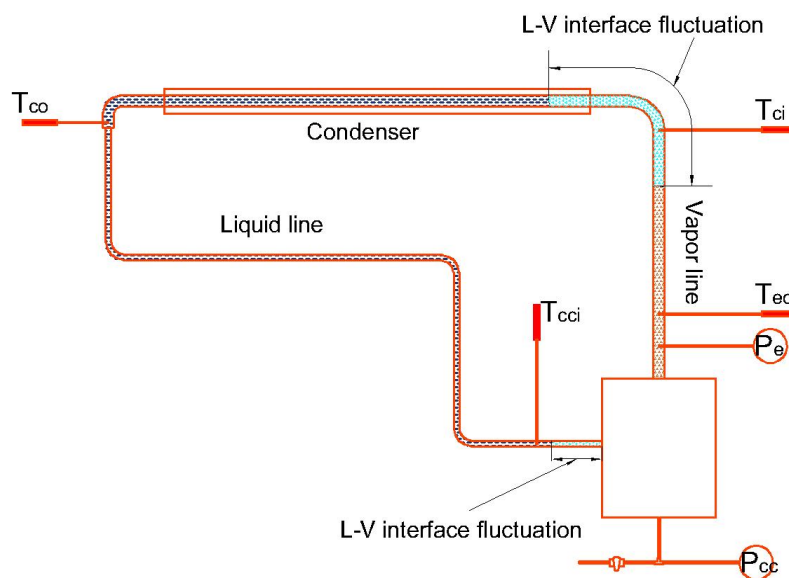


Figure 6.8: Phase distribution when LHP operating at the heating power at 25 W and CR was around 58.7%. The L-V interface fluctuation existed not only in the liquid line but also in the vapor line.

However, when heating power was increased to 50 W (Fig. 6.9), the oscillating behavior almost disappeared, the LHP operation could be considered as stable state. The L-V interface existed stably inside the condenser section, there were no interface in the liquid line because of T_{cci} and T_{co} existed at the same values after circulation happened.

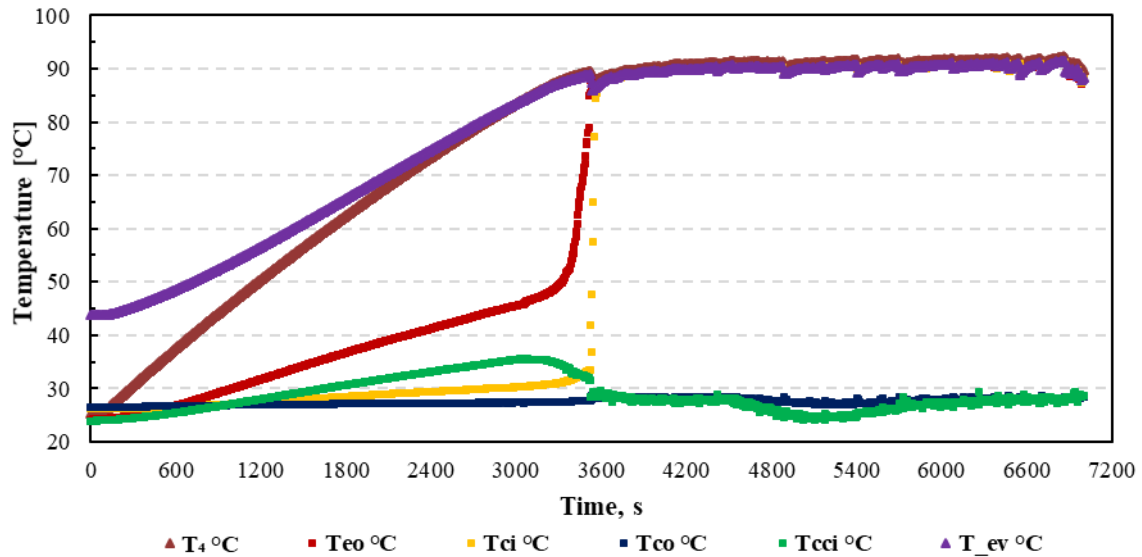


Figure 6.9: Temperature in the base of evaporator T_4 and temperatures at different positions of LHP after the first time of reducing amount of charged water (heating power at 50 W – CR was around 58.7%)

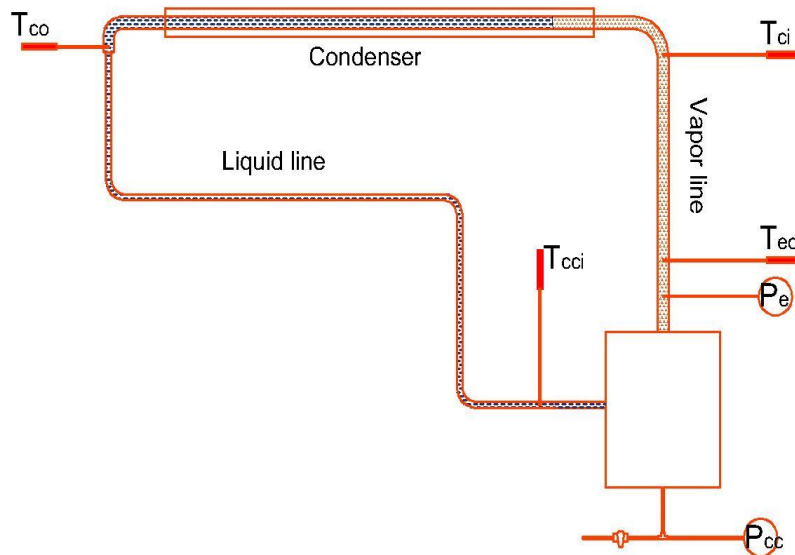


Figure 6.10: Phase distribution when LHP operating at the heating power at 50 W and CR was around 58.7%. The L-V interface only existed in the condenser section

6.3.3 Thermal performance of LHP after the second time reducing the amount of charged water (CR = 53%)

To confirm that the LHP behaved the oscillation characteristics in the above experiment because of the overcharged condition, the amount of water inside the LHP was reduced again. The taken amount was 2.6 ml by conducting the removal procedure two times; therefore, the new charging ratio was around 53%.

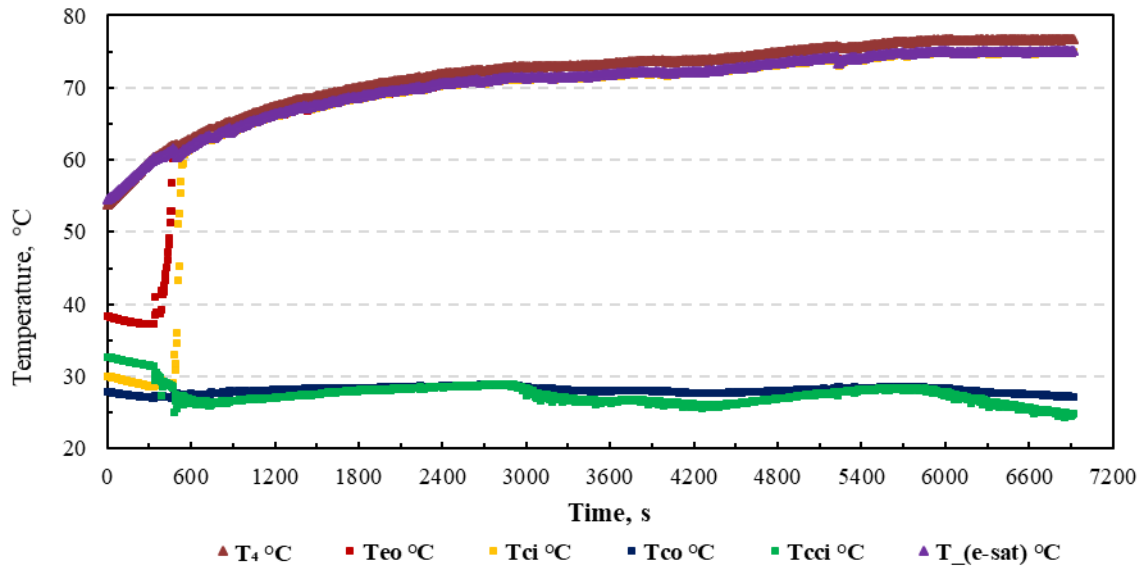


Figure 6.11: Temperature in the base of evaporator T_4 and temperatures at different positions of LHP after the second time of reducing amount of charged water (heat input power at 45W – CR was around 53%)

The performance of LHP under heating power at 45W is displayed in Fig. 6.11. Although at the begin of experiment, value of T_4 were 54.5°C, it was clear that the startup of LHP became easier because the circulation almost accomplished when T_4 was around 62°C. Different with results demonstrated in Fig. 6.5, the temperature T_{ci} were equal to the temperature T_{eo} while T_{cci} was same as or a little lower than T_{co} . Although there was a little change of T_{eo} and T_{ci} , their changes were inconsiderable. These results demonstrated that the first liquid-vapor interface existed stably in the condenser section, and there was no vapor phase in the liquid pipe.

Figure 6.12 shows the maximum, minimum and mean values of total thermal resistance R_t changing with heat flow rate through the LHP with CR at 58.7% and 53% after the first and second time of reduction amount of working fluid, respectively. In general, in company with the increase of heating power, both average value of R_t and its changing range reduced or LHP performance became more stable. In addition, in the second case, the total thermal resistance value and the range of oscillation were smaller. This result indicates that under the first conditions, more working fluid presenting inside the LHP caused the unstable performance of the LHP. Besides, The LHP with more working fluid than the optimum value had the higher thermal resistances, lower heat transfer capacity to achieve the cooling goal.

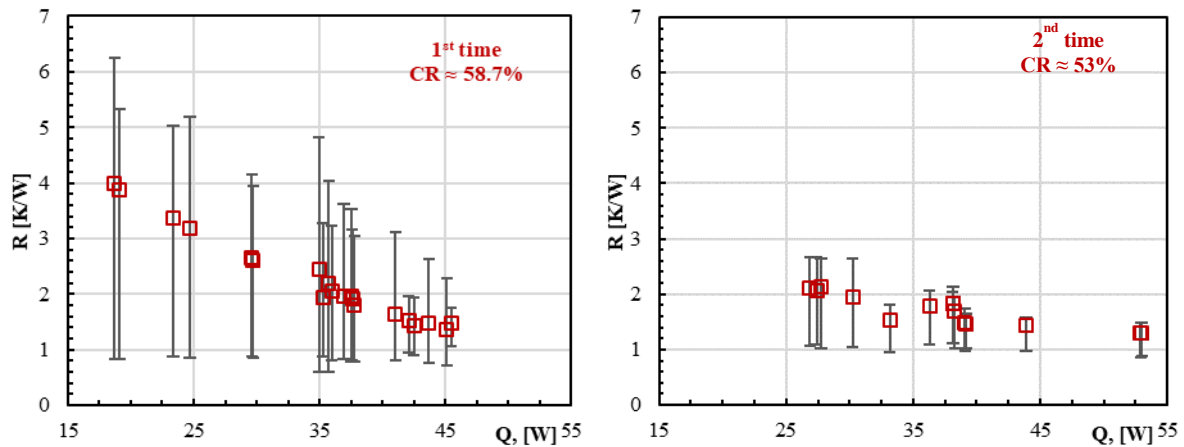


Figure 6.12: Total thermal resistance of LHP under the first and the second time of reducing working fluid

6.4 CONCLUSION

In this chapter, the LHP with flat-rectangular evaporator was fabricated and investigated its thermal performance under different CR when functioning on the horizontal orientation. The experimental results indicated that this LHP could not start up if the charging ratio of working fluid was around 61%. After the first time reducing the working fluid (CR was 58.7%), the LHP behaved two types of oscillating characteristics when working under medium and low heat input power. The first oscillation had the low amplitude, high frequency while the second type demonstrated the high amplitude and low frequency. It could be explained that the oscillating movement of liquid-vapor interface inside the condenser section caused the first type of oscillation. On the other hand, when the LHP functioned under at the low heat load condition, this interface changed its location on the wider range between the condenser and vapor line; as a result, creating the high amplitude, low-frequency oscillation of operating temperature of the LHP. This oscillation could be eliminated when heat input power was increased, or more working fluid was taken out of the LHP.

REFERENCES

- [1] J. R. Jentung Ku, “Low frequency high amplitude temperature oscillation in loop heat pipe operation,” in *SAE 33rd International Conference on Environmental Sciences (ICES)*, 2003, p. Paper No. 2003-01-2388.
- [2] S. V. Vershinin and Y. F. Maydanik, “Investigation of pulsations of the operating temperature in a miniature loop heat pipe,” *Int. J. Heat Mass Transf.*, vol. 50, pp. 5232–5240, 2007.
- [3] H. Nagano, E. Onogawa, F. Fukuyoshi, H. Ogawa, and H. Nagai, “Effect of Amount of Fluid Charge in Thermal Performance of Loop Heat Pipe,” *Heat Transf. Res.*, vol. 39, no. 6, pp. 355–364, 2010.
- [4] J. Xu, Z. Wang, H. Xu, and L. Zhang, “Experimental research on the heat performance of a flat copper-water loop heat pipe with different inventories,” *Exp. Therm. Fluid Sci.*, vol. 84, pp. 110–119, 2017.
- [5] SMC Coporation, Sinter metal element (EB/ES Series) Nov, 27th, 2017 from https://www.smcworld.com/products/en/s.do?ca_id=537.

Chapter 7

CONCLUSION

In this study, the idea of the LHP's evaporator with the array of fins or the crossing grooves system machined on the heat transfer area of evaporator was suggested. From this ideal, there were two patterns of evaporator that were designed, fabricated and invested performance by experiments.

- The first pattern of evaporator was accompanied with the sintered stainless-steel wick, and water was the working fluid inside the LHP. With this pattern, the experiments were setup to investigate the LHP performance when working under both of gravity assisted and horizontal condition.
 - In the experiment that LHP worked in condition advantage in gravity, the condenser was cooled by water at 27.5°C with mass flow rate at 27 kg/h, the LHP could operate stably in the range of 50 to 520 W (19.2 W/cm²) and maintain the temperature on the top surface of the heater not be higher than 105°C. The total thermal resistance of LHP had the minimum value at 0.149 K/W when LHP worked at the heat load of 520 W. For the target of cooling, this LHP could take the heat at the rate of 350 W (12.9 W/cm²) from the heater while the temperature on the top surface of heating block at 85°C. In addition, the start-up characteristics and the cooling performance of the LHP after turning heaters off were also analyzed and discussed. The experimental results also included the changing of evaporation heat transfer coefficient on the heat flux. Through the results, an assumption about boiling phenomenon happening inside the evaporator was introduced.
 - Within the horizontal condition, the performance of LHP was investigated when the inlet temperature of cooling water was adjusted at different values including 18.5°C, 28.5°C, 36.5°C. When cooled by water at 28.5°C, the LHP could operate in the range of heat load from 10 W to 94 W and maintain temperature at the top surface of heating block lower than 100°C. Experimental results also show that the total thermal resistance of LHP, when cooled by water at 28.5°C and 36.5°C, are nearly equal together and smaller than the case that cooling water was set at 18.5°C. This result indicates that

LHP can function efficiently with natural water without cooled in advance. Besides, the experiment of horizontal condition also found out the overcharged of working fluid is one of reasons caused the LHP behave different types of oscillation characteristics.

- The second pattern of the evaporator was investigated in the LHP operating under gravity assisted condition with different working fluids that were water and ethanol. The sintered stainless-steel wick was the capillary structure of this LHP. The experimental results show that the performance of water LHP was almost similar to one working with the first pattern of evaporator although the elevation difference between evaporator and condenser was smaller (350mm → 235mm). Comparison between water and ethanol LHP, the LHP with water as working fluid had better performance. In the case of water LHP, when heating power was changed from 33 to 535 W, the temperature at the top surface of the heating block raised from 38°C to 110°C. With the ethanol LHP, this temperature reached the value of 133°C at the heating power of 395 W. If temperature limitation of microprocessors functioning inside the DCs is recognized at 85°C, the cooling capability of LHP will be 220 W and 350 W corresponding to the working fluid was ethanol and water respectively. In addition, the results of the evaporator heat transfer coefficient obtained from the experiments of water and ethanol LHP in this study also confirmed for the assumption of boiling heat transfer characteristics that presented in the previous study. Moreover, the assumption about the effect of convection heat transfer mechanism on the boiling heat transfer when heat flux was more than 100 kW/m² was also considered in this study to explain the difference in changing evaporator HTC with heat flux when LHP was charged with water and ethanol.

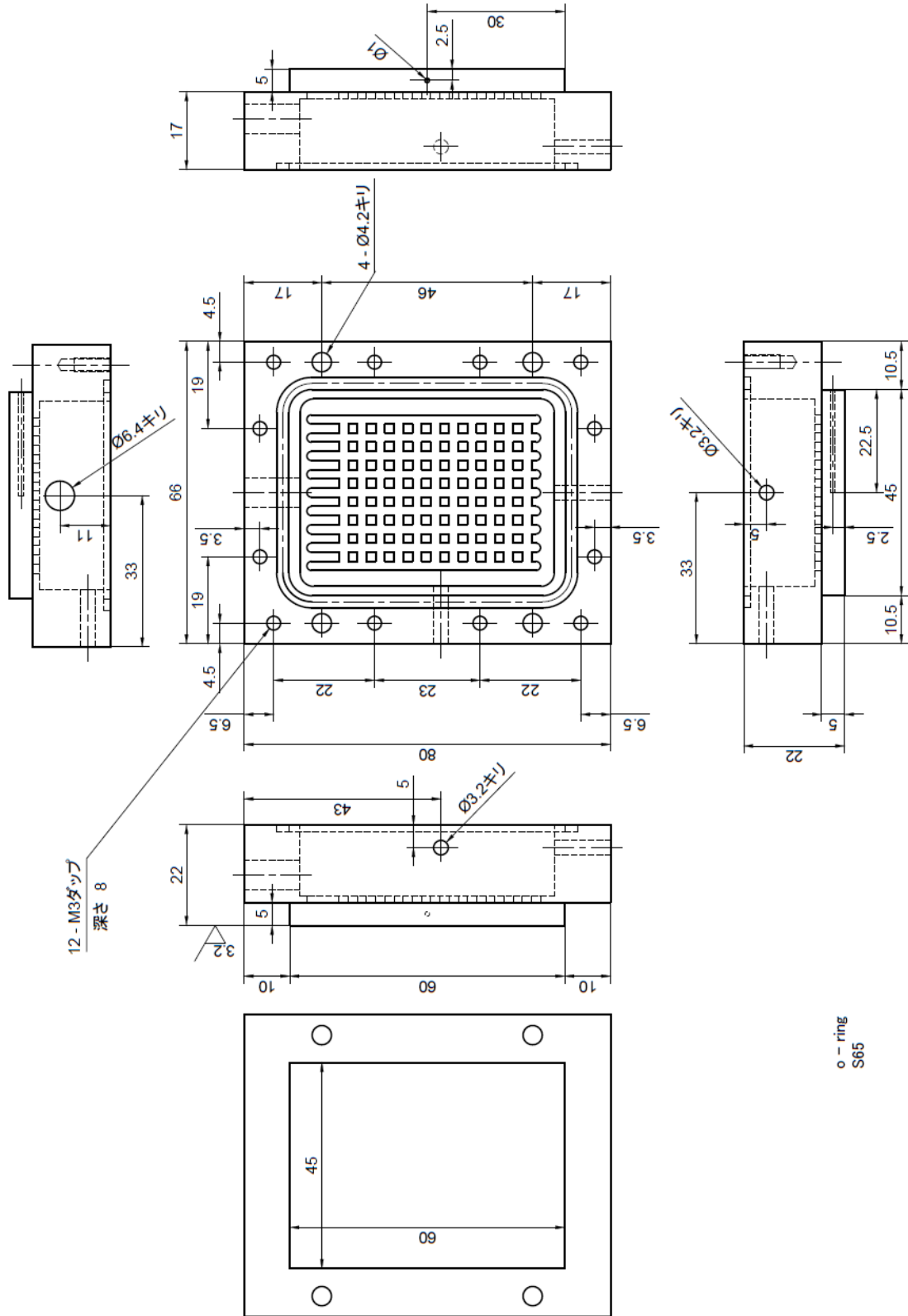
However, this study just commenced the research on the LHP with flat-rectangular shape evaporator. It is necessary to conduct not only experiment but also computational research to more valuable results. Following are the topics that can be carried out in future

- Although the performance of LHP under gravity assisted condition was investigated well, it is necessary to modify the experimental setup that can increase heating power to find out the operation limitation (dry out, capillary limitation, etc.) of LHP when water is working fluid.
- It is important to conduct the experiment on the effect of operating temperature on compatibility between stainless-steel and water.
- More experiments are needed for the horizontal condition and anti-gravity for understand more about the capillary force created by the wick.

- In addition, it is also important to conduct more theoretical or experimental studies that focus the following problems
 - Find out the optimum geometry of the fins on the inner surface of the evaporator.
 - To support more the assumption of the effect of convection heat transfer mechanism on the boiling heat transfer inside the evaporator.
 - Compensation chamber is a component that dominates the performance of the LHP. It is necessary to investigate the heat and mass transfer process happen inside.
 - The opportunity of using non-metallic wick for the low cost and lightweight to the LHP
 - Binary – working fluid (a mixture of water and alcohol working fluid) for using Marangoni effect, especially in the horizontal and anti-gravity LHP.

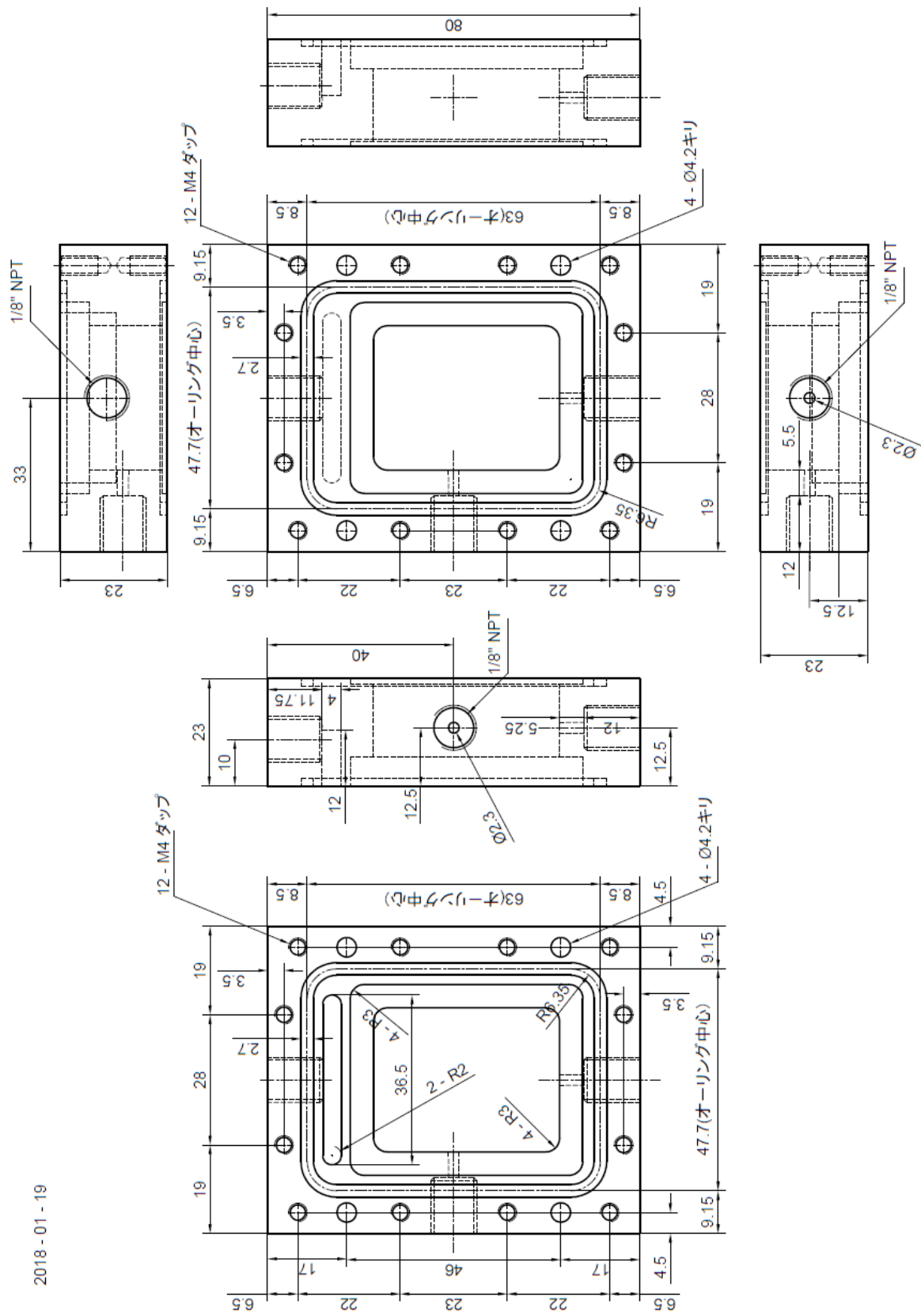
APPENDIX A: MANUFACTURED DRAWINGS

APPENDIX A-1: MANUFACTURED DRAWING OF THE FIRST PATTERN OF EVAPORATOR



o-ring
S65

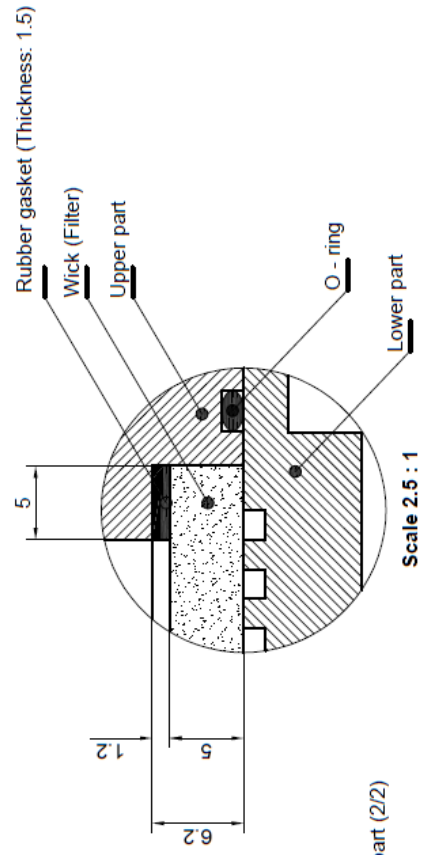
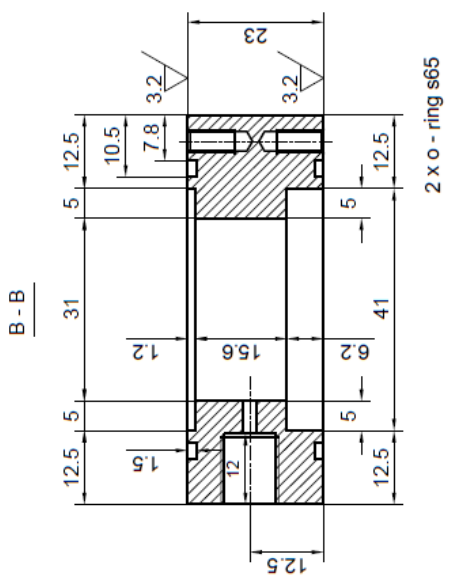
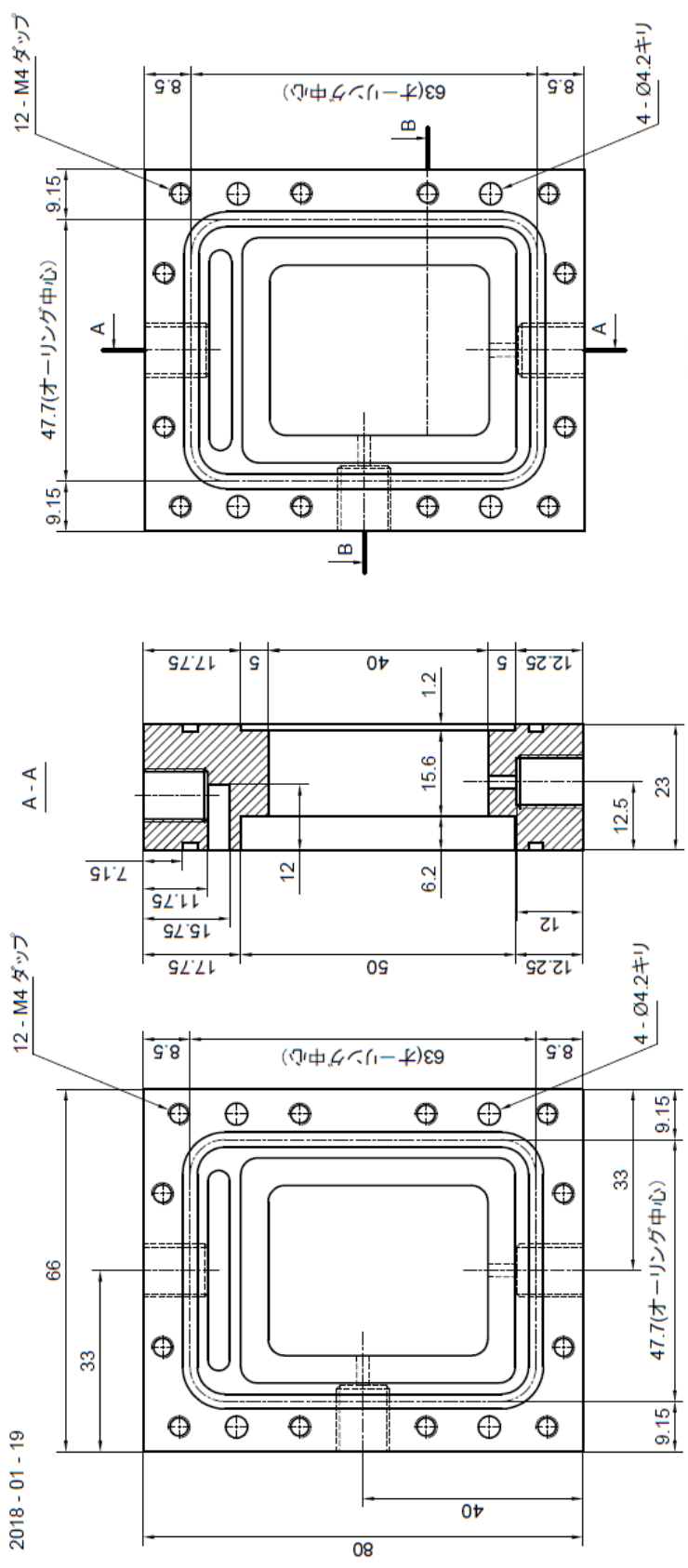
APPENDIX A-2: MANUFACTURED DRAWING OF THE SECOND PATTERN OF EVAPORATOR



2018 - 01 - 19

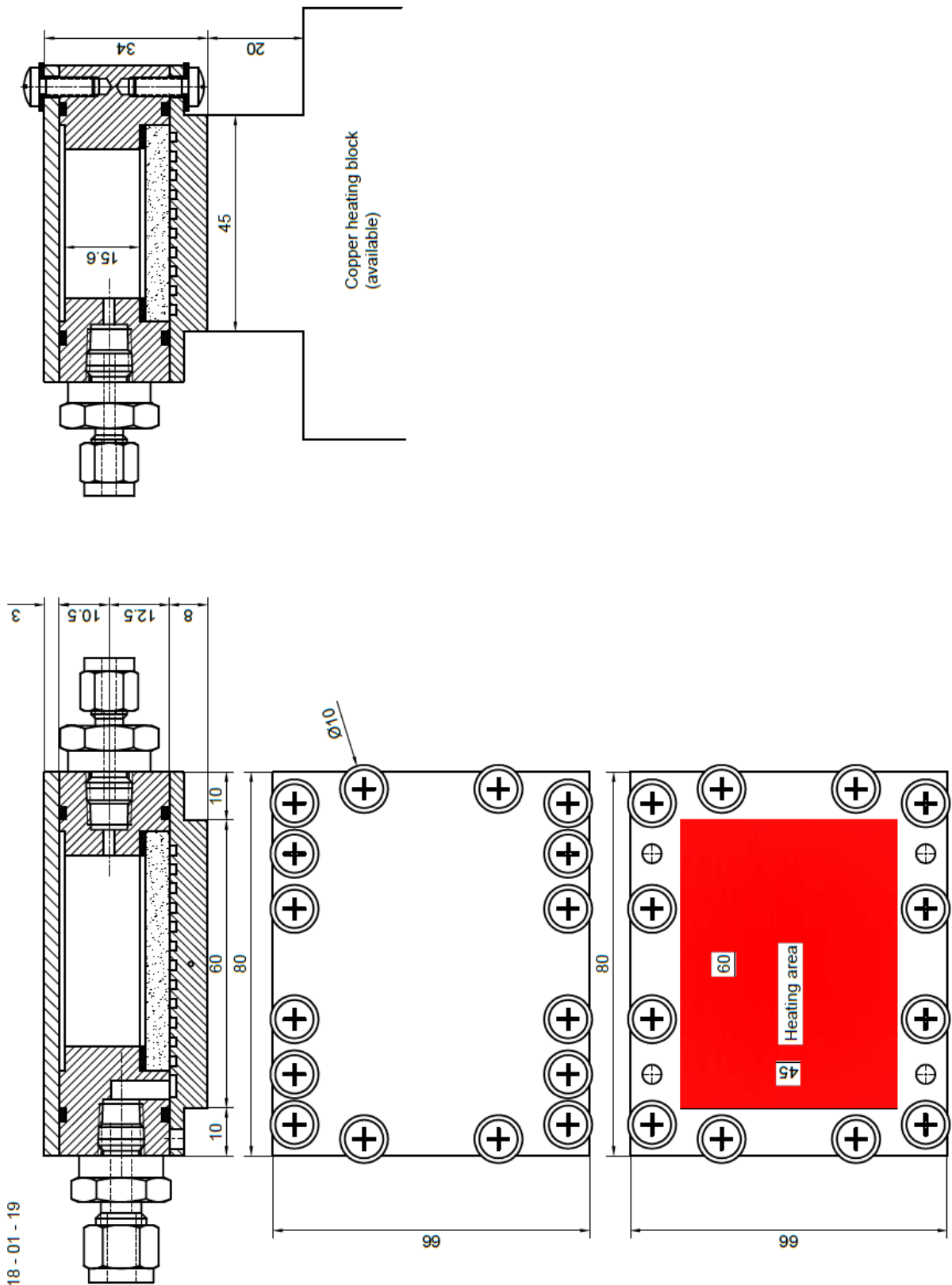
Upper part (1/2)

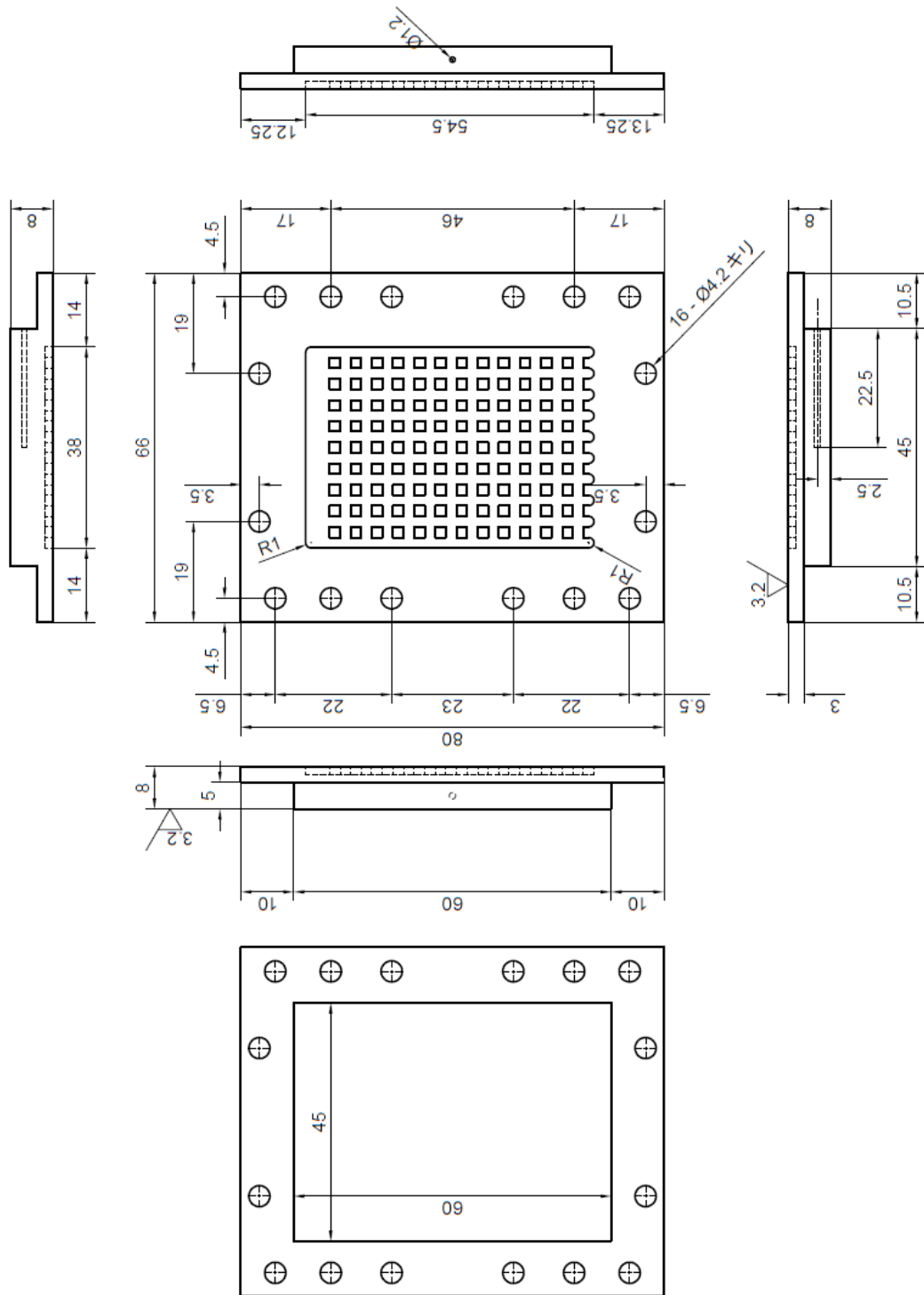
2018 - 01 - 19



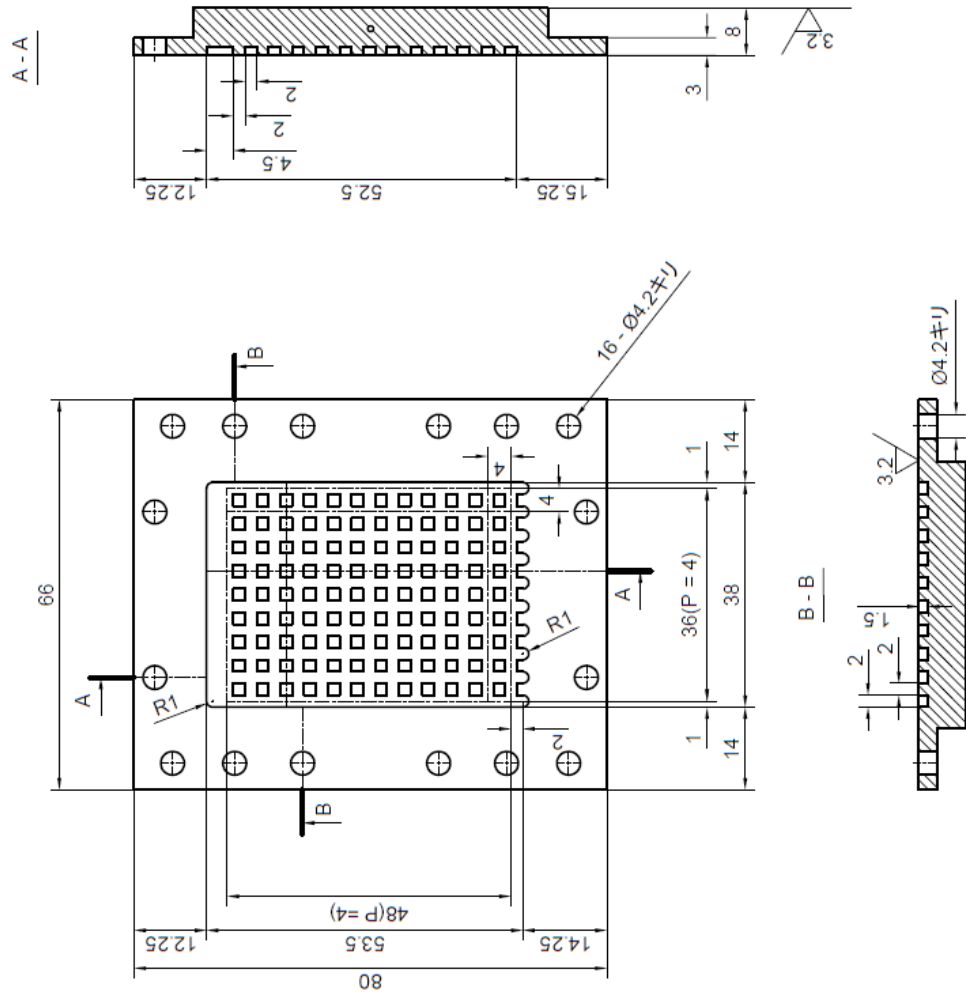
Upper part (2/2)

2018 - 01 - 19





Lower part (1/2)



Lower part (2/2)

APPENDIX B: WICK'S SPECIFICATIONS

APPENDIX B-1: MEASURING SINTERING WICK VOID RATIO

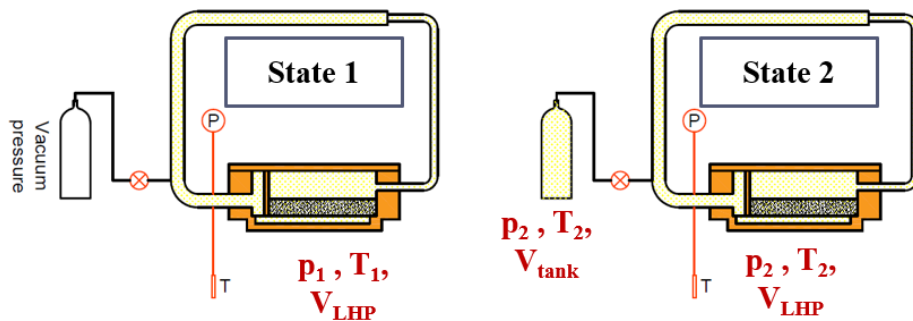
Porosity or void fraction is a fraction of the volume of voids over the total volume

$$\varepsilon = \frac{V_{\text{void}}}{V_{\text{total}}} = \frac{(V_{\text{total}} - V_{\text{solid}})}{V_{\text{total}}} = 1 - \frac{V_{\text{LHPwOW}} - V_{\text{LHPwW}}}{V_{\text{total}}}$$

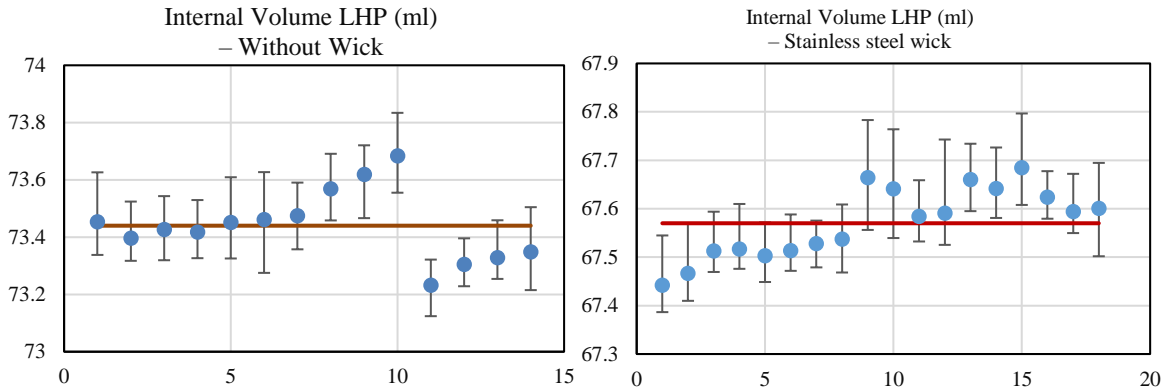
V_{solid} is the volume of solid phase in the wick, which is estimated from the difference between the internal volume of LHP without the wick V_{LHPwOW} and internal volume of LHP with the wick inside V_{LHPwW} . Therefore, internal volume of the LHP with and without wick had to be determined. The internal volume was measured basing on the ideal gas law and mass conservation through 2 steps

Step 1: the whole volume of LHP was charged with N_2 gas while the pressure of standard tank was maintained at vacuum condition. The pressure p_1 and temperature T_1 of the N_2 in the LHP was collected by the data logger.

Step 2: opening the valve V , collecting the data p_2, T_2 after system becomes equilibrium state



$$\frac{p_1 V_{\text{LHP}}}{RT_1} = \frac{p_2 (V_{\text{LHP}} + V_{\text{tank}})}{RT_2} \Leftrightarrow V_{\text{LHP}} = \frac{(p_2 T_1)}{p_1 T_2 - p_2 T_1} * V_{\text{tank}}$$



Internal volume of LHP without wick

$$V_{\text{LHP-wow}} = 77.43 \text{ ml}; \text{STDEV} = 0.125 \text{ ml}$$

Internal volume of LHP with SS wick

$$V_{\text{LHP-SS}} = 67.57 \text{ ml}; \text{STDEV} = 0.072 \text{ ml}$$

Wick total volume

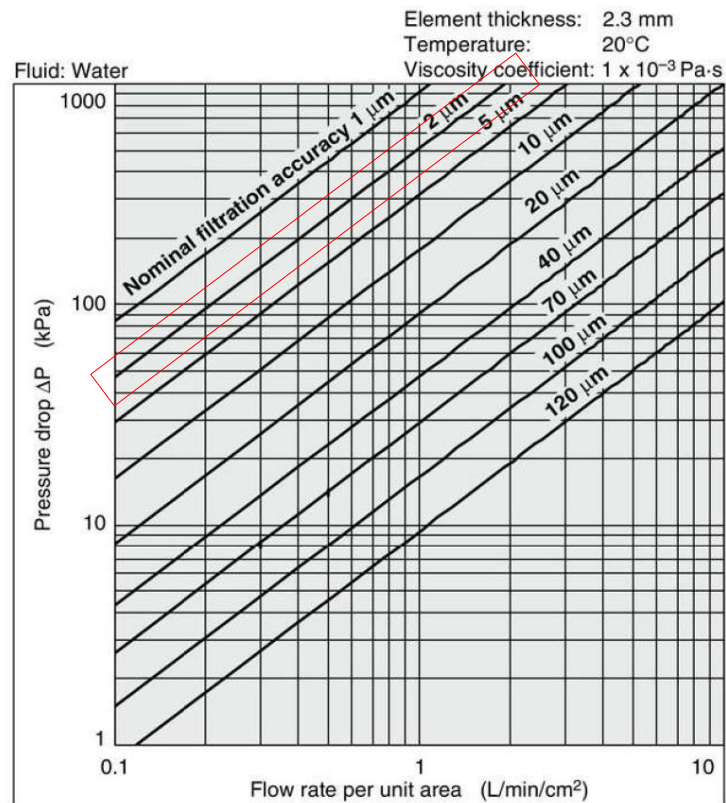
$$V_{\text{total}} = 10.21 \text{ ml}$$

Porosity SS wick

$$42.51\%$$

The internal volume of the LHP in chapter 4 and the porosity of stainless-steel wick

APPENDIX B-2: FLOW RATE CHARACTERISTICS OF STAINLESS-STEEL SINTERING WICK



Wick permeability K can be estimated from the flow rate characteristic and the Darcy's law

$$\Delta P = (\mu_l l_{\text{eff}} m) \frac{1}{\rho_l K A_w}$$

Flow rate (L/min/cm ²)	Pressure drop (kPa)	Viscosity (Pa·s)	Thickness (m)	A _w (m ²)	K (m ²)
0.4	200	0.001	0.0023	0.0001	7.67·10 ⁻¹³
0.6	300	0.001	0.0023	0.0001	7.67·10 ⁻¹³
0.8	400	0.001	0.0023	0.0001	7.67·10 ⁻¹³

APPENDIX B-3: WICK EFFECTIVE THERMAL CONDUCTIVITY

Wick effective thermal conductivity can be estimated from following correlations

Average method

$$k_{\text{eff}} = k_s(1 - \varepsilon) + \varepsilon k_f$$

Maxwell

$$k_{\text{eff}} = \frac{k_s \left(2 + \left(\frac{k_f}{k_s} \right) - 2\varepsilon \left(1 - \frac{k_f}{k_s} \right) \right)}{\left(2 + \left(\frac{k_f}{k_s} \right) + 2\varepsilon \left(1 - \frac{k_f}{k_s} \right) \right)}$$

Alexander

$$k_{\text{eff}} = k_f \left(\frac{k_f}{k_s} \right)^{-(1-\varepsilon)^{0.59}}$$

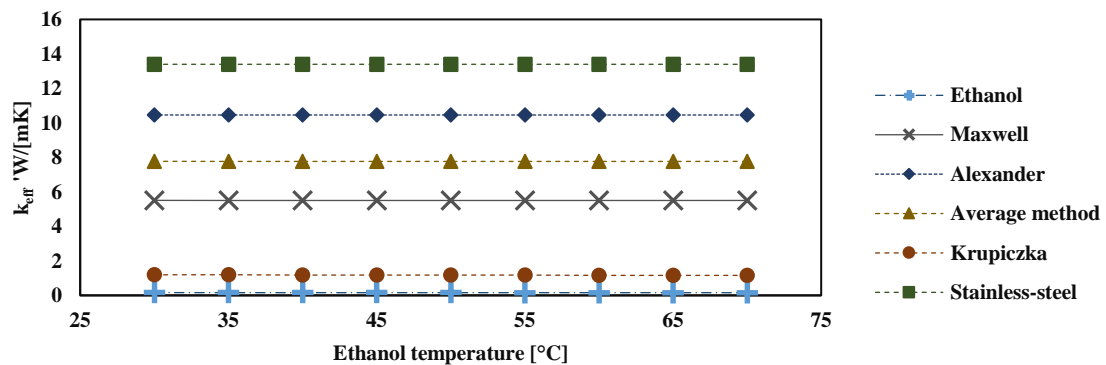
Krupiczka

$$k_{\text{eff}} = k_f \left(\frac{k_s}{k_f} \right)^\eta$$

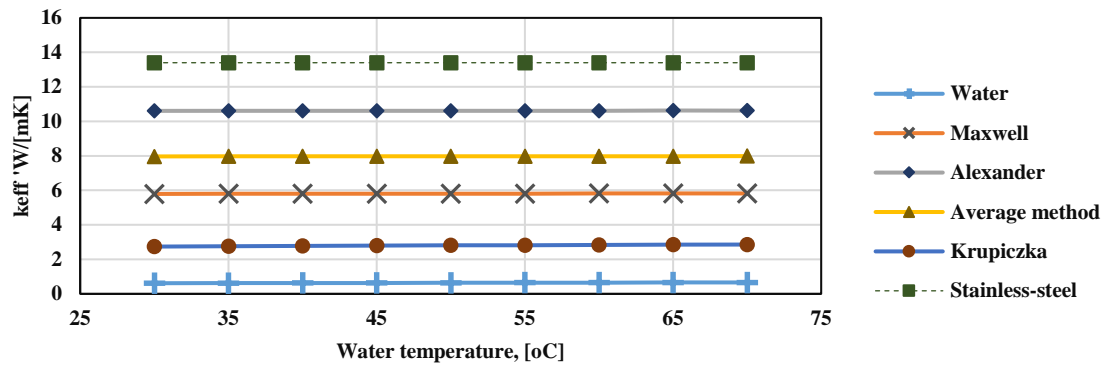
$$\eta = 0.28 - 0.757 \log \varepsilon - 0.057 \log \left(\frac{k_s}{k_f} \right)$$

Where: ε is wick porosity; k_f thermal conductivity of fluid; k_s thermal conductivity of wick material

Wick's effective thermal conductivity when saturated by Ethanol



Wick's effective thermal conductivity when saturated by Water

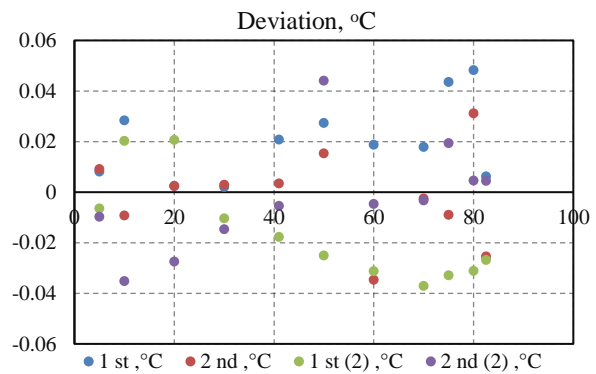
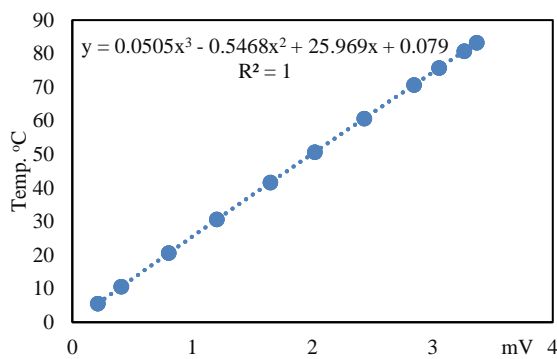


APPENDIX C: THERMOCOUPLES CALIBRATION RESULTS

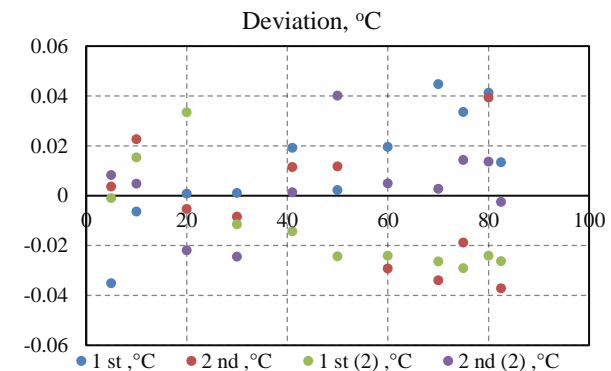
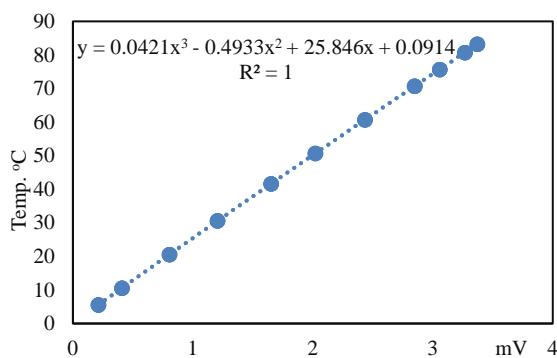
Thermocouples used in the experiment were calibrated by using the thermal resistance Pt100 (Chino Co. Model – R900-F25AT)

APPENDIX C-1: Thermocouples inserted into the heating block T₁ T₂ T₃ and thermocouple inserted into the evaporator base T₄

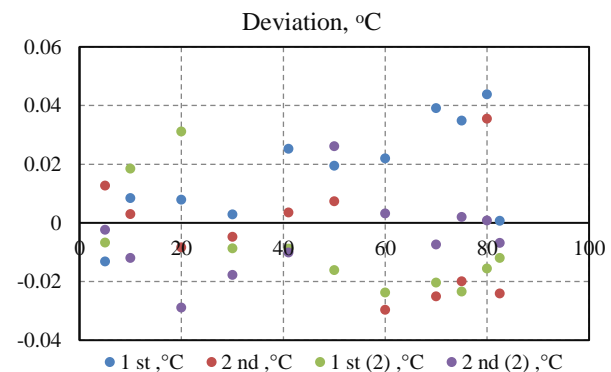
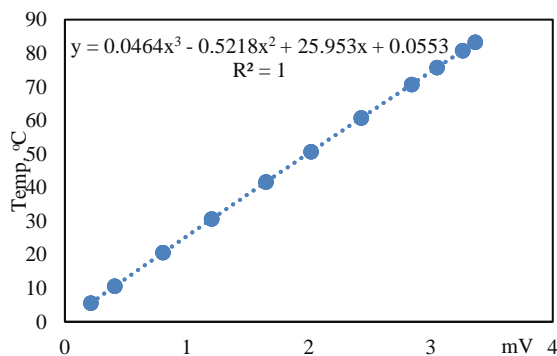
Thermocouple T₁



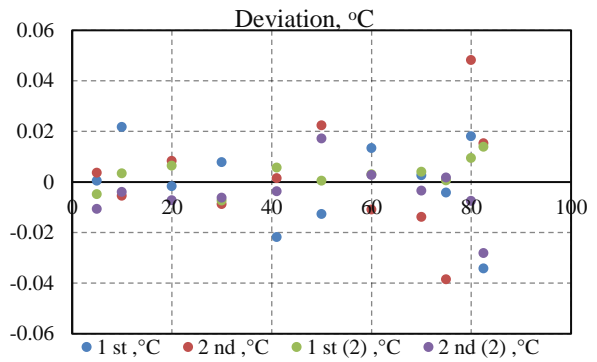
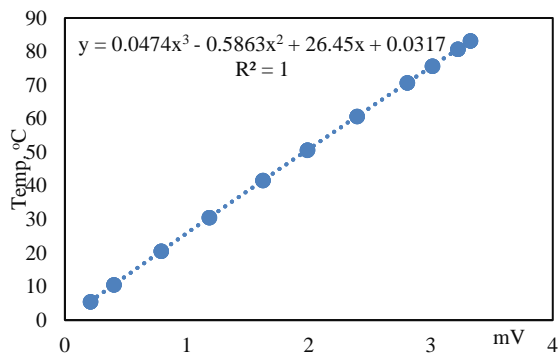
Thermocouple T₂



Thermocouple T₃

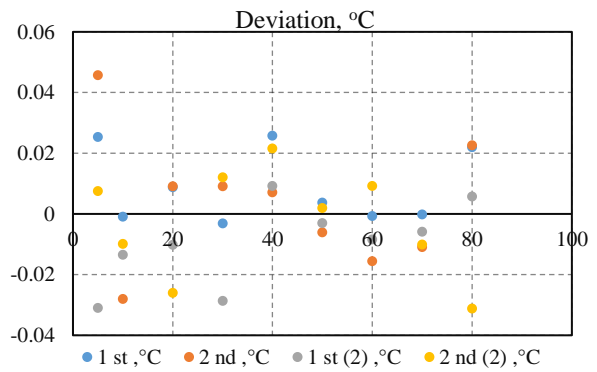
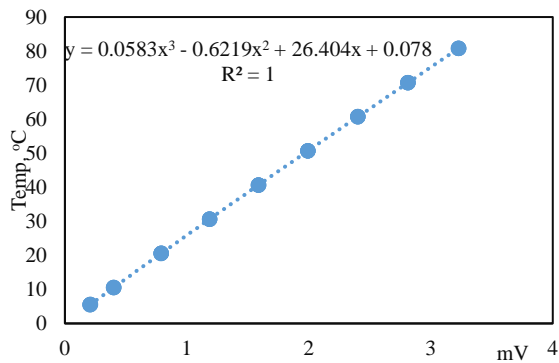


Thermocouple T₄

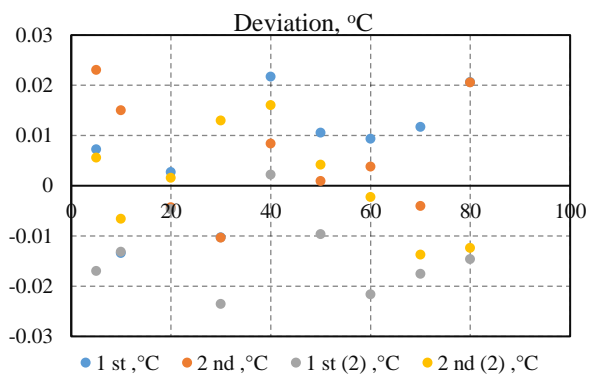
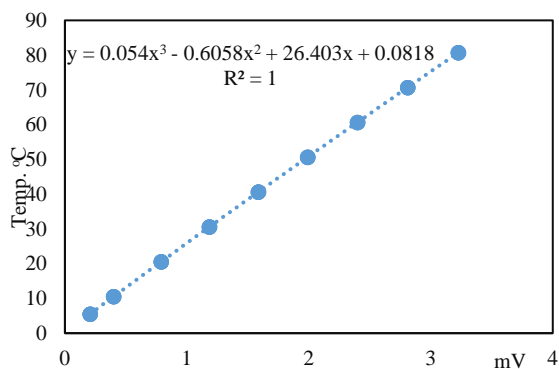


APPENDIX C-2: Thermocouples inserted inside the LHP

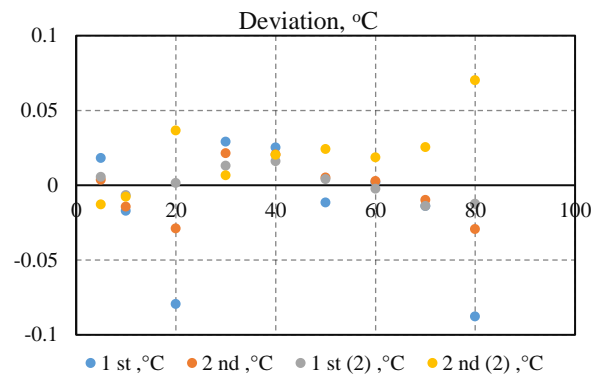
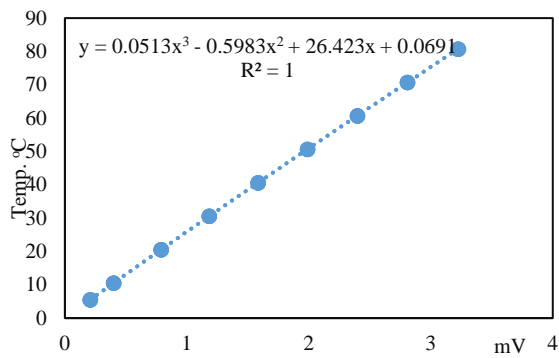
Thermocouple T_{eo} – outlet of the evaporator



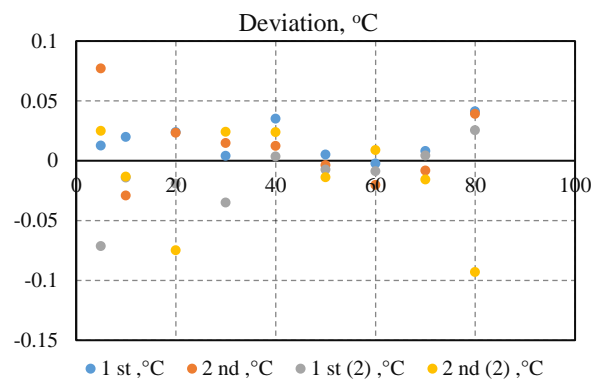
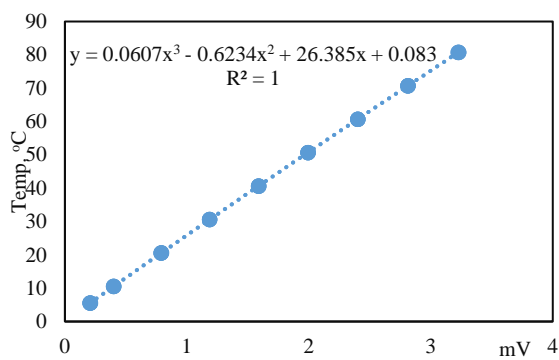
Thermocouple T_{ci} – inlet of the condenser



Thermocouple T_{co} – outlet of the condenser

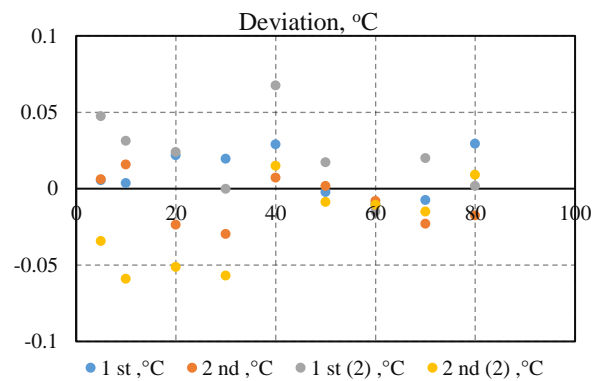
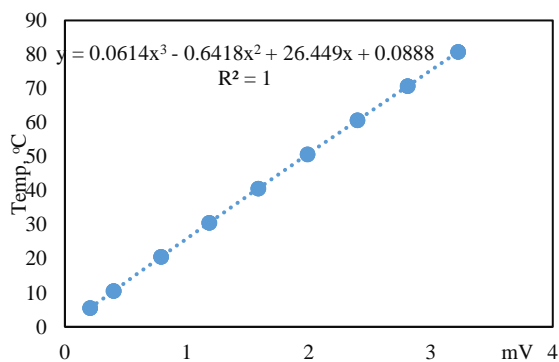


Thermocouple T_{cci} – inlet of compensation chamber

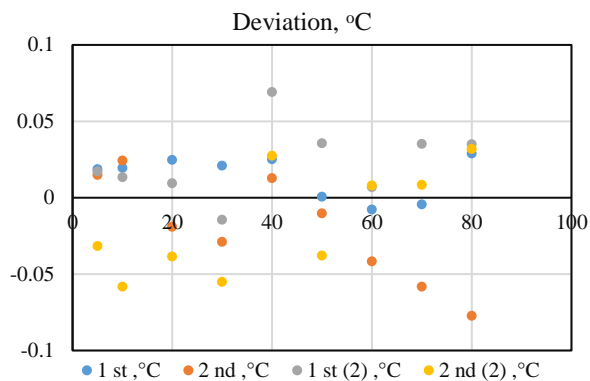
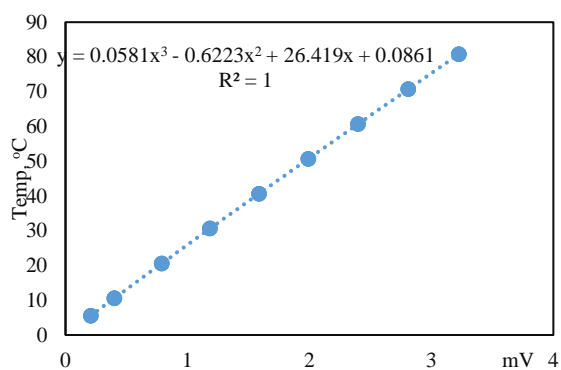


APPENDIX C-3: Other thermocouples

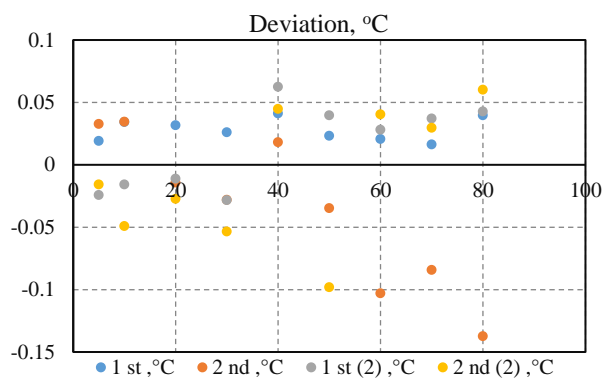
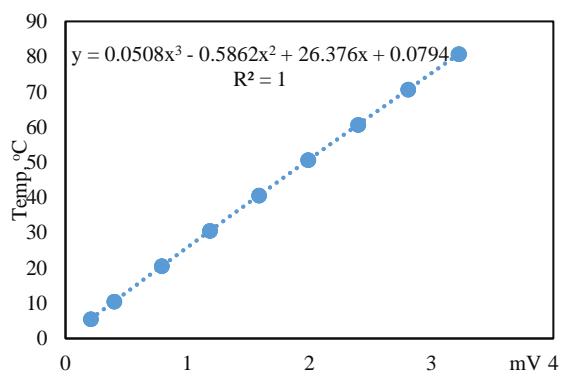
Thermocouple T_{wa-i} – cooling water temperature at inlet of condenser



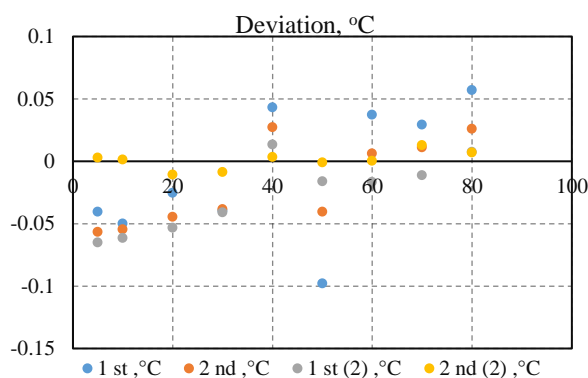
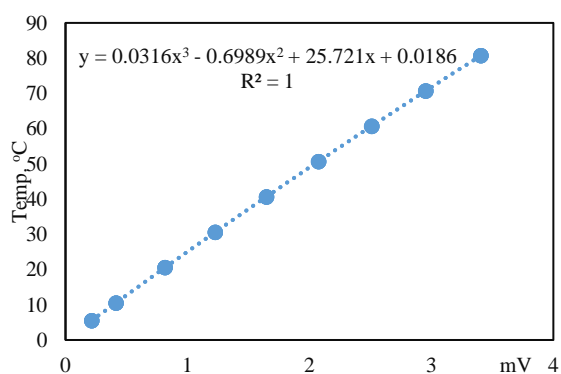
Thermocouple T_{wa-o} – cooling water temperature at outlet of condenser



Thermocouple T_a – ambient temperature

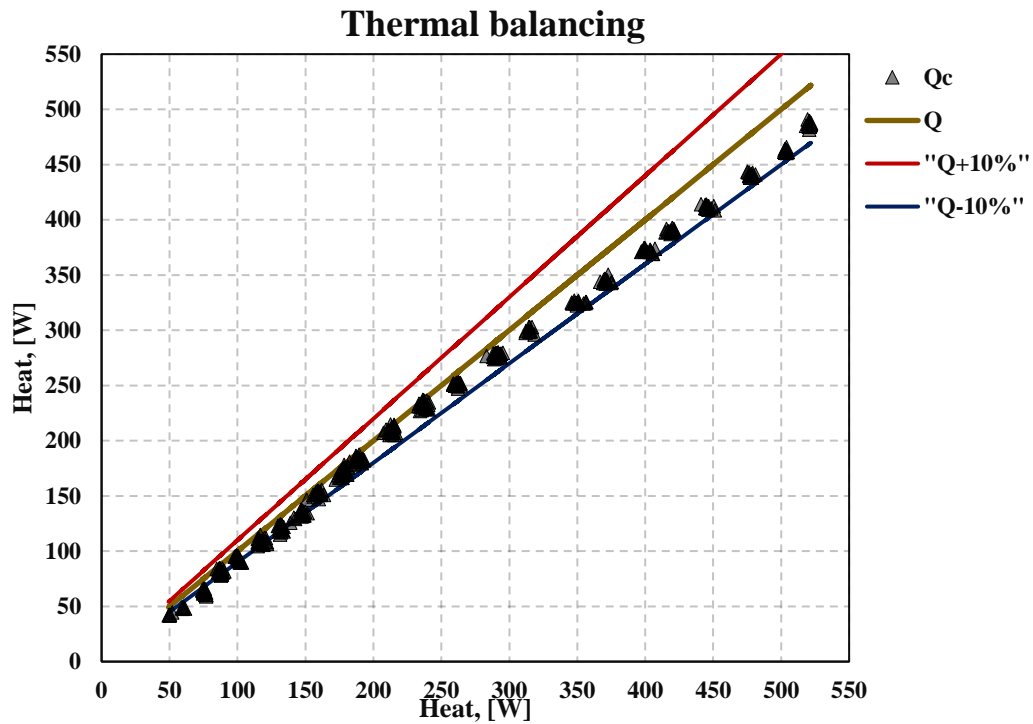


Thermocouples T_{cw1} to T_{cw5} condenser wall temperature

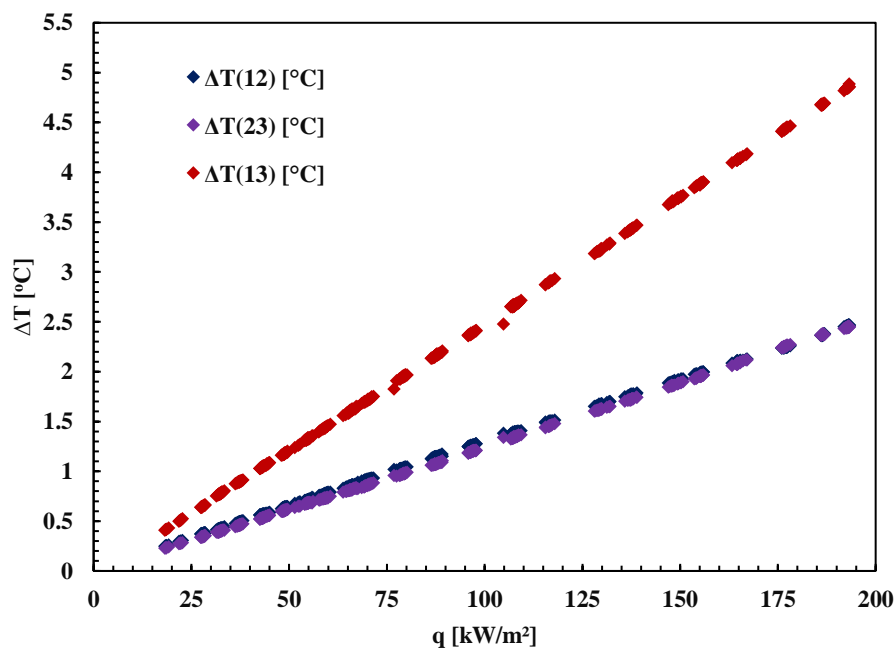


APPENDIX D: THERMAL BALANCING & GRADIENT TEMPERATURE MEASUREMENT

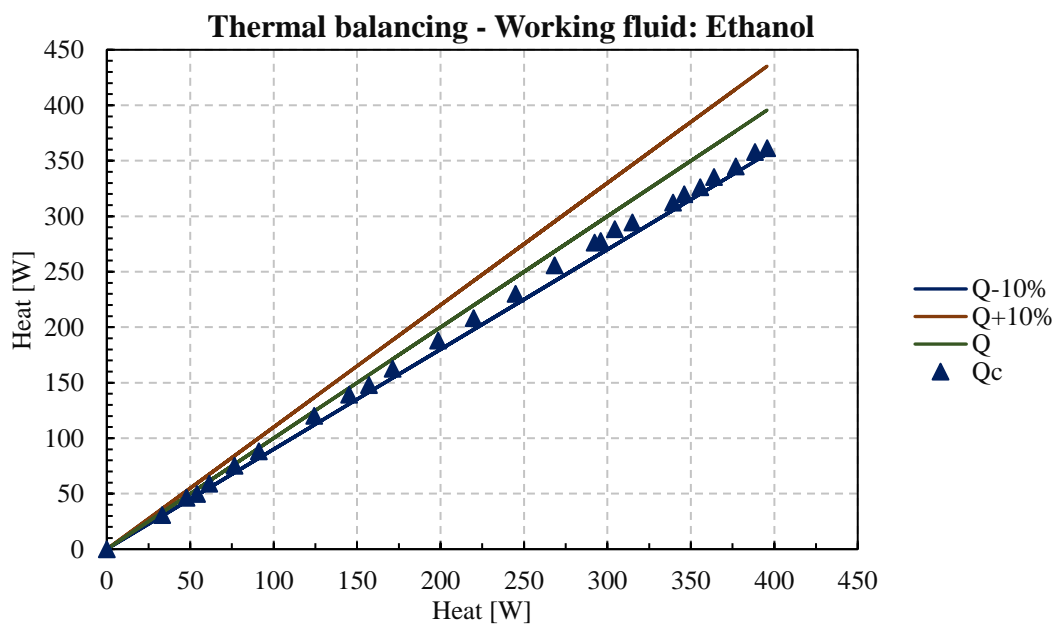
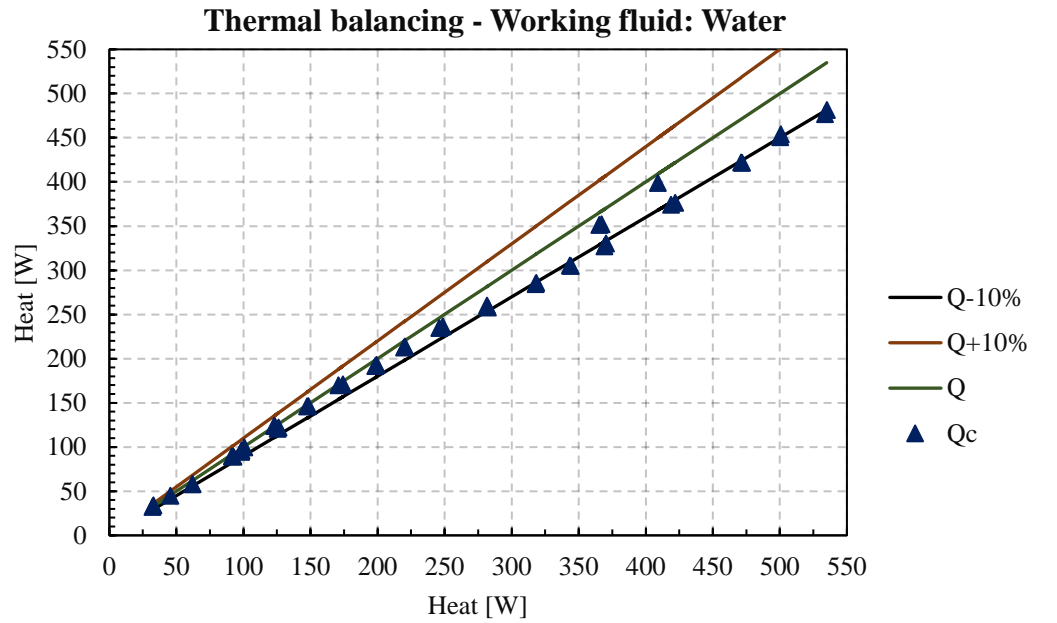
APPENDIX D-1: Thermal balancing in the experiment investigating LHP performance under gravity-assisted condition – the first pattern of evaporator



APPENDIX D-2: Temperature gradient measured in the experiment investigating LHP performance under gravity-assisted condition – the first pattern of evaporator

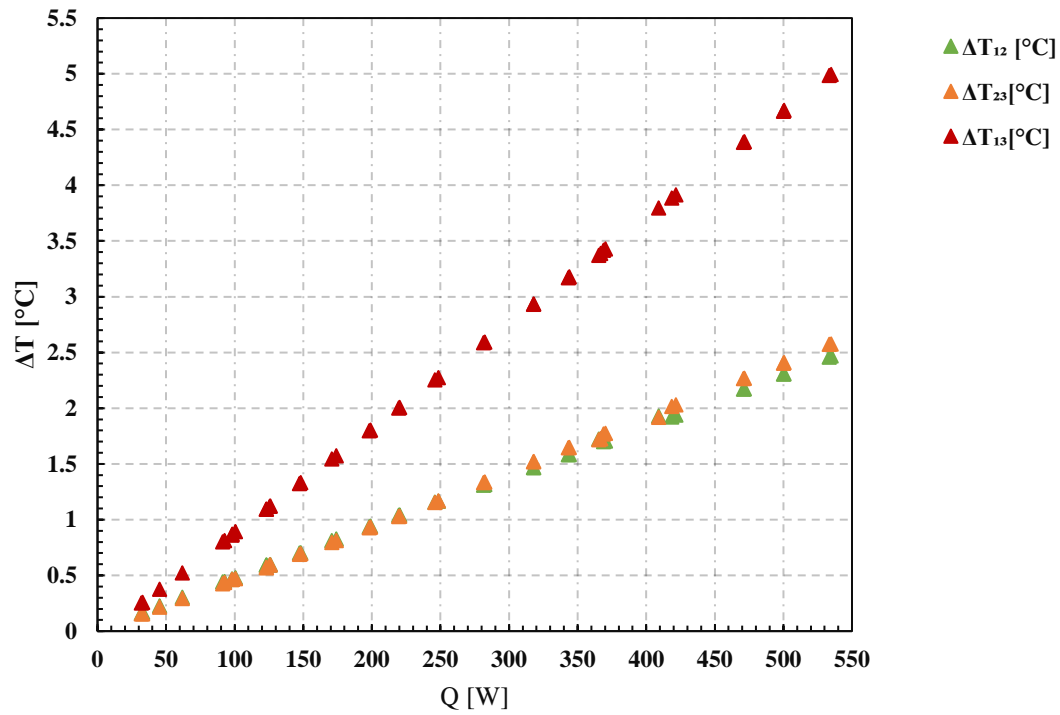


APPENDIX D-3: Thermal balancing in the experiment investigating LHP performance under gravity-assisted condition – the second pattern of evaporator

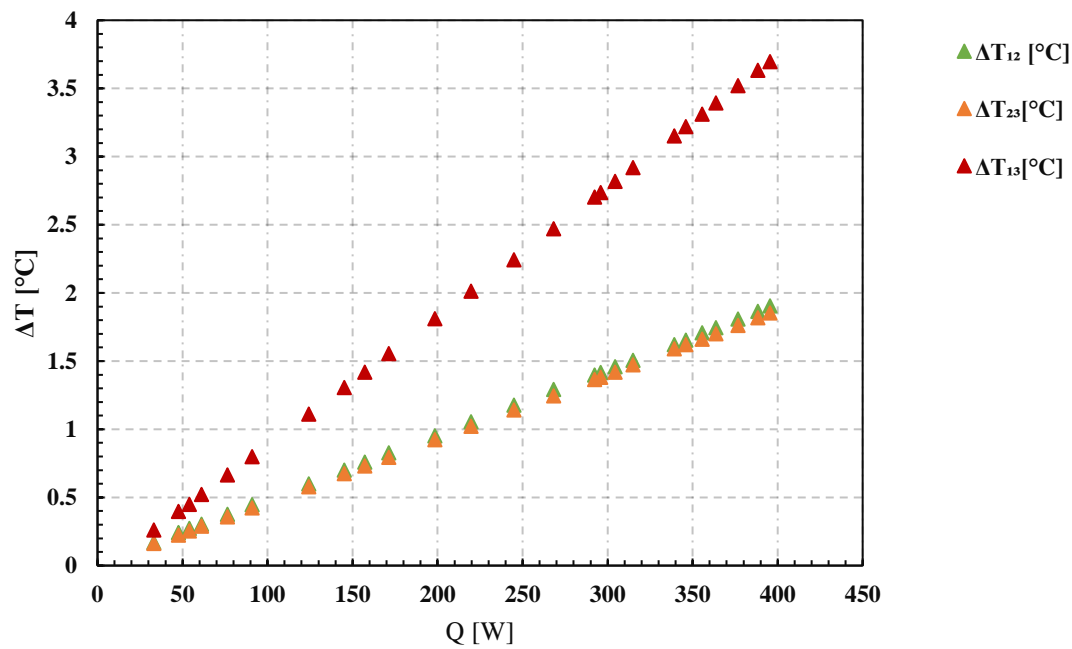


APPENDIX D-4: Temperature gradient measured in the experiment investigating LHP performance under gravity-assisted condition – the second pattern of evaporator

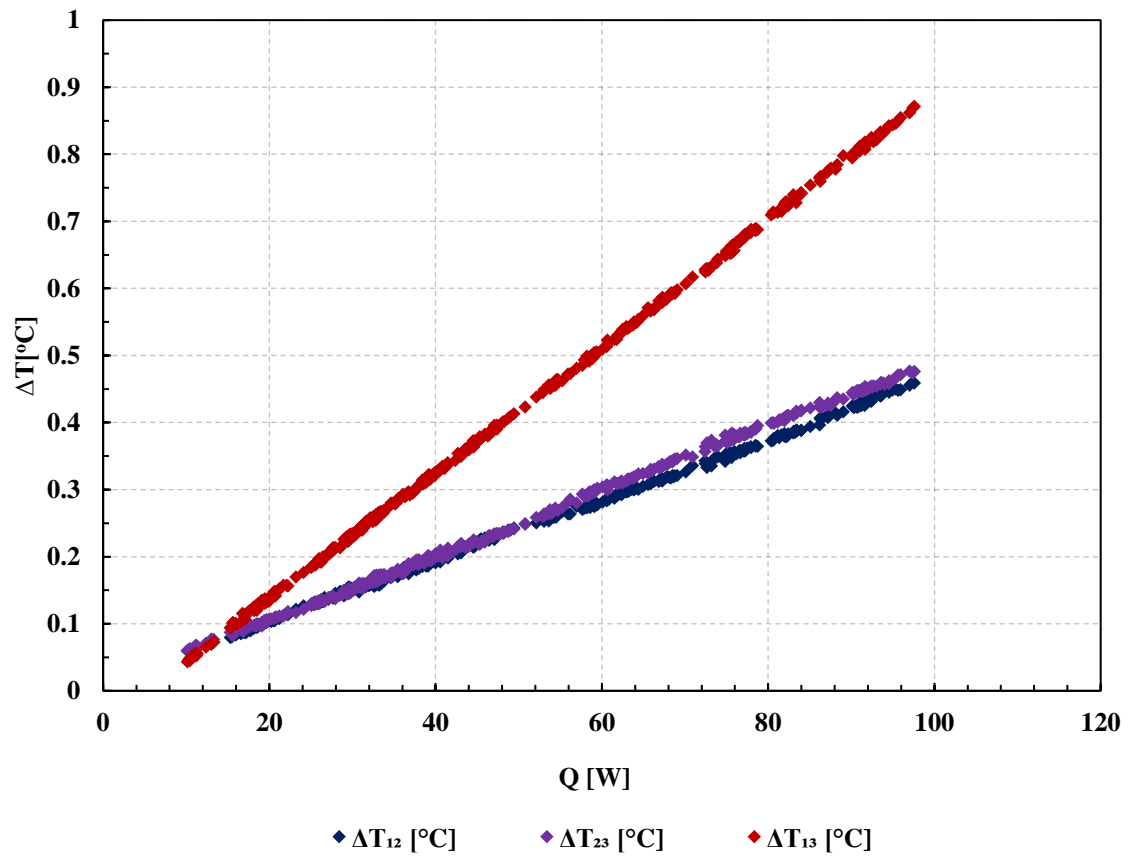
Temperature gradient - Working fluid: Water



Temperature gradient - Working fluid: Ethanol



APPENDIX D-5: Temperature gradient measured in the experiment investigating LHP performance at horizontal orientation– the first pattern of evaporator



APPENDIX E: EXPERIMENTAL UNCERTAINTY ANALYSIS

According to Robert J. Moffat [1], the result R of the experiment is assumed to be calculated from a set of measurements using a data interpretation program presented by

$$R = R(X_1, X_2, X_3, \dots, X_N)$$

The effect of each measurement uncertainty on the calculated result if only that one measurement were in error would be

$$\delta R_{X_i} = \frac{\partial R}{\partial X_i} \delta X_i$$

The partial derivative of R with respect to X_i is the sensitivity coefficient for the result R with respect to the measurement X_i .

When several independent variables are used in the function R , the individual terms are combined by a root-sum-square method

$$\delta R_{X_i} = \left\{ \sum_{i=1}^N \left(\frac{\partial R}{\partial X_i} \delta X_i \right)^2 \right\}^{\frac{1}{2}}$$

Parameter	Uncertainty
$\Delta T_{12} = T_1 - T_2$	$\delta(\Delta T_{12}) = (\delta T_1^2 + \delta T_2^2)^{\frac{1}{2}}$
$\Delta T_{23} = T_3 - T_2$	$\delta(\Delta T_{23}) = (\delta T_3^2 + \delta T_2^2)^{\frac{1}{2}}$
$\Delta T_{13} = T_1 - T_3$	$\delta(\Delta T_{13}) = (\delta T_1^2 + \delta T_3^2)^{\frac{1}{2}}$
$\Delta T_{wa} = T_{wa-o} - T_{wa-i}$	$\delta(\Delta T_{wa}) = (\delta T_{wa-o}^2 + \delta T_{wa-i}^2)^{\frac{1}{2}}$
$q = k \frac{\Delta T_{12}}{\delta_1}$	$\delta q = \frac{k}{\delta_1} \delta(\Delta T_{12})$
$Q = qA$	$\delta Q = \delta q A$
$Q_c = m_{wa} c_p \Delta T_{wa}$	$\delta Q_c = \left((c_p \Delta T_{wa} \delta m_{wa})^2 + (m_{wa} c_p \delta \Delta T_{wa})^2 \right)^{\frac{1}{2}}$
$T_{s1} = T_1 - 3 \frac{q \delta_1}{k}$	$\delta(T_{s1}) = \left((\delta T_1)^2 + \left(3 \frac{\delta_1}{k} \delta q \right)^2 \right)^{\frac{1}{2}}$
$T_{s2} = T_4 + \frac{q \delta_2}{k}$	$\delta(T_{s2}) = \left((\delta T_4)^2 + \left(\frac{\delta_2}{k} \delta q \right)^2 \right)^{\frac{1}{2}}$
$T_{bf} = T_4 - \frac{q \delta_2}{k}$	$\delta(T_{bf}) = \left((\delta T_4)^2 + \left(\frac{\delta_2}{k} \delta q \right)^2 \right)^{\frac{1}{2}}$
$T_{sat} = f(P_{ev})$	$\delta T_{sat} = \frac{\partial T_{sat}}{\partial P_e} \delta P_e$
$R_{LHP} = \frac{T_{s1} - T_{wa-i}}{Q}$	$\delta(R_{LHP}) = \left(\left(\frac{\delta T_{s1}}{Q} \right)^2 + \left(\frac{\delta T_{wa-i}}{Q} \right)^2 + \left(\frac{T_{s1} - T_{wa-i}}{Q^2} \delta Q \right)^2 \right)^{\frac{1}{2}}$
$R_e = \frac{T_{s2} - T_{eo}}{Q}$	$\delta(R_e) = \left(\left(\frac{\delta T_{s2}}{Q} \right)^2 + \left(\frac{\delta T_{eo}}{Q} \right)^2 + \left(\frac{T_{s2} - T_{eo}}{Q^2} \delta Q \right)^2 \right)^{\frac{1}{2}}$

$R_c = \frac{T_{ci} - T_{wa-i}}{Q}$	$\delta(R_c) = \left(\left(\frac{\delta T_{ci}}{Q} \right)^2 + \left(\frac{\delta T_{wa-i}}{Q} \right)^2 + \left(\frac{T_{ci} - T_{wa-i}}{Q^2} \delta Q \right)^2 \right)^{\frac{1}{2}}$
$R_{ct} = \frac{T_{s1} - T_{s2}}{Q}$	$\delta(R_{ct}) = \left(\left(\frac{\delta T_{s1}}{Q} \right)^2 + \left(\frac{\delta T_{s2}}{Q} \right)^2 + \left(\frac{T_{s1} - T_{s2}}{Q^2} \delta Q \right)^2 \right)^{\frac{1}{2}}$
$h_{e-T} = \frac{q}{T_{eo} - T_{bf}}$	$\delta(h_{e-T}) = \left(\left(\frac{\delta q}{T_{eo} - T_{bf}} \right)^2 + \left(\frac{q \delta T_{eo}}{(T_{eo} - T_{bf})^2} \right)^2 + \left(\frac{q \delta T_{bf}}{(T_{eo} - T_{bf})^2} \right)^2 \right)^{\frac{1}{2}}$
$h_{e-P} = \frac{q}{T_{sat} - T_{bf}}$	$\delta(h_{e-P}) = \left(\left(\frac{\delta q}{T_{sat} - T_{bf}} \right)^2 + \left(\frac{q \delta T_{sat}}{(T_{sat} - T_{bf})^2} \right)^2 + \left(\frac{q \delta T_{bf}}{(T_{sat} - T_{bf})^2} \right)^2 \right)^{\frac{1}{2}}$

APPENDIX E-1: Estimating the uncertainty of parameters in the experiments of gravity assisted loop heat pipe with the first pattern of evaporator

q, (W/m ²)		Q, (W)		T _{s1} , (°C)		R _t , (K/W)		R _{ct} , (K/W)		h _e , W/(m ² ·K)	
Mean	δq (%)	Mean	Mean	Mean	δT _{s1} (%)	Mean	δR _t (%)	Mean	δR _{ct} (%)	Mean	δh _e (%)
18598	30.41	50.22	40.33	0.39	0.2494	30.24	0.0055	67.19	1329	62.04	
37144	15.20	100.29	49.22	0.32	0.2138	15.16	0.0072	27.53	2132	37.35	
54783	10.29	147.91	53.13	0.29	0.1712	10.29	0.0053	24.07	3931	32.03	
69693	8.08	188.17	58.72	0.27	0.1650	8.06	0.0062	16.82	4718	24.92	
87835	6.40	237.2	67.47	0.23	0.1680	6.39	0.0072	11.95	5560	17.44	
107420	5.22	290.03	76.69	0.20	0.1695	5.20	0.0086	8.63	6382	12.46	
129896	4.31	350.72	84.20	0.18	0.1615	4.31	0.0093	6.82	7569	9.71	
148767	3.76	401.67	91.55	0.17	0.1593	3.76	0.0098	5.78	8160	7.67	
165137	3.38	445.87	96.34	0.16	0.1542	3.39	0.0098	5.19	9102	6.68	
186470	2.99	503.47	102.94	0.15	0.1497	3.00	0.0101	4.51	10410	5.61	
192854	2.89	520.7	105.44	0.15	0.1492	2.90	0.0097	4.46	10681	5.23	

APPENDIX E-2: Estimating the uncertainty of parameters in the experiments of gravity assisted loop heat pipe with the second pattern of evaporator – Ethanol is working fluid

q, (W/m ²)		Q, (W)		T _{s1} , (°C)		R _t , (K/W)		R _{ct} , (K/W)		h _{e-T} , W/(m ² ·K)		h _{e-P} , W/(m ² ·K)	
Mean	δq (%)	Mean	Mean	Mean	δT _{s1} (%)	Mean	δR _t (%)	Mean	δR _{ct} (%)	Mean	δh _{e-P} (%)	Mean	δh _{e-P} (%)
12240	46.3	33.05	32.94	0.47	0.2179	46.33	0.0067	90.62	5612	46.5	5587	110.8	
22683	24.9	61.25	40.65	0.38	0.2433	24.94	0.0060	53.60	5600	25.1	5750	51.8	
46000	12.2	124.2	59.36	0.26	0.2702	12.26	0.0068	24.14	6679	12.3	6962	19.0	
58188	9.7	157.11	71.26	0.22	0.2889	9.67	0.0071	18.33	7796	9.8	8156	13.1	
73468.6	7.6	198.37	80.01	0.19	0.2728	7.64	0.0076	13.86	9378	7.7	9814	9.9	
89824	6.2	242.52	92.22	0.17	0.2736	6.23	0.0065	12.75	9886	6.3	10235	7.3	
108261	5.2	292.31	99.9	0.16	0.2534	5.16	0.0077	9.33	10309	5.2	9962	5.8	
128132	4.3	345.96	114.66	0.14	0.2572	4.35	0.0083	7.49	12039	4.4	9369	4.6	
146516	3.8	395.59	133.4	0.12	0.2726	3.79	0.0080	6.66	10104	3.8	7679	3.9	

APPENDIX E-3: Estimating the uncertainty of parameters in the experiments of gravity assisted loop heat pipe with the second pattern of evaporator – Water is working fluid

q, (W/m ²)		Q, (W)	T _{sl} , (°C)		R _i , (K/W)		R _{ct} , (K/W)		h _{e-T} , W/(m ² ·K)		h _{e-P} , W/(m ² ·K)	
Mean	δq (%)	Mean	Mean	δT _{sl} (%)	Mean	δR _i (%)	Mean	δR _{ct} (%)	Mean	δh _{e-P} (%)	Mean	δh _{e-P} (%)
12151	46.6	32.8	37.83	0.41	0.3657	46.52	0.0077	84.0	2341	46.4	1513	88.7
22934	24.6	61.9	45.41	0.34	0.3172	24.61	0.0081	42.5	5728	24.7	3871	69.5
36318	15.6	98.1	45.99	0.34	0.2059	15.58	0.0065	31.6	6293	15.7	5795	64.1
54907	10.3	148.3	53.43	0.29	0.1860	10.29	0.0066	20.4	9451	10.4	9536	49.3
73401	7.7	198.2	61.08	0.25	0.1780	7.66	0.0071	14.6	9660	7.5	10020	29.8
92074	6.1	248.6	69.66	0.22	0.1763	6.11	0.0080	10.7	11337	6.1	11685	21.7
117720	4.8	317.9	80.65	0.19	0.1727	4.77	0.0089	7.8	15423	4.9	11139	13.0
136657	4.1	369.0	88.30	0.18	0.1698	4.11	0.0092	6.6	16509	4.3	11751	9.8
155045	3.6	418.6	93.80	0.17	0.1631	3.62	0.0082	6.2	18229	3.8	13693	8.4
174701	3.2	471.7	101.90	0.15	0.1621	3.20	0.0089	5.2	18846	3.4	13138	6.3
185410	3.0	500.6	105.83	0.15	0.1603	3.02	0.0087	5.0	19994	3.2	13836	5.7
198121	2.8	534.9	109.94	0.14	0.1577	2.82	0.0089	4.6	20147	3.0	13353	4.9